






The Combia Volcanic Province: Miocene Post-Collisional Magmatism in the Northern Andes

Marion WEBER^{1*} , José Fernando DUQUE² , Susana HOYOS³ ,
Andrés L. CÁRDENAS-ROZO⁴ , Jorge GÓMEZ TAPIAS⁵ , and Rob WILSON⁶

Abstract A transtensional basin setting originated the Combia Volcanic Province in the northern Andes of Colombia. Volcanism is heterogeneous encompasses tholeiitic, calc-alkaline, and shoshonitic magmatic series. A review of existing geochemical and geochronological data suggests that all magma series coexisted between 12 and 6 Ma but originated from different processes. Tholeiites formed via the melting of a modified primitive mantle source, with limited sedimentary or continental-contaminant input. Calc-alkaline magmas are mainly adakitic and formed from fractionation of garnet and amphibole at high pressures from a hydrous melt from an enriched source. Petrographic and mineral chemistry of garnet-bearing rocks indicate that magmas underwent at least three ascent phases that include: (1) crystallization of high-pressure phenocryst phases at 900 °C and 1200 GPa in a mantle-derived melt, (2) stalling of differentiated magma at lower-pressure conditions, and (3) stalling at shallower conditions, where decompression occurred. Shoshonitic magmas formed from a mantle with sedimentary or continental-contaminant input source in the plagioclase stability field. Finally, the Combia Volcanic Province's formation was enhanced by the Caldas Tear, a slab window developed by the subduction of the Sandra Ridge beneath the South American Plate.

Keywords: *Combia Formation, shallow-volcanic intrusions, tholeiitic magmatism, calc-alkaline magmas, adakites, shoshonitic magmatism, igneous garnet.*

Resumen La Provincia Volcánica de Combia en el norte de los Andes de Colombia se formó en un ambiente de cuenca transtensional. El vulcanismo es heterogéneo y comprende series magmáticas toleíticas, calcoalcalinas y shoshoníticas. Una revisión de los datos geoquímicos y geocronológicos existentes sugiere que las tres composiciones de magma coexistieron entre 12 y 6 Ma, pero se originaron por diferentes procesos. Las toleitas se formaron a partir de una fuente de manto primitivo modificada, con limitado suministro de contaminante sedimentario o continental. Los magmas calcoalcalinos son principalmente adakíticos y se formaron del fraccionamiento de granate y anfíbol a altas presiones a partir de un fundido hidratado proveniente de una fuente enriquecida. Los datos petrográficos y de química mineral de rocas con granate indican que estos magmas experimentaron por lo menos tres fases de ascenso que incluyen: (1) cristalización de las fases de fenocristales de alta presión a 900 °C y 1200 GPa en un fundido derivado del manto, (2) estancamiento del magma diferenciado a más bajas

Citation: Weber, M., Duque, J.F., Hoyos, S., Cárdenas-Rozo, A.L., Gómez, J. & Wilson, R. 2020. The Combia Volcanic Province: Miocene post-collisional magmatism in the northern Andes. In: Gómez, J. & Mateus-Zabala, D. (editors), The Geology of Colombia, Volume 3 Paleogene – Neogene. Servicio Geológico Colombiano, Publicaciones Geológicas Especiales 37, p. 355–394. Bogotá. <https://doi.org/10.32685/pub.esp.37.2019.12>

<https://doi.org/10.32685/pub.esp.37.2019.12>
Published online 26 November 2020

- 1 mweber@unal.edu.co
Universidad Nacional de Colombia
Sede Medellín
Departamento de Geociencias y Medio Ambiente
Carrera 80 n.º 65-223
Medellín, Colombia
 - 2 jduquet@eafit.edu.co
Universidad EAFIT
Departamento de Ciencias de la Tierra
Carrera 49 n.º 7 sur-50
Medellín, Colombia
 - 3 shoyosm1@eafit.edu.co
shoyos@mit.edu
Universidad EAFIT
Departamento de Ciencias de la Tierra
Carrera 49 n.º 7 sur-50
Medellín, Colombia
Massachusetts Institute of Technology
Department of Earth, Atmospheric, and Planetary Sciences
77 Massachusetts Avenue, 54-918, Cambridge, MA 02139
USA
 - 4 acarde17@eafit.edu.co
Universidad EAFIT
Departamento de Ciencias de la Tierra
Carrera 49 n.º 7 sur-50
Medellín, Colombia
 - 5 mapageo@sgc.gov.co
Servicio Geológico Colombiano
Dirección de Geociencias Básicas
Grupo Mapa Geológica de Colombia
Diagonal 53 n.º 34-53
Bogotá, Colombia
 - 6 robnewwilson@gmail.com
University of Leicester
School of Geography, Geology & the Environment
Leicester LE1 7RH
United Kingdom
- * Corresponding author

Supplementary Information:

- S1: <https://www2.sgc.gov.co/LibroGeologiaColombia/tgc/sgcpubesp37201912s1.pdf>
- S2: <https://www2.sgc.gov.co/LibroGeologiaColombia/tgc/sgcpubesp37201912s2.pdf>
- S3: <https://www2.sgc.gov.co/LibroGeologiaColombia/tgc/sgcpubesp37201912s3.pdf>
- S4: <https://www2.sgc.gov.co/LibroGeologiaColombia/tgc/sgcpubesp37201912s4.pdf>

condiciones de presión y (3) estancamiento en condiciones superficiales, donde ocurrió la descompresión. Los magmas shoshoníticos se formaron a partir de una fuente mantélica con aporte sedimentario o continental, en el campo de estabilidad de la plagioclasa. La formación de la Provincia Volcánica de Combia fue acentuada por el *Caldas Tear*, una ventana en la placa desarrollada por la subducción del *Sandra Ridge* bajo la Placa de Suramérica.

Palabras clave: *Formación Combia, intrusivos volcánicos someros, magmatismo toleítico, magmas calcoalcalinos, adakitas, magmatismo shoshonítico, granate ígneo.*

1. Introduction

The Andes are among the most extensive active volcanic chains in the world (Figure 1). They represent an essential record of continental–crust construction and modification processes. Volcanic activity is caused by the eastward subduction of the Nazca Plate beneath the South American Plate (Harmon et al., 1984). It is divided into four distinct zones (from south to north): The Austral Volcanic Zone, the Southern Volcanic Zone, the Central Volcanic Zone, and the Northern Volcanic Zone (Figure 1; Stern & Kilian, 1996; Thorpe et al., 1984). Each of these zones is characterized by differences in the magmatic activity related to variances in the subduction configuration (e.g., subduction angle, velocity) and intrinsic, differential properties in both subducting and overriding plates (e.g., age and thickness). Of these segments, the Northern Volcanic Zone remains the least studied and well known due to a long history of political unrest in the region.

In Colombia, the Andean belt comprises three cordilleras separated by deep, fluvial valleys (i.e., Western, Central, and Eastern Cordilleras) (Figure 1). The geographic limit between the Western and Central Cordilleras is marked by the Cauca River valley, which is the superficial expression of the Cauca–Romeral Fault System. Today, this paleosubduction zone constitutes a suture zone between a Permian – Triassic, continental–basement domain to the east and a Cretaceous, oceanic–basement domain to the west (e.g., Aspden & Litherland, 1992) (Figure 2), which resulted from the complex history of subduction–accretion that occurred throughout the Late Cretaceous until today (Horton et al. 2010; Kennan & Pindell, 2009; Pindell et al., 2005).

The establishment of the current subduction configuration and Neogene magmatism along the Western Cordillera started in the mid–Miocene, with the accretion of the Panamá–Chocó Block onto the South American margin (Duque–Caro, 1990; Montes et al., 2012, 2015). Recent studies suggest that normal subduction of the Nazca Plate initiated around 14 to 9 Ma, and accretion of the Panamá–Chocó Block occurred before 12 Ma (Montes et al., 2012, 2015; Wagner et al., 2017). Magmatism ceased between 6 and 4 Ma due to the flat–slab subduction of the Nazca Plate underneath South America. Magmatism resumed at 3 Ma along the length of the arc, south of the *Caldas Tear* (Wagner et al., 2017).

Among the Neogene magmatic events in the Cauca River valley, the Combia Formation (CF) comprises a middle to upper Miocene (ca. 12 to 6 Ma) volcanoclastic–sedimentary sequence located in the middle and northern parts of the valley, and represents a distinctive magmatic occurrence (Figure 2). The CF was deposited within the intramontane, semi–isolated Amagá Basin, which formed between the basement rocks from the Western and Central Cordilleras in the northernmost Colombian Andes (Figure 2; Lara et al., 2018). The CF mainly comprises basic tholeiitic magmas, linked to crustal thinning and basin extension (Bernet et al., 2020; Dunia, 2005; Jaramillo, 1976; Jaramillo et al., 2019). Furthermore, calc–alkaline, andesitic to dacitic, shallow, volcanic porphyries of the Cauca Shallow Volcanic Intrusions (CSVI) are spatially associated with the CF, even though some authors define them as a single, separate unit (e.g., Borrero & Toro–Toro, 2016; Calle & González, 1980; Tassinari et al., 2008). Moreover, the cartographic resolution of the volcanic products recorded in the CF does not record individual event levels. Only a few studies have discussed their genesis and tectonic setting (e.g., Bernet et al., 2020; Jaramillo et al., 2019; Marriner & Millward, 1984; Rodríguez & Zapata, 2014). Several authors (Bissig et al., 2017; Jaramillo, 1976; Ramírez et al., 2006) suggest that the CSVI and the CF were generated by a subduction zone related to the magmatic arc. In addition, they argue that the magmatic setting started as a protoarc (tholeiitic series) and then moved towards a more mature arc (calc–alkaline series). Additionally, these studies also suggest differentiation and contamination from the input of a mature crustal end–member (Dunia, 2005; Marriner & Millward, 1984).

The CF has been traditionally considered late Miocene in age (ca. 6 to ca. 10 Ma; Ramírez et al., 2006), mostly based on cross–cutting relationships with the CSVI. Recent studies on basaltic andesites (formerly considered part of the CF) have suggested the presence of an older, magmatic arc, located to the west of the Amagá Basin (Rodríguez & Zapata, 2014; Zapata & Rodríguez, 2011). Consequently, these authors propose to splitting the middle Miocene magmatism into two different magmatic arcs with different ages and geographical locations: The earlier shoshonitic arc and a later tholeiitic and calc–alkaline arc represented by the CF and CSVI magmas. The shoshonitic arc comprises El Botón basalts and El Morito basaltic andesites (Figure 2; Rodríguez & Zapata, 2014; Zapata & Rodríguez, 2011).

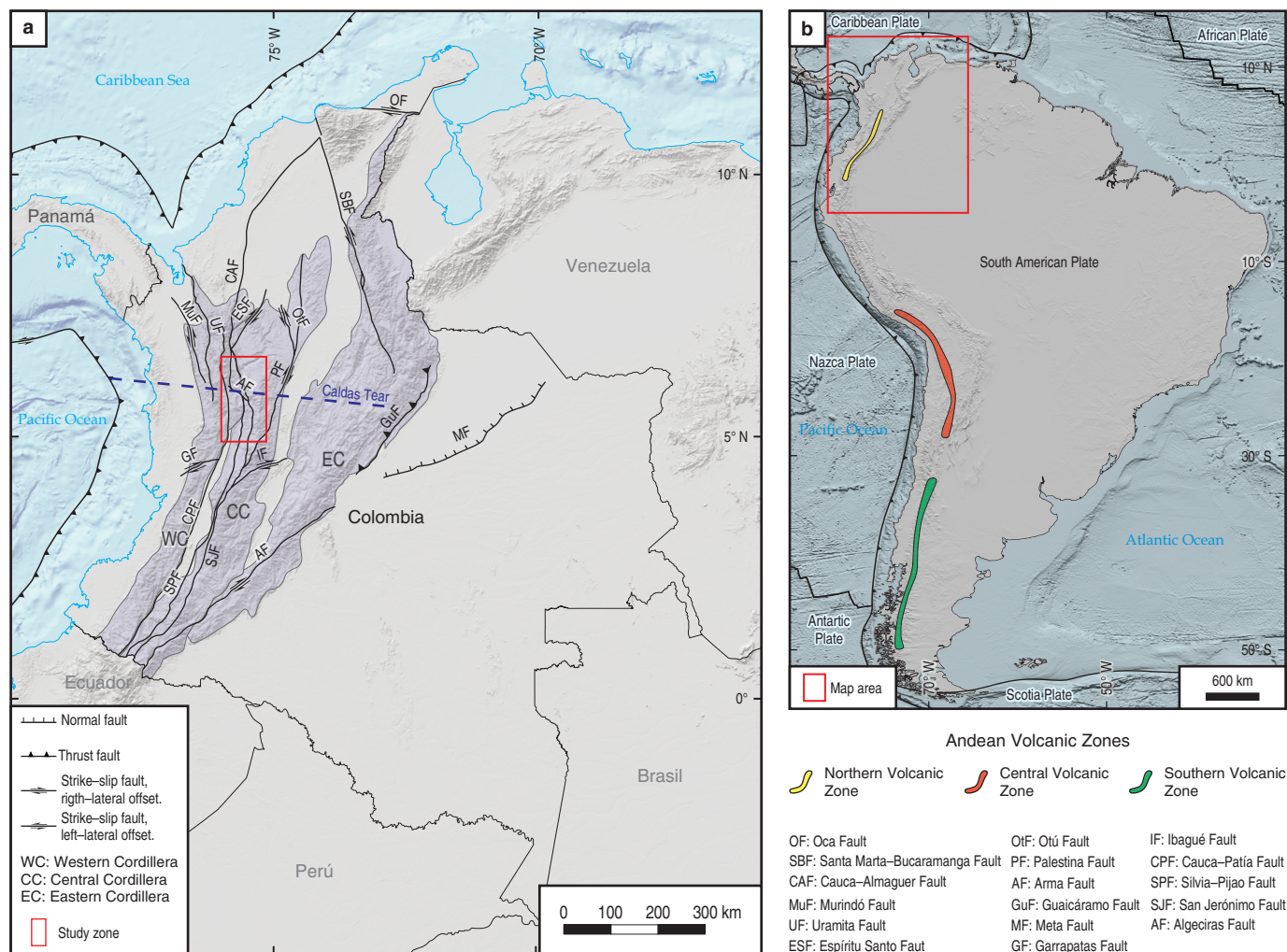


Figure 1. (a) Tectonic setting of the Andes in Colombia. The CVP is located within the rectangle. **(b)** Geographic distribution of the volcanic zones in the Andes (after Harmon et al., 1984).

The present work represents an effort to synthesize an essential amount of petrography, field relationships, mineral chemistry, geochronological, and geochemical data previously reported associated with volcanic, volcanoclastic, hypabyssal, porphyritic magmatism and sedimentary rocks of the Combia Formation found along the Cauca River valley. The authors here combine unpublished petrography, mineral chemistry, geochronological, and geochemical data with previous data available from Jaramillo (1976), Álvarez (1983), Marriner & Millward (1984), Ordóñez-Carmona (2001), Dunia (2005), Tejada et al. (2007), Tassinari et al., (2008), Leal-Mejia (2011), Borrero & Toro-Toro (2016), Bissig et al. (2017), Jaramillo et al. (2019), and Bernet et al. (2020) to better understand this unique geological occurrence in Colombia.

2. The Combia Formation

In this chapter, we present the previous studies published on the Combia Formation.

The CF was first defined by Grosse (1926) as the “Neo-Tertiary volcanics” and “Neo-Tertiary sediments” in the Alto Combia locality (Fredonia, Colombia; Figure 3). In this work, he also divided the CF into a Lower Member (Volcanic Neo-Tertiary) and an Upper Member (Sedimentary Neo-Tertiary). In general, Grosse (1926) described the CF as a mixture of sedimentary and volcanoclastic packages: “Conglomerates, sandstones, schistose clay, tuffitic conglomerates, tuffitic sandstones, tuffs, crystal tuffs, ash and agglomerate tuffs, and basaltic and andesitic lava flows”. Later, the unit was renamed the Combia Formation by Calle et al. (1980), who, based on lithology, divided it into two members (i.e., Sedimentary and Volcanic).

Jaramillo (1976) conducted a detailed petrographic and geochemical study of the volcanic rocks and determined the tholeiitic character of the basaltic to andesitic flows of the CF, which are interbedded with pyroclastic material, as well as the calc-alkaline nature of magmas from the Cauca porphyritic intrusions (cf. CSMV). Petrographically, based on phenocryst content, he divided the basalts into three types: plagioclase, hypersthene, and augite

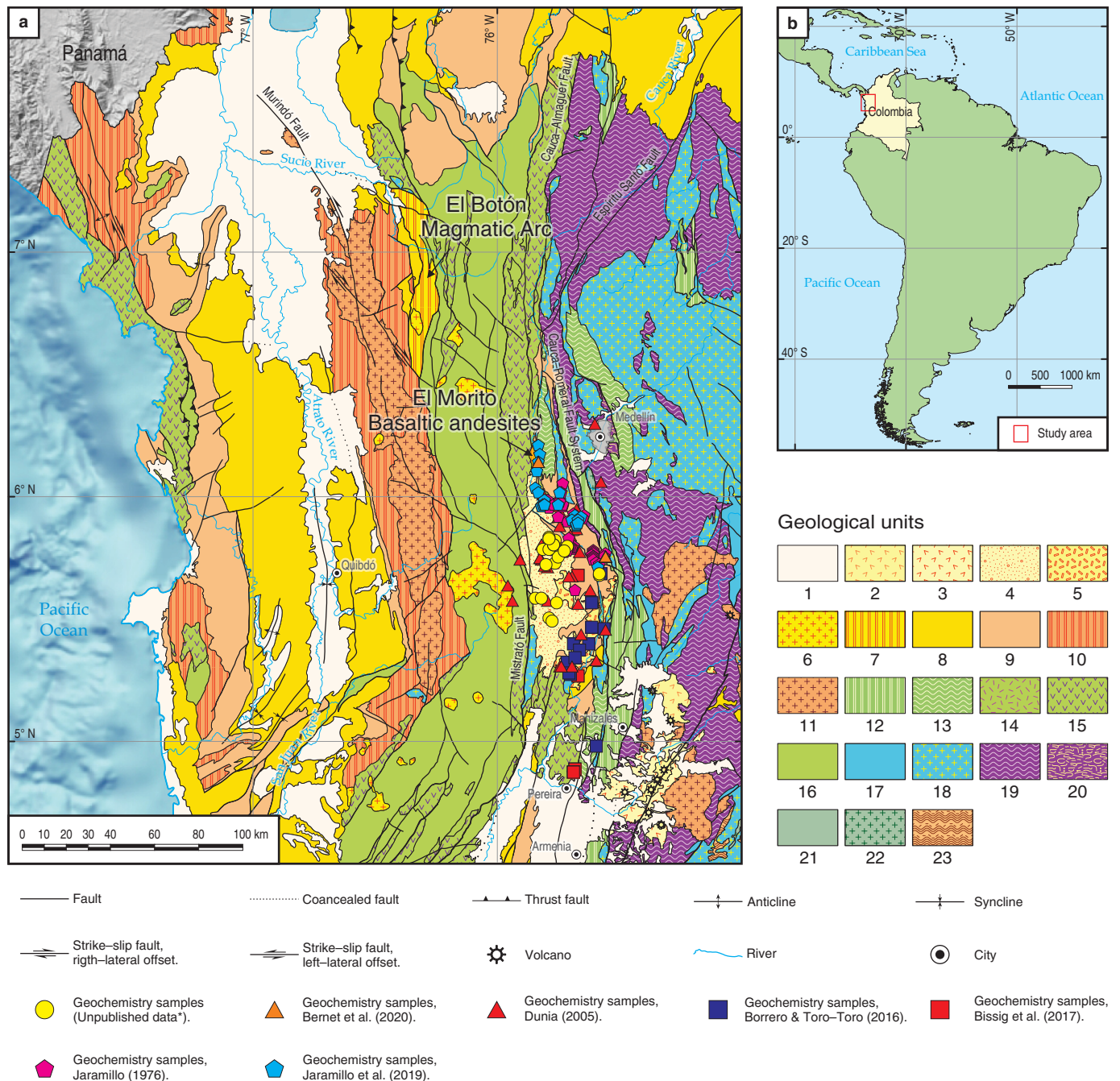


Figure 2. (a) Geological map of the Western of Colombia simplified from Alcárcel & Gómez (2017), and location of the geochemistry samples used in this study. Geological units: (1) Quaternary deposits and volcanoclastic deposits; (2) Quaternary volcanites; (3) Pliocene volcanites; (4) Combia Formation; (5) Miocene sub-volcanic bodies; (6) Miocene plutons; (7) El Botón Magmatic Arc; (8) Neogene sedimentites; (9) Eocene – Miocene sedimentites; (10) Paleogene volcanites and volcanosedimentites; (11) Paleogene plutons; (12) Cretaceous sedimentites, volcanites, gabbros, and ultramafic rocks; (13) Lower Cretaceous metamorphic rocks; (14) Upper Cretaceous gabbros and ultramafic rocks; (15) Upper Cretaceous basalts; (16) Upper Cretaceous sedimentites; (17) Mesozoic sedimentary and volcanoclastic rocks; (18) Mesozoic plutons; (19) Triassic metamorphic rocks and plutons; (20) Triassic ultramafic rocks; (21) Paleozoic sedimentites; (22) Paleozoic plutons; and (23) Stenian – Tonian metamorphic rocks. **(b)** Location of the geological map area. Unpublished data* from Tejada et al. (2007) and Project “Caracterización Estratigráfica, Petrogenética y Geocronológica de la Formación Combia, Acuerdo Específico No 009–2004 con la Universidad Nacional de Colombia”.

basalts. Furthermore, Jaramillo (1976) determined that some basic dikes that intruded the Amagá Formation (AF) are part of the CF (i.e., in the areas of the Quebrada Popala and Río Poblano).

The AF is a terrestrial, siliciclastic succession dominated by meandering (Lower Member) to braided (Upper Member) rivers in a pull-apart, tectonic regime during the late Oligocene to middle

Miocene (Lara et al., 2018). Jaramillo (1976) also reported two dikes that cut the CF at the Alto Combia location and described them as an alkaline–rock unit similar to absarokites. Finally, he suggested that both the CF and CSVI are the outcome of the presence of a ‘permeable zone’, which allowed the migration of different magma batches, generated under different conditions and/or depths, through the continental crust.

Later, Marriner & Millward (1984), in an integrated geochemical study of Colombian volcanism, and based on the tholeiitic, chemical character of the CF, suggested an island–arc tectonic setting for its formation. Based mainly on geographic location and age, they proposed a single province in northern Colombia, which includes both the CF and the recent axial, calc–alkaline volcanism of the Central Cordillera (Figure 1).

Extensive geological mapping has been performed over time by various projects of the Servicio Geológico Colombiano (Figure 2; e.g., Álvarez, 1983; Calle & González, 1980, 1982; Dunia, 2005; Mahecha et al., 2006; Tejada & Betancourt, 2006; Tejada et al., 2007). Among these studies, Dunia’s (2005) report integrates petrographic, geochemical, and geophysical analyses of the Amagá Basin, including the CF and CSVI. Mafic rocks of the volcanic member are described as agglomerates, andesites, and feldspathic basalts. Moreover, the latter are divided (based on textural features) into porphyritic basalts, augite basalts, amygdalar basalts, and glomeroporphyritic basalts. Furthermore, Dunia (2005) also included andesitic and basaltic dikes and sills that cut through both the AF and CF and suggested that they are genetically linked to basaltic rocks. Finally, the Farallones Batholith and Támesis Stock are coetaneous with Combia–magmatic activity (González, 2010; Zapata & Rodríguez, 2013). According to Dunia (2005), the two compositional–magma series formed during juvenile–arc activity, which later evolved into a mature calc–alkaline, volcanic arc via differentiation, and the accretion of the Chocó Block, as proposed by Duque–Caro (1990), which may be responsible for the magmatism.

Detailed mapping of the area near the municipalities of Pueblorrico and Jericó (Tejada & Betancourt, 2006) enabled Tejada et al. (2007) to locally divide the CF into eight units based on lithological differences and age, from oldest to youngest: (i) tuffs 1 (N1ct1); (ii) basalts 1 (N1cb1); (iii) hornblende, basaltic andesites (N1cab); (iv) basalts 2 (N1cb2); (v) agglomerates (N1ca); (vi) interspersed basalts, tuffs and agglomerates (N1cbta); (vii) tuffs 2 (N1ct2); and (viii) hypabyssal rocks that comprise basalt dikes and sills, hornblende, andesitic porphyries and one garnet–bearing, hornblende, andesitic porphyry (N1cds, N1cp, and N1cpg, respectively). Moreover, they suggested that the presence of garnet indicates wet conditions during calc–alkaline magma formation at 9 Kbar and 1000 °C. Subsequently, the CF originated from various explosive and extrusive stages, and the basaltic rocks may have formed in a back–arc or immature arc. In contrast, the porphyries represent

typical magmas of a subduction zone with an added continental component (Tejada et al., 2007).

Additional geochemical research on the CSVI on the lower volcanic rocks from the Cauca and Amagá regions (Borrero & Toro–Toro, 2016) shows that adakitic signature magmas could be related to melts originated in a previously metasomatized mantle located in a subduction zone.

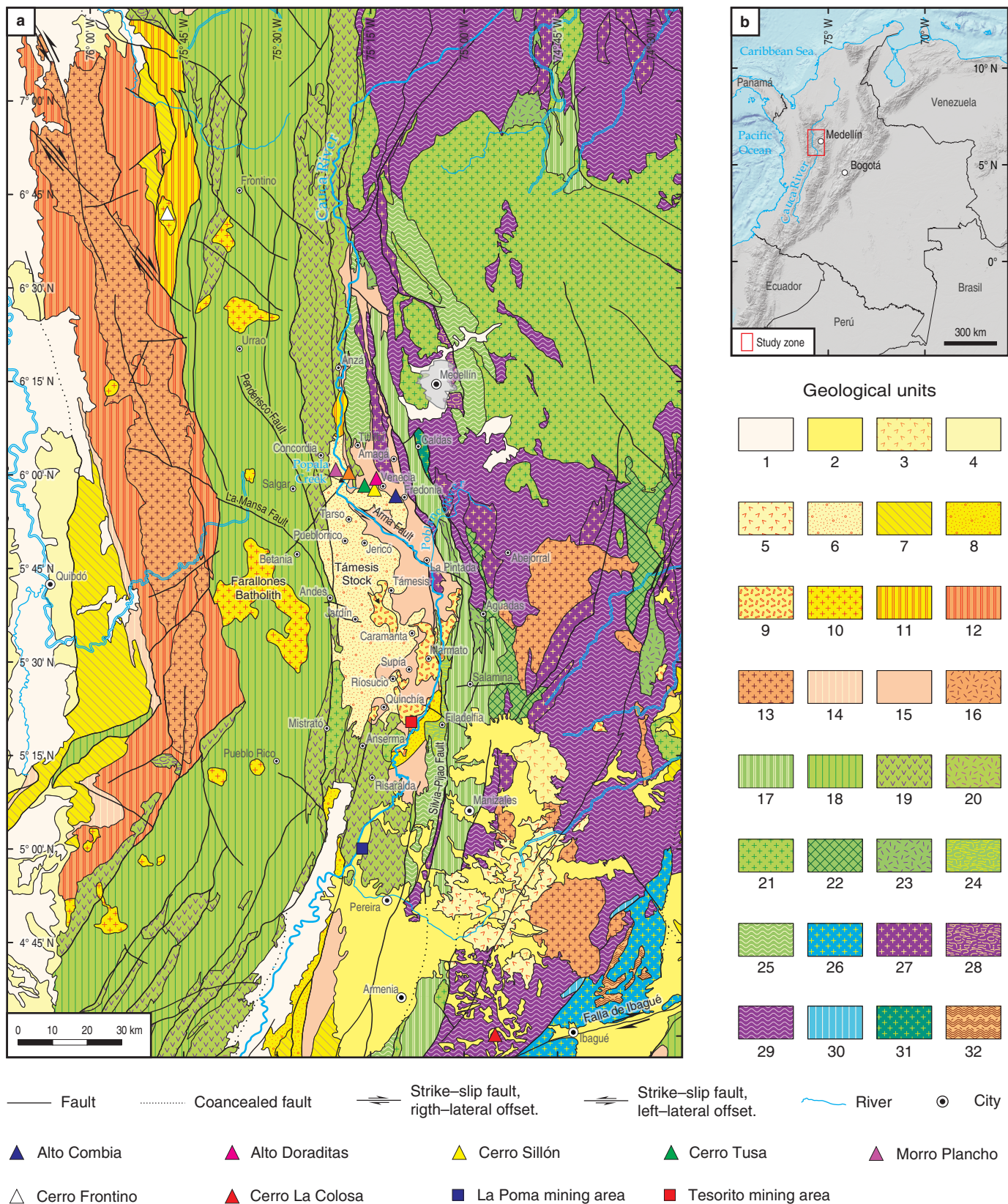
Additional interest in the CF has arisen because of copper, gold, and molybdenum deposits associated with the CSVI. Tassinari et al. (2008) studied the origin of Marmato gold deposits. Leal–Mejía (2011), Leal–Mejía et al. (2019), and Shaw et al. (2019) focused their studies on Phanerozoic gold metallogeny in the northern Andes, including gold–bearing associated porphyries in the CF. Most recently, Bissig et al. (2017) studied the origin of garnet–bearing magmas in the Colombian Middle Cauca Metallogenic Belt.

Tassinari et al. (2008) suggested a juvenile, mantle–derived magma as the primary source of calc–alkaline to tholeiitic magmatism, based on isotopic data. However, they did not exclude a minor magmatic contribution resulting from the partial melting of the lower continental crust. In the Marmato Stock, hydrothermal activity occurred at 5.6 Ma, which is later than the reactivation of the Cauca–Romeral Fault System at approximately 6.3 Ma.

Bissig et al. (2017) described the garnet–bearing porphyry systems of Tesorito and El Poma located in the Colombian Middle Cauca Metallogenic Belt. They interpreted their formation as occurring from a rapidly ascending magma that melted in the lower crust, at pressures above 1 GPa. Furthermore, they suggested that a change in the geodynamic environment may have removed garnet from the melt. This enabled the generation of middle– to upper–crustal magma chambers, which accounts for the later, garnet–free, porphyritic rocks.

Finally, new interest has arisen in the CF that is associated with the magmatic evolution of the northern Andes after the fragmentation of the Farallón Plate ca. 23 Ma (Lonsdale, 2005; Marriner & Millward, 1984), and the development of diverse magmatic activity. Two recent contributions, which include geochemical, geochronological, and isotopic data, focus on the petrogenesis and tectonic setting of the CF (Bernet et al., 2020; Jaramillo et al., 2019).

Jaramillo et al. (2019) suggested that 9 to 5.2 Ma magmatism in the area comprising the Combia Volcanic Complex, formed mainly from the mantle, interacted with older crustal material and underwent magmatic differentiation. They suggested that the basalts represent the oldest, erupting phase at ca. 9 Ma and are overlain by more differentiated, calc–alkaline rocks. They related the different magmatic compositions (i.e., tholeiitic, calc–alkaline, and adakitic) to differences in dry– and wet–melting conditions in the continental crust associated with crustal thickness. Their proposed formation model suggests that Combia magmatism is related to oblique subduction and substantial structural inheritance.



Bernet et al. (2020) presented three stratigraphic sections in the eastern Amagá Basin and proposed that the origin of magmas of the CF resulted from a metasomatized mixture of a

mantle source with the lower crust. Chemical signatures were created by differences in the depth of melting and other possible processes, such as AFC and MASH. These authors determined

Figure 3. (a) Geological map of the area, simplified from Gómez et al. (2015). Geological units: (1) Quaternary deposits; (2) Quaternary volcanoclastic deposits; (3) Quaternary volcanites; (4) Pliocene sedimentites; (5) Pliocene volcanites; (6) Combia Formation; (7) Neogene marine sedimentites; (8) Miocene volcanoclastic deposit; (9) Miocene sub-volcanic bodies; (10) Miocene plutons; (11) El Botón Magmatic Arc; (12) Santa Cecilia La Equis Complex; (13) Paleogene plutons; (14) Oligocene–Miocene marine sedimentites; (15) Oligocene continental sedimentites; (16) Paleocene mafic plutons; (17) Cretaceous sedimentites, volcanites, gabbros, and ultramafic rocks; (18) Upper Cretaceous sedimentites; (19) Upper Cretaceous basalts; (20) Upper Cretaceous gabbros and ultramafic rocks; (21) Upper Cretaceous plutons; (22) Lower Cretaceous sedimentites; (23) Lower Cretaceous mafic rocks; (24) Lower Cretaceous ultramafic rocks; (25) Lower Cretaceous metamorphic rocks; (26) Jurassic plutons; (27) Triassic plutons; (28) Triassic ultramafic rocks; (29) Triassic metamorphic rocks; (30) Permian–Triassic sedimentites; (31) Ordovician plutonic rocks; (32) Stenian–Tonian metamorphic rocks. **(b)** Location of the geological map area.

that Miocene – Pliocene magmatism is associated with an extension–compression regime and that an extensional pull–apart event (12–9 Ma) was followed by convergence (9–6 Ma) that formed calc–alkaline magmas.

3. Petrography and Outcrop Evidence

The CF unconformably overlies the AF. Both units were emplaced and restricted to the Amagá Basin, which, as well as similar basins aligned along the Cauca–Patía River depression, formed as a pull–apart basin due to Oligocene – Miocene Cauca–Romeral Fault System activity (Sierra, 1994).

The CF has generally been divided into a Lower Member, mainly recording volcanic activity, both explosive (pyroclastic–density current and fall–out deposits) and extrusive (lava flows), and an Upper Member, dominated by reworked primary volcanoclastic rocks and secondary volcanoclastics (such as lahars and debris avalanches; Murcia et al., 2013), as described by Grosse (1926), Calle & González (1980; 1982), Ríos & Sierra (2004), and Marín–Cerón et al. (2019). In this review, to obtain a synthesized, petrological understanding of the variety of rocks found in the CF, we have classified them into volcanic, sedimentary, and intrusive lithofacies.

3.1. Volcanic Lithofacies

The magmatic rocks that constitute the CF can be separated into two major groups: (1) Volcanic effusive deposits, which here include La Popala and Río Poblano Dikes, as well as El Sillón Stock, given their geochemical similarity with basaltic, lava flows (Álvarez, 1983; Dunia, 2005; Jaramillo, 1976; Tejada et al., 2007), and (2) pyroclastic density current deposits.

3.1.1. Volcanic Effusive Deposits

Within this group, there are both intrusive and extrusive rock bodies with basaltic and intermediate compositions.

3.1.2. Basaltic Lava Flows

These rocks can be divided according to textural variation into porphyritic, glomeroporphyritic, and vesicular basalts. The for-

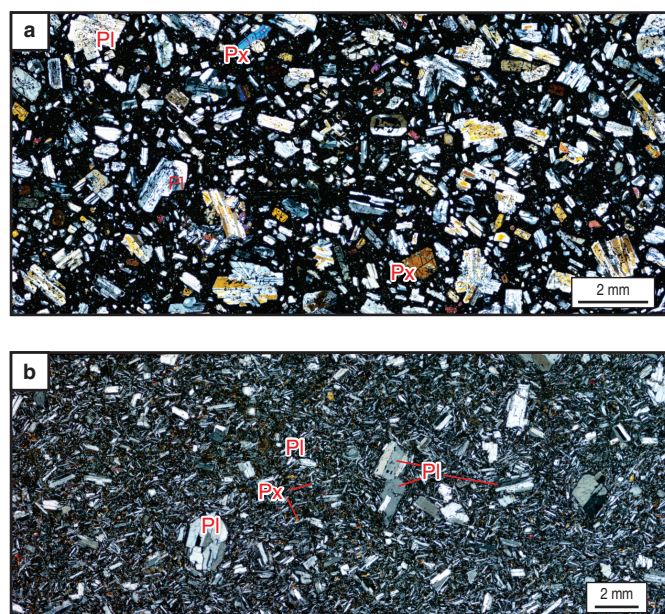


Figure 4. Panoramic microphotographs of porphyritic basalts, under crossed polarized light. **(a)** Large plagioclase (Pl) and pyroxene (Px) phenocrysts in a matrix of plagioclase, pyroxene (orthopyroxene and clinopyroxene), and opaque microliths in glass. Sieve texture is conspicuous in the plagioclase crystals. Sample MJG-011 from Tejada & Betancourt (2006). **(b)** The trachytic texture is shown by basalt with plagioclase phenocrysts in a groundmass of plagioclase and pyroxene microliths. Sample HJ-11 from Mahecha et al. (2006).

mer is also subdivided into three types based on the significant phenocryst phase (i.e., plagioclase, augite, and hypersthene).

Porphyritic basalts: These rocks are characterized by plagioclase and pyroxene phenocrysts in an aphanitic matrix, varying from holocrystalline to hypocrySTALLINE. The matrix is mostly composed of tabular–shaped plagioclase and pyroxene microliths and glass, which are commonly locally altered to palagonite and other clay materials (Figure 4a). In general, a chaotic texture dominates, although a well–defined trachytic–flow texture can be seen (Figure 4b).

Plagioclase is the most common phenocryst in these samples. Crystals are subhedral to euhedral and range in size from approximately 0.5 to 3 mm. Albite and albite–carlsbad twinning are present in the majority of crystals and are normal to oscillato-

ry zonation. In some samples, plagioclase–overgrowth textures, skeletal crystals, and spongy rims are evident (Figure 4a). The microliths vary in size from 0.5 to >0.1 mm and show albite twinning. Augite phenocrysts and microlith crystals are anhedral to subhedral and are commonly associated with abundant disseminated opaque minerals (magnetite), and glass. Normal zonation and twinning are conspicuous, and exsolution and embayment textures are also common. In general, crystals are fractured. Hypersthene crystals are less abundant and are euhedral to subhedral, in some cases with exsolution lamellae and carlsbad twinning. In some examples, coronas composed of augite or other clinopyroxenes surround orthopyroxene. Mineral embayments are evidence of the dissolution of pyroxene–phenocryst phases.

Glomeroporphyritic basalts: These rocks are characterized by plagioclase, augite, and olivine, phenocrystal clusters of 1 to 3 mm, and microphenocrysts that also show this cumulative texture. The matrix comprises plagioclase, pyroxene, olivine microliths, opaques, and glass (Figure 5). The olivine phenocrysts and microliths are subhedral, commonly fractured and altered to iddingsite. In all major minerals, zonation is less common than in the other two classifications.

Vesicular basalts: These rocks are the least common of the basaltic lava flows. They contain abundant vesicles and amygdules of up to 4 mm in diameter. These basalts comprise scarce, plagioclase phenocrysts in a vitreous matrix with microliths of plagioclase and pyroxene (Figure 6). Fractures and vesicles are filled with slightly oxidized zeolites, mainly heulandite, chabazite, mordenite, and philipsite, but celadonite, quartz, and calcite are also present (Gelves et al., 2016).

3.1.2.1. Andesitic Volcanics

Intermediate (andesitic) dikes and flows described by Dunia (2005), Tejada & Betancourt (2006), and Jaramillo et al. (2019) are intercalated within pyroclastic rocks in the CF. These are characterized by a fine-grained matrix with pyroxene and amphibole phenocrysts with intersertal, glomeroporphyritic, and subophitic textures. They show evidence of silicification and contain amygdules filled with zeolites.

Due to their composition, age, stratigraphic position, and field relationships, these rocks could be genetically related to the CSVI.

3.1.3. Pyroclastic Density Current Deposits

Different pyroclastic deposits, which are products of explosive eruptions, have been reported by various authors in several sections within the CF (Calle & González, 1980; Hoyos & Duque–Trujillo, 2017; Ramírez et al., 2006). The most commonly reported explosive products are fall tuffs, followed by pyroclastic density current deposits. The latter are scarce but, when found, constitute an unambiguous indication of for-

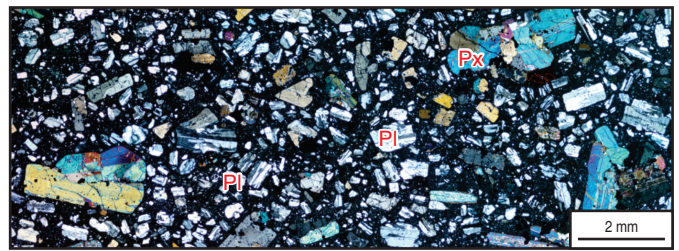


Figure 5. Panoramic microphotograph of a glomeroporphyritic basalt, under crossed polarized light. Sample exhibits seriate porphyritic texture, with phenocrystal clusters of plagioclase (Pl) and augite in a matrix of plagioclase, pyroxene (Px; orthopyroxene and clinopyroxene), opaques, and glass. Sample HJ–180 from Mahecha et al. (2006).

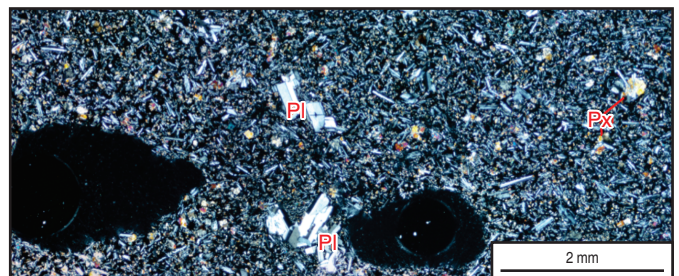


Figure 6. Microphotograph of vesicular basalt, under crossed polarized light. The sample exhibits porphyritic texture, with plagioclase (Pl) phenocrysts in a vitreous matrix with plagioclase and pyroxene (Px; orthopyroxene and clinopyroxene) microliths. Vesicles are two large dark areas, both with air bubbles in the resin. Sample from the Igneous Rocks Collection of Universidad EAFIT, Medellín.

mation by pyroclastic density currents because of its high-welding grade, the vitrophyric texture of the matrix, fiamme texture, vitreous, and pumiceous cognate clasts, columnar jointing, etc.

On the other hand, unequivocally identifying tuffaceous deposits is challenging, particularly where the reworking processes of primary volcanic sequences have been intense. Nevertheless, Hoyos & Duque–Trujillo (2017) reported extended, pyroclastic density current deposits only in the western margin of the Cauca River valley, specifically along the Bolombolo–Concordia section, and small sequences of the same pyroclastic density current deposits in the eastern margin of the Cauca River valley, where the Amagá River discharges into the Cauca River.

These pyroclastic density current deposits are mainly composed of broken plagioclase, pyroxene, and amphibole crystals. Moreover, lithic fragments are also common (mainly basaltic andesites and glass shards). Pumice fragments exhibit eutaxitic and fiamme textures, indicating that these deposits were formed by pyroclastic–flow density currents and were emplaced hot enough to be welded. The matrix of these rocks

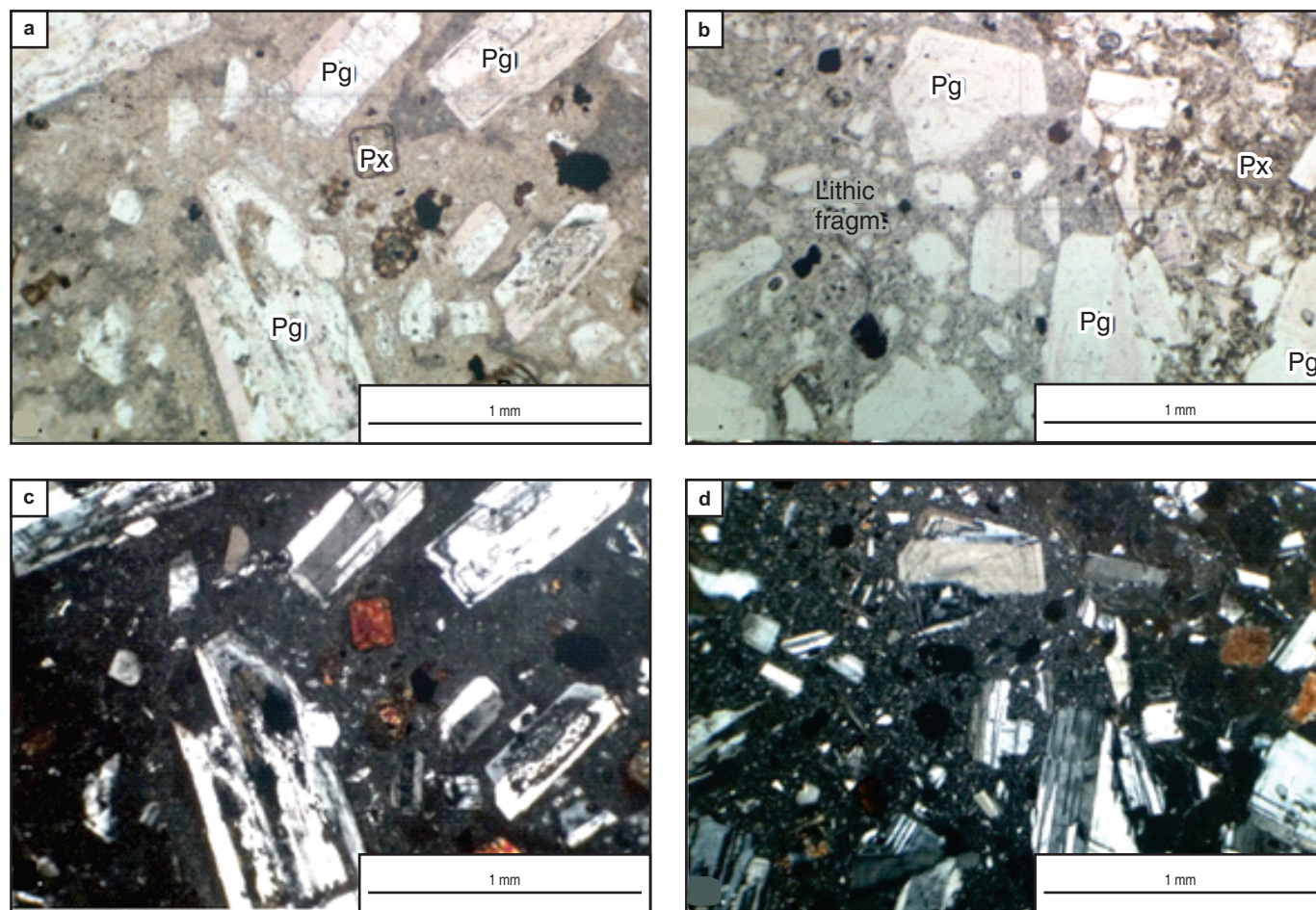


Figure 7. Microphotograph of a welded pyroclastic density current deposit (Sample Conc 03) from the Bolombolo–Concordia section. Note the boundary between lithic fragment and matrix in (b). (a) and (c) parallel polarized light and, (b) and (d) cross-polarized light. (Pg) Plagioclase, (Px) Pyroxene.

is coherent and presents eutaxitic and trachytic textures with microlites of the main-forming minerals and rock fragments. Minerals and rock fragments show the same textures as already described for the lavas and CSVI. Finally, the composition of the welded pyroclastic density current deposits in the CF, combined with the fluidal textures observed in most of the lithic clasts in the samples, is characterized by eruptive pulses, which include parts of the volcanic edifice, possibly domes, and lava flows. Juvenile materials (pumice and glass shards) were also involved during those eruptions and were then flattened (more or less bed oriented), forming a fiamme texture in these deposits (Figure 7).

Several authors (e.g., Calle & González, 1980, 1982; Grosse, 1926; Jaramillo, 1976; Jaramillo et al., 2019; Tejada et al., 2007) have described “agglomerates” as a common constituent of the CF. These have been described as thick layers of block or breccia tuffs with massive structures, including rounded and subspherical fragments, with sizes varying between 1 and 50 cm, with occasional larger blocks (up to 1 m). The included blocks are composed of massive porphyritic basalts,

vesiculated basalts, andesites, garnet-bearing andesites, and other pyroclastic rocks. Most of these fragments show thermal alteration in their boundaries. The matrix is mainly composed of glass, which varies from relatively fresh to palagonite, with plagioclase microlites, pyroxene, hornblende, and olivine. Because the term agglomerate is used for fluidal-shaped, volcanic bombs deposited near a volcanic vent (Németh & Martin, 2007), we suggest using the term lithic-breccia, as suggested by McPhie et al. (1993).

These volcanic, lithic-breccia deposits are interpreted as proximal facies formed from explosion-derived, highly concentrated, pyroclastic density currents (Németh & Martin, 2007), which were involved in the eruptive process of some of the volcanic rocks, volcanoclastic rocks, and porphyritic intrusions related to this volcanism. These lithic-breccia deposits are associated with basaltic lava flows along the Jericó–Puente Iglesias (Tejada & Betancourt, 2006), Jericó–Tarso, and Jericó–Tamesis roads. Jaramillo et al. (2019) reported that these rocks are intercalated with other pyroclastic rocks (primary and secondary) and cut by andesitic dikes in the Fredonia region.

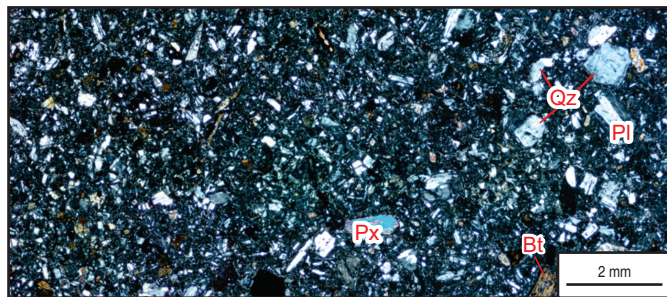


Figure 8. Microphotography of a medium-coarse sandstone, under cross-polarized light. The sample exhibits subangular clasts of plagioclase (Pl), quartz (Qz), pyroxene (Px; orthopyroxene and clinopyroxene), and biotite (Bt). Sample CPG-392 from Ríos & Sierra (2004).

3.2. Sedimentary Lithofacies

These lithofacies contain the non-volcanic, clastic sedimentites of the CF. These sedimentary sequences are composed (in clast-size order) of conglomerates and breccias, fine- to medium-coarse-grained sandstones (Figure 8), and siltstones. The sediment supply of these rocks is derived from the Amagá and Combia (volcanic lithofacies) Formations. Specifically, conglomerates and breccias contain clasts composed of basalt, andesite, and tuff (CF), as well as sandstones (AF; Calle & González, 1980; Grosse, 1926; Ríos & Sierra, 2004).

Ríos & Sierra (2004) synthesized sedimentary sequences into four facies assemblages: (i) fluvial channels, (ii) debris and hyperconcentrated flows, (iii) debris flows intercalated with fluvial channels and alluvial plains, and (iv) pyroclastic flows intercalated with alluvial plains and reworked pyroclastic material. These facies assemblages were obtained from the study of Bolombolo–Peñalisa (140 m thickness) and Guineales–Peñalisa (167 m thickness) surface sections. The Bolombolo–Peñalisa section documents an alluvial-plain deposit interbedded with pyroclastic and debris flows. On the other hand, the Guineales–Peñalisa section shows fluvial channels interbedded with debris and hyperconcentrated flows. Both alluvial plain and fluvial channels are adjacent environments in a fluvial-sedimentary complex. Therefore, based on Ríos & Sierra (2004) report, it is possible to establish that changes in sedimentary facies assemblages in the CF are limited to autocyclic processes. Moreover, the beds formed by pyroclastic and debris-hyperconcentrated flows show short-term interruptions in the fluvial system due to the CF's volcanic activity, thereby promoting the formation of local lacustrine deposits.

3.3. Intrusive Lithofacies (Cauca Shallow Volcanic Intrusions; CSVI)

In general, the middle to late Miocene (ca. 12 to 6 Ma) shallow volcanic intrusions located along the Cauca River valley (north

of ca. 4° N) (Figure 3) are considered a continuous magmatic belt in the northern part of the Western Cordillera with an extension of ca. 100 km (e.g., Álvarez, 1983; Borrero & Toro-Toro, 2016; Leal-Mejía, 2011). The CSVIs are commonly distinguishable in the field due to their positive relief from the sedimentary country rocks (AF and CF) and the Romeral mélange (Cediel *et al.*, 2003).

According to Leal-Mejía (2011), the CSVI can be grouped into four segments according to their geographic location: (1) Quinchía–Dos Quebradas, (2) Marmato–Supia–Orofino, (3) La Quebradona–La Aurora, and (4) Titiribí. Nevertheless, these shallow volcanic bodies can be split into two different groups of shallow volcanic intrusives based on their geomorphological and compositional features: (1) Those that are restricted to the Amagá Basin (Amagá Basin), and (2) those emplaced outside the Amagá Basin along the Cauca River (Cauca River) (Figure 3).

Although some authors have considered that the volcanoclastic sequence of the CF and CSVI may correspond to the same magmatic event (Borrero & Toro-Toro, 2016; Calle & González, 1980; Grosse, 1926; Jaramillo *et al.*, 2019; Leal-Mejía, 2011), there is no agreement as to whether both the Amagá Basin–CSVIs and Cauca River–CSVIs were formed from the same magmatism (Borrero & Toro-Toro, 2016; Leal-Mejía, 2011).

The CSVIs are mostly round-shaped bodies in map view (e.g., La Pintada and Marmato, intruding the Quebradagrande Complex and the Amagá, Irra, and Combia Formations) (Figure 9). These intrusives are mostly andesitic-dacitic in composition, characterized by a seriate, porphyritic texture, in a gray, microlithic-groundmass. Centimetric plagioclase constitutes a typical phenocryst phase in all CSVIs. Furthermore, they have phenocrysts of quartz, amphibole, biotite, and/or occasional garnet as accessory phases. Plagioclase crystals are subhedral, with a tabular habit and oscillatory zonation. Sieve and skeletal textures are also common in the plagioclase (Figure 10a). Hornblende phenocrysts are sometimes zoned and embayed and occasionally show dehydration-reaction rims to secondary amphibole and opaques (Figure 10b). Although uncommon, when present, most garnet crystals are either euhedral phenocrysts or show breakdown rims often surrounded by a plagioclase corona (Figure 10c). Garnet is also commonly present as inclusions in plagioclase and amphibole, indicating early crystallization. Phenocrysts float in an aphanitic to microlithic, pilotaxitic- or fine-granular matrix composed of microliths of plagioclase, amphibole, pyroxene, opaques, and devitrified glass. Textures are porphyritic, microporphidic, and trachytic. Some of these bodies contain xenoliths of the surrounding rocks (basalts and schists).

Characteristic of the the Amagá Basin–CSVIs are intrusions of laccoliths and dikes of different sizes into the sedimentary AF (e.g., Cerro Tusa and Cerro Corcovado; Figure 11). These intrusives are mostly basaltic to andesitic in composition, contrasting with the slightly more differentiated composition of the Cauca River–CSVIs. In general, these intrusives are porphyritic to glom-



Figure 9. Panoramic view of La Pintada Intrusives, part of the Cauca Shallow Volcanic Intrusions (CSV). The Combia Formation (CF) sediments and Amagá Formation (AF) can also be seen. Picture from Mauricio Montoya (<https://www.flickr.com/photos/mauriciomontoya/>). The picture was taken towards the east at 11 km from the CSVI (1200 masl).

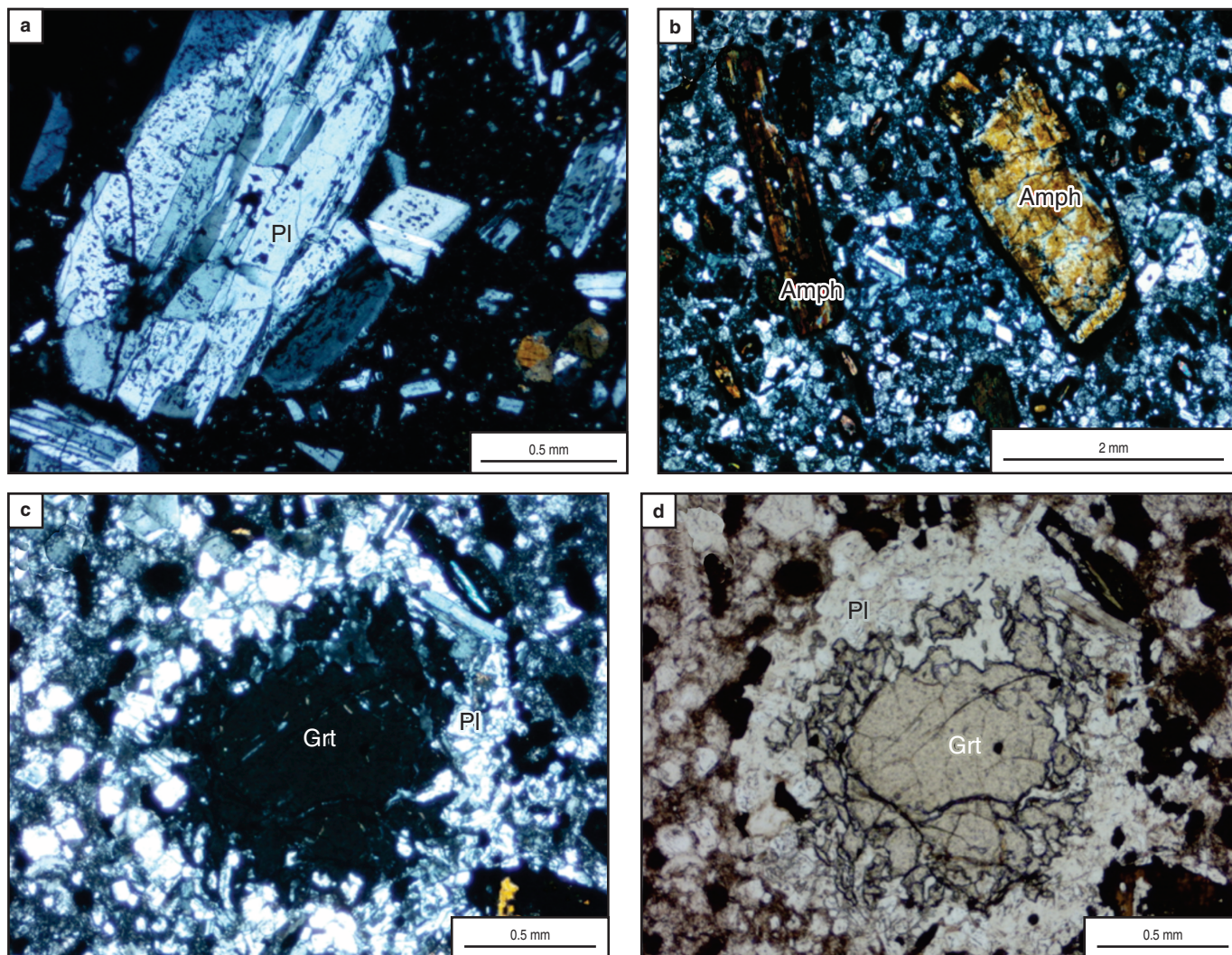


Figure 10. Common petrographic textures from volcanic rocks of the Combia Formation. **(a)** Sieve and skeletal textures in plagioclase (Pl) crystals. Note also the presence of oscillatory zoning on the edges of the crystal. Sample MJG-46-1 from Tejada & Betancourt (2006). **(b)** Dehydration rims around amphibole (Amph). Sample MJG-132 from Tejada & Betancourt (2006). **(c), (d)** Plagioclase (Pl) corona rims around garnet (Grt). Sample MJG-132 from Tejada & Betancourt (2006). Sample under cross polarized light is shown in (c) and under parallel polarized light in (d).

eroporphyritic in texture. Plagioclase is the most common phenocryst, although amphibole is also common. Glomeroporphyritic textures are formed by plagioclase, amphibole, biotite, and olivine. The groundmass consists mainly of plagioclase microliths and amphibole, pyroxene, biotite, and/or olivine in a trachytic texture.

Petrographic evidence, such as sieve and skeletal textures, oscillatory zonation in plagioclase, clinopyroxene coronas over orthopyroxene, and olivine breakdown, indicates that magma mixing, and disequilibrium were common processes in these magmas before being emplaced.

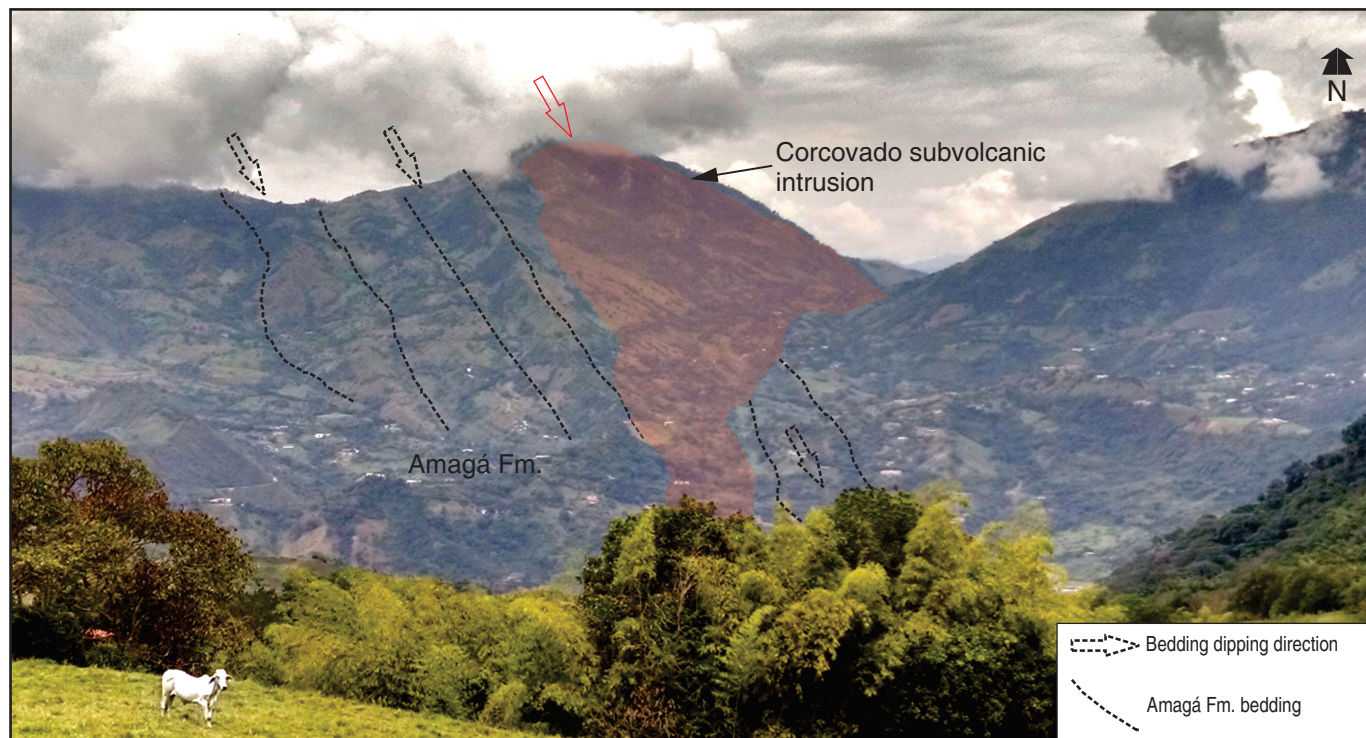


Figure 11. View of the Cerro Corcovado from the south. Notice that the intrusion has the same dipping as the Amagá Formation strata, indicating that it must have intruded as a sill and then was tilted together with the Amagá Formation.

4. Major and Trace Element Geochemistry

A complete dataset (see Table 1 of the Supplementary Information 1) of 202 analyses of the igneous rocks of the CVP has been analyzed (Bernet et al., 2020; Bissig et al., 2017; Borrero & Toro–Toro, 2016; Dunia, 2005; Jaramillo, 1976; Jaramillo et al., 2019; Marriner & Millward, 1984; Tejada et al., 2007). Data from the project “Caracterización Estratigráfica, Petrogenética y Geocronológica de la Formación Combia, Acuerdo Específico No 009–2004 con la Universidad Nacional de Colombia” are also included. For representation, volcanoclastic rocks were excluded, as well as samples with high LOI values (≥ 3 wt%), as these are possibly related to alteration and secondary processes associated with hydrothermal alteration and mineralization (e.g., Leal–Mejía, 2011; Tassinari et al., 2008). Most of the excluded samples are basalts (alteration in these rocks is also evident by abundant zeolite and secondary calcite). Samples from the shoshonitic El Botón and El Morito (Rodríguez & Zapata, 2014; Zapata & Rodríguez, 2011) may represent the first magmatism of modern subduction and are also included in the dataset. In this case, only samples with LOIs higher than 5 wt% were excluded, as determined by Müller et al. (1992) for these rocks. Finally, the geochemistry of the CF and CSVI, as initially determined by Jaramillo (1976), reflects a tholeiitic and calc–alkaline series (Figure 12). Both series are separated by a compositional gap at ca. 58 wt% SiO_2 . It is important to

note that dikes and sills of both series intrude the AF and CF (Bernet et al., 2020; Dunia, 2005; Jaramillo, 1976; Jaramillo et al., 2019; Tejada et al., 2007).

4.1. Tholeiitic Series

This series comprises the lava flows of the CF and some mafic intrusives (e.g., La Popala, Río Poblano, Alto Doraditas, and Cerro Sillón), as well as one sample from Quebrada La Popala. The tholeiitic series is mainly basalts to andesites that conform to a tight compositional cluster, according to the total alkali vs. silica plot of LeMaitre et al. (2002) (Figure 13). SiO_2 ranges from 50.30 to 61.53 wt%, and Al_2O_3 ranges from 12.89 to 19.49 wt%. MgO and FeOt vary from 1.43 to 6.98 wt% and 6.06 to 10.93 wt%, respectively. CaO varies between 4.48 and 12.24 wt%; Na_2O is low, between 1.74 and 4.11 wt%; and K_2O is relatively high, between 0.66 and 2.99 wt% (Figures 12, 14). Most samples cluster in the tholeiitic field of the AFM triangular plot of Miyashiro (1974) and the medium–K to high–K area of the K_2O vs. SiO_2 diagram (Gill, 1981) (Figure 12).

The N–MORB normalized (Sun & McDonough, 1989), multielement diagrams of the tholeiitic series have similar patterns and relative abundances of incompatible elements (Figure 15). Three different groups within the tholeiitic series can be identified under slightly different La/Yb and La/Sm ratios (Figure 14) and the different sizes of element anomalies: Group

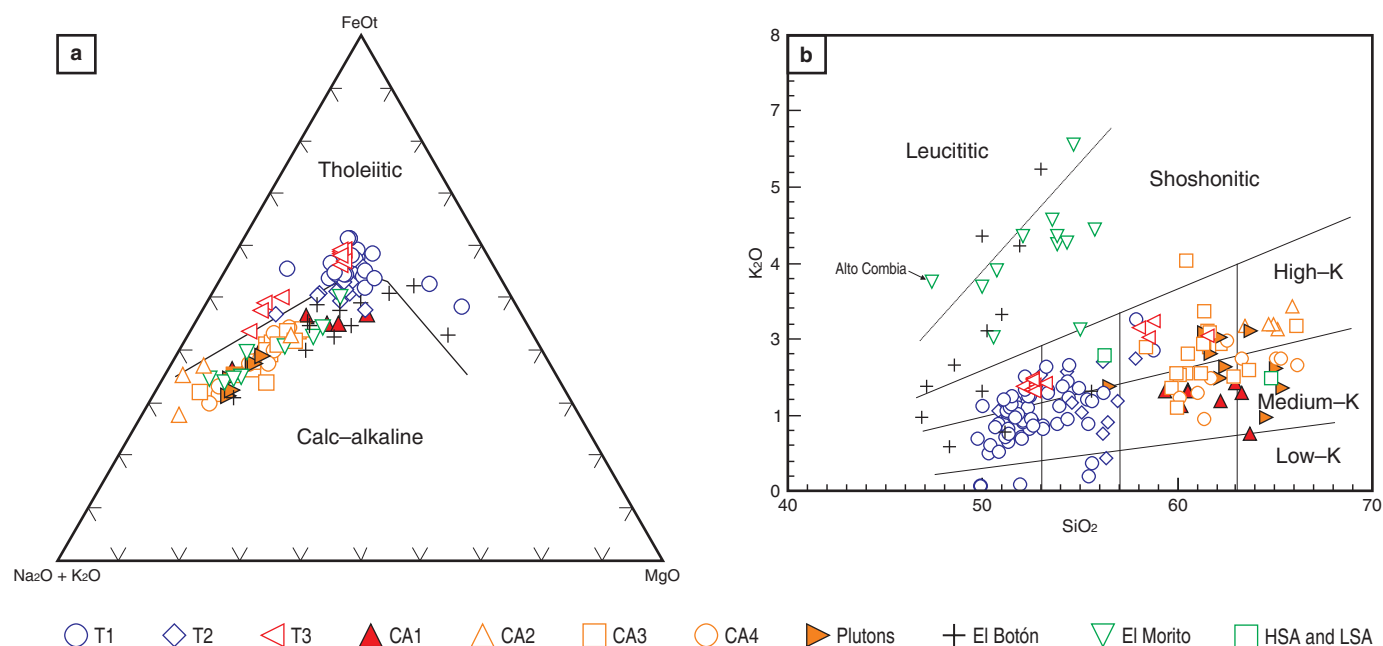


Figure 12. (a) AFM diagram for differentiation of tholeiitic vs. calc-alkaline magma series, after Miyashiro (1974). (b) K_2O vs. SiO_2 diagram distinguishing low-K, medium-K, and high-K series, after Gill (1981). High Silica Adakites (HSA), Low Silica Adakites (LSA) after Martin et al. (2005).

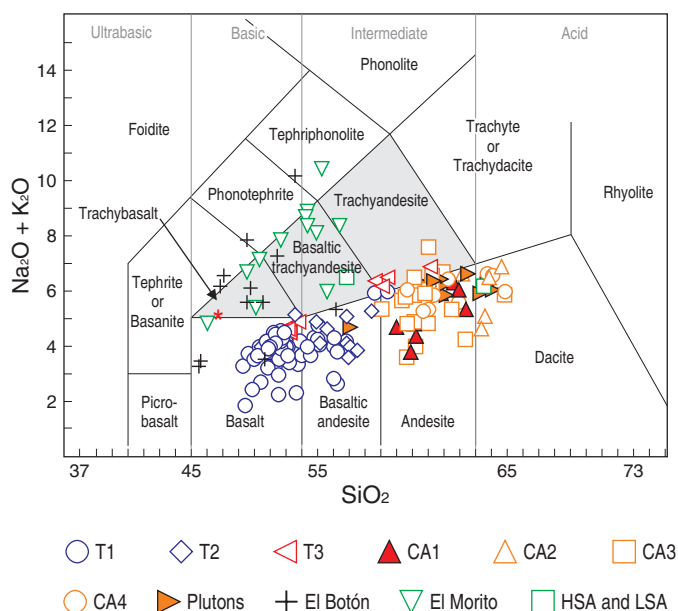


Figure 13. Rock classification diagram after Le Maitre et al. (2002). The Alto Combia sample (Jaramillo, 1976) is highlighted with a red star. Green squares denote High Silica Adakites (HSA), Low Silica Adakites (LSA) after Martin et al. (2005).

T1, Group T2, and Group T3. Overall, the patterns show a negative anomaly for Nb and a slightly less marked anomaly for Ti (Figure 14), all of which have been considered indicative of subduction-related origin for these rocks (Bernet et al., 2020; Dunia, 2005; Jaramillo et al., 2019; Marriner & Millward, 1984;

Tejada et al., 2007). Furthermore, positive Ba and Sr anomalies are also evident (Figure 14). La Popala sample is the most differentiated of the Group T1 rocks, with a parallel REE pattern, indicating crystal fractionation. Nevertheless, variation diagrams define two separate trends for Group T2 and T3 (Figures 14, 16), which suggests that differentiation through crystal fractionation is not the only process involved forming of these rocks. Group T2 overbridges the compositional gap toward the calc-alkaline series. Group T3 includes trachy-andesitic magmas and can be differentiated from other groups based on low Sr/Y and the highest absolute concentrations of Y, Zr, and high FeOt (Figures 14, 15).

REE patterns for the tholeiitic series are relatively flat and somewhat LREE enriched compared to HREEs (Figure 17). Group T1 has a lower La/Yb ratio than the other groups. Some samples show a slight positive Eu anomaly, possibly due to plagioclase as a phenocryst phase.

4.2. Calc-Alkaline Series

The calc-alkaline series comprises mainly andesites and dacites of the CSVI. Nevertheless, samples from El Poma and Tesorito localities are also integrated into the dataset (Bisig et al., 2017; Dunia, 2005). The two associated coetaneous plutonic units, the Farallones Batholith and the Tamesis Stock, are also shown (Dunia, 2005). The calc-alkaline series shows a better-defined trend in the variation diagrams than the tholeiitic series. SiO_2 content varies from 54.97 wt% (basaltic andesites) to 66.13 wt% (dacites) (Figure 14). The MgO

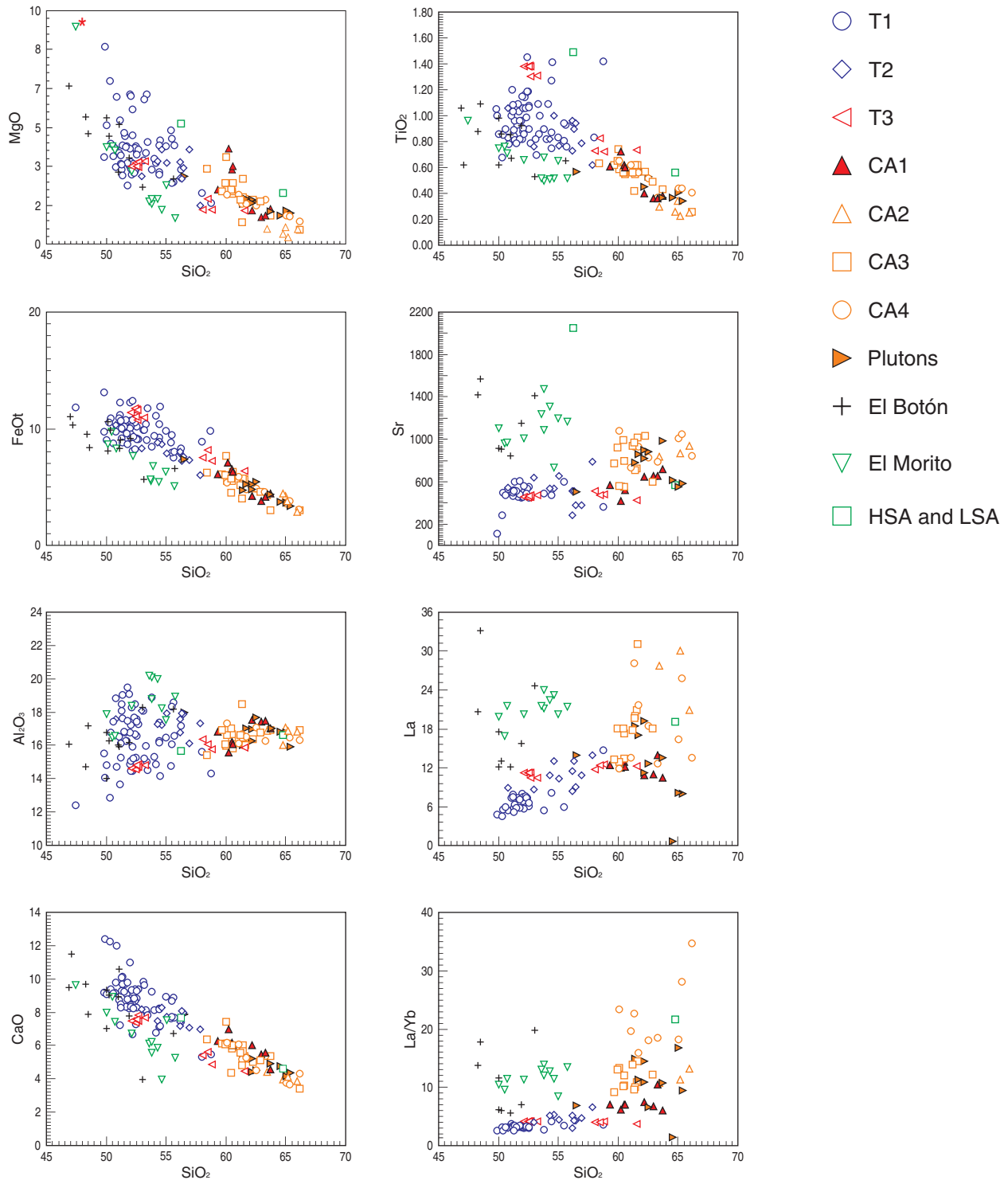


Figure 14. Harker variation diagrams of selected major and trace elements for the Combia Volcanic Province lavas. The Alto Combia sample (Jaramillo, 1976) is highlighted with a red star. High Silica Adakites (HSA), Low Silica Adakites (LSA) after Martin et al. (2005).

content ranges from 0.31 to 4.09 wt%; Al_2O_3 content ranges from 15.56 to 18.50 wt%; and K_2O contents ranges from 0.62 to 4.04 wt% (Figure 12). Samples follow the calc-alkaline field trend (Figure 12) and the medium-K to high-K area of

the K_2O vs. SiO_2 diagram, and therefore, some are high-K calc-alkaline rocks. Garnet-bearing samples of Tejada et al. (2007) and Bissig et al. (2017) are included here, as these samples plot in the calc-alkaline field.

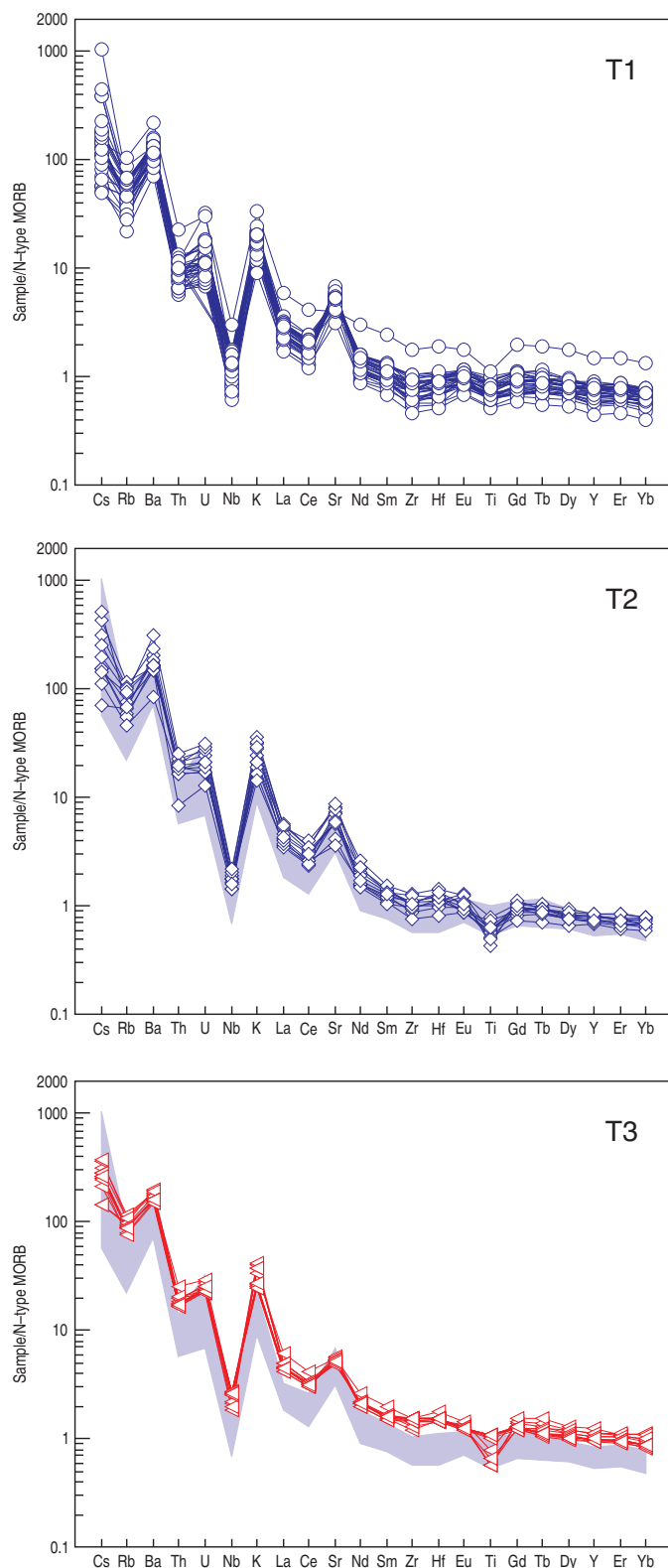


Figure 15. N-MORB-normalized trace-element patterns for the tholeiitic series of the Combia Volcanic Province. Normalization values from Taylor & McLennan (1985). Symbols as in Figure 12.

The N-MORB (Sun & McDonough, 1989) multielement diagrams are more differentiated (Figure 18), and the La/Yb

ratios are higher than those of the tholeiitic samples. Sr and Y content ranges from 374 to 1200 ppm and 5.6 to 27.3 ppm, respectively (Figure 14). Additionally, the negative Nb and Ti and positive K and Sr anomalies are more evident, and there is a positive Hf anomaly in some samples.

REE patterns are more variable than those of the tholeiitic series (Figure 19). Samples were divided into several calc-alkaline groups: Group CA1 (includes garnet-bearing samples) has the lowest La/Yb of the calc-alkaline suite, Group CA2, and CA3 have an intermediate La/Yb, and Group CA4 has the highest La/Yb values of the series. Overall, these samples show a spoon-shaped pattern (Figure 19), indicating that amphibole was significant in magma formation and evolution processes. This is particularly evident in Group CA2.

In general, the Farallones Batholith and Tamesis Stock (Dunja, 2005) have similar compositions when compared to the calc-alkaline series, and variations within these rocks overlap the variations shown by the CSVI. Therefore, a similar petrogenetic origin is likely. Unfortunately, due to the nature of these rocks, no cross-cutting or field relationship has been reported to support this observation.

Some characteristics of the calc-alkaline series are typical of adakites (Figures 12, 20). These characteristics include: $\text{SiO}_2 > 56 \text{ wt\%}$, $\text{Al}_2\text{O}_3 > 15 \text{ wt\%}$, MgO generally $< 3 \text{ wt\%}$, low Y ($< 15 \text{ ppm}$), and HREE relative to the island arc ADR, high Sr $> 400 \text{ ppm}$, $\text{Na}_2\text{O} > 3.5 \text{ wt\%}$, $\text{K}_2\text{O}/\text{Na}_2\text{O}$ approximately 0.4, and low $^{87}\text{Sr}/^{86}\text{Sr}$ ratios (ca. 0.7040) (Castillo, 2012; Defant & Drummond, 1990; Martin et al., 2005). Therefore, these rocks can be classified as adakites (e.g., Borrero & Toro-Toro, 2016). They also plot within the compositional field of High Silica Adakites, as proposed by Martin et al. (2005) (Figure 20b). Nevertheless, La/Yb is relatively low for most of the Group CA1 (garnet-bearing) compared to the typical adakite signatures. Possible differences may be due to the presence of garnet, which would lower this ratio, as will be discussed further in the text.

4.3. Shoshonite Series

Eleven samples, mainly trachybasalts and trachyandesite, define this series (Figure 12). They comprise El Morito basaltic andesites and the Alto Combia absarokite, mirroring El Botón basalts of Zapata & Rodríguez (2011). SiO_2 for these rocks ranges between 55.78 and 50 wt%, MgO between 1.12 and 4.18 wt%, and Al_2O_3 between 16.48 and 20.02 wt%. These rocks have high alkalis, with K_2O ranging from 2.7 for the more mafic rocks to 6.08 wt% for the more felsic rocks (Figure 12). The N-MORB (Sun & McDonough, 1989) multielement diagrams are more differentiated (Figure 21), and the La/Yb ratios are higher. The Sr and Y contents range from 374 to 1200 ppm, and 5.6 to 27.3, respectively (Figure 14). Additionally, they show negative Nb and Ti and positive K and Sr anomalies.

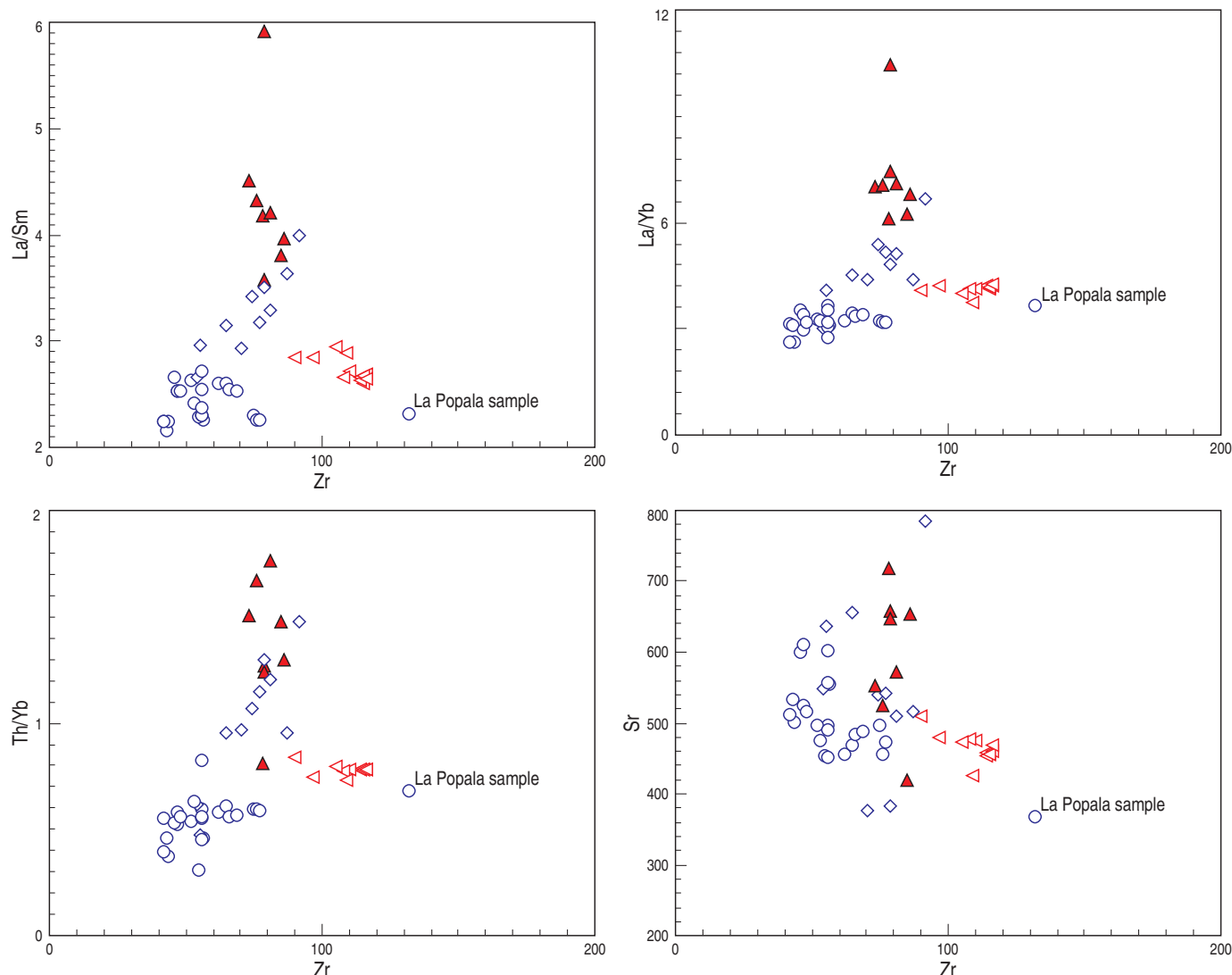


Figure 16. Harker variation diagrams of selected trace elements and ratios vs. Zr for the tholeiitic series of the Combia Volcanic Province. Samples of Group CA1, which includes garnet-bearing samples, of the calc-alkaline series also shown. Symbols as in Figure 12.

4.4. Isotope Data

Present-day $^{87}\text{Sr}/^{86}\text{Sr}$ ratios versus $^{143}\text{Nd}/^{144}\text{Nd}$ isotope values of published (Bernet et al., 2020; Jaramillo et al., 2019; Leal-Mejía, 2011; Ordóñez-Carmona, 2001; Tassinari et al., 2008) and unpublished samples are presented in Figure 22 (see Table 2 of the Supplementary Information 1). The CF and CSVI define a tight sub-linear array, which generally extends from 0.70378 to 0.70533 and 0.512906 to 0.512612, although some outliers are present. Most of the data fall within the mantle array. In general, the data spread towards the lower crust or sediment fields. Most Group T1 and T3 samples cluster at ca. $^{87}\text{Sr}/^{86}\text{Sr}$ 0.79390 and $^{143}\text{Nd}/^{144}\text{Nd}$ at 0.52195, and calc-alkaline samples are slightly more enriched. Some samples, including the garnet-bearing rocks, tend toward lower Sm–Nd and higher Rb–Sr

isotope ratios, indicating either variable sedimentary input or assimilation of older basement rocks.

Pb–isotope analysis from the CVP, Farallones Batholith, and Támesis Stock (data from Bernet et al., 2020; Leal-Mejía, 2011; Tassinari et al., 2008) shows isotopic ratios of $^{206}\text{Pb}/^{204}\text{Pb}$, $^{208}\text{Pb}/^{204}\text{Pb}$, and $^{207}\text{Pb}/^{204}\text{Pb}$ ranging from 18.91 to 19.22, 38.59 to 38.93, and 15.56 to 15.68, respectively (Figure 23). In general, samples show a linear trend that falls within the Northern Volcanic Zone (Compilation by Marín-Cerón et al., 2019). Although the lead-isotope signatures of two CF samples and the Farallones Batholith and the Támesis Stock (Leal-Mejía, 2011) are in the same linear trend as the CF samples, they are more radiogenic. The data generally plot between the altered oceanic crust, Pacific sediments, and the Cretaceous basement, suggesting crust mantle contamination and assimilation.

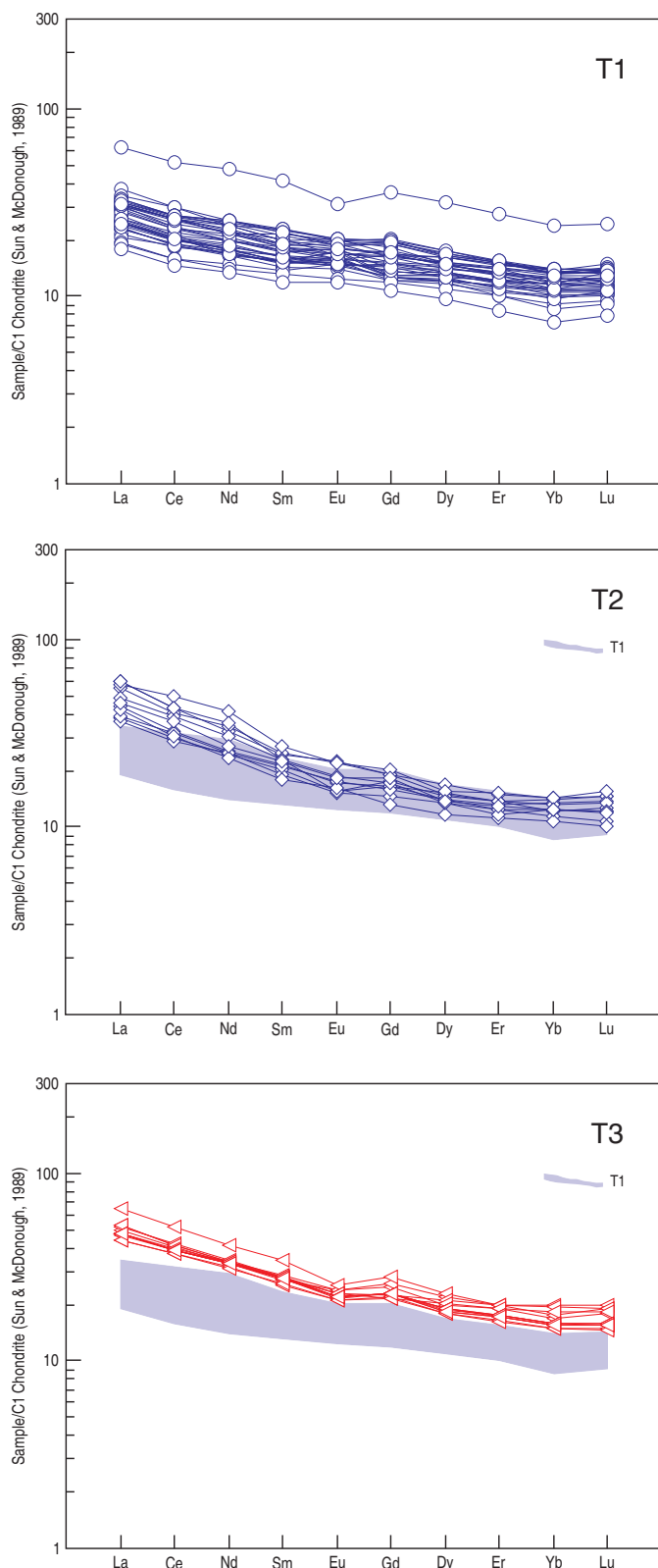


Figure 17. Figure REE patterns normalized to chondrite for the tholeiitic series of the Combia Volcanic Province. Normalization values from Sun & MacDonough (1974). Group T1 tholeiitic lavas are shown for comparison. Symbols as in Figure 12.

5. Geochronology

Recently, Rodríguez & Zapata (2014) proposed to split the middle Miocene magmatism into two different magmatic arcs with different ages and geographical locations: An earlier shoshonitic El Botón arc and a later tholeiitic and calc-alkaline arc of the CF, including CSVI magmas.

El Botón magmatic arc constitutes a series of magmatic products, all of them emplaced on accreted rocks with oceanic affinity from the Western Cordillera and Cauca River basin, including rocks from the Amagá Basin, the Cañasgordas Block, and Romeral suture zone. These magmas have geochemical characteristics of shoshonitic affinity and ages ranging between 12.5 and 9 Ma (Rodríguez & Zapata, 2014). Moreover, Zapata & Rodríguez (2013) define El Botón magmatic arc based on magmatic units such as: El Morito basaltic andesites and El Cangrejo latibasalt (9.1 ± 0.7 Ma in Restrepo et al., 1981a), Cerro Frontino gabbro (10.17 ± 0.41 Ma in Zapata & Rodríguez, 2013), and El Botón basalts (10.55 ± 0.28 Ma, in Zapata & Rodríguez, 2011).

The CF, constituted by volcanic and subvolcanic products, has a tholeiitic to calc-alkaline affinity and is younger than the shoshonitic El Botón Magmatic Arc (Figure 2), as shown by their radiometric ages with an age span between 9 and 6 Ma (Jaramillo et al., 2019; Rodríguez & Zapata, 2014). Nevertheless, it is common to find inherited zircons between 12 and 11 Ma in CF magmatic rocks (cf. Bernet et al., 2020; Hoyos et al., submitted; Jaramillo et al., 2019). These rocks probably originally crystallized in magmas coeval with El Botón and El Morito units.

Analyzing the distribution of different ages obtained over middle Miocene volcanic products in Colombia, a general pattern of younging to the east is evident (Figure 24; see Table 1 of the Supplementary Information 2). Middle Miocene magmatism in Colombia began in the northernmost part of the Western Cordillera with the intrusion of several mostly basic magmas between 17 and 10 Ma. After 10 Ma, this magmatism migrated to the Cauca valley, and no more magmatism is registered in the Western Cordillera after that (Figure 24; see Table 1 of the Supplementary Information 2). Gabbroic intrusions represent early magmatism as Cerro Frontino and basaltic flows as the Santa Cecilia, La Equis, and El Botón. After ca. 10 Ma, the magmatism migrated and was established on the northern segment of the Cauca valley, specifically in the Amagá Basin, represented by several shallow volcanic intrusions and some lava flows (e.g., El Cangrejo latibasalt). South of the Amagá Basin, in the middle Cauca valley, there is another critical intrusion cluster, La Colosa (Leal-Mejía, 2011), constituted by a series of dioritic porphyries and granodioritic intrusions.

Along with the basic magmatism in western Colombia, volumetrically important magmatism with ages ranging between ca.

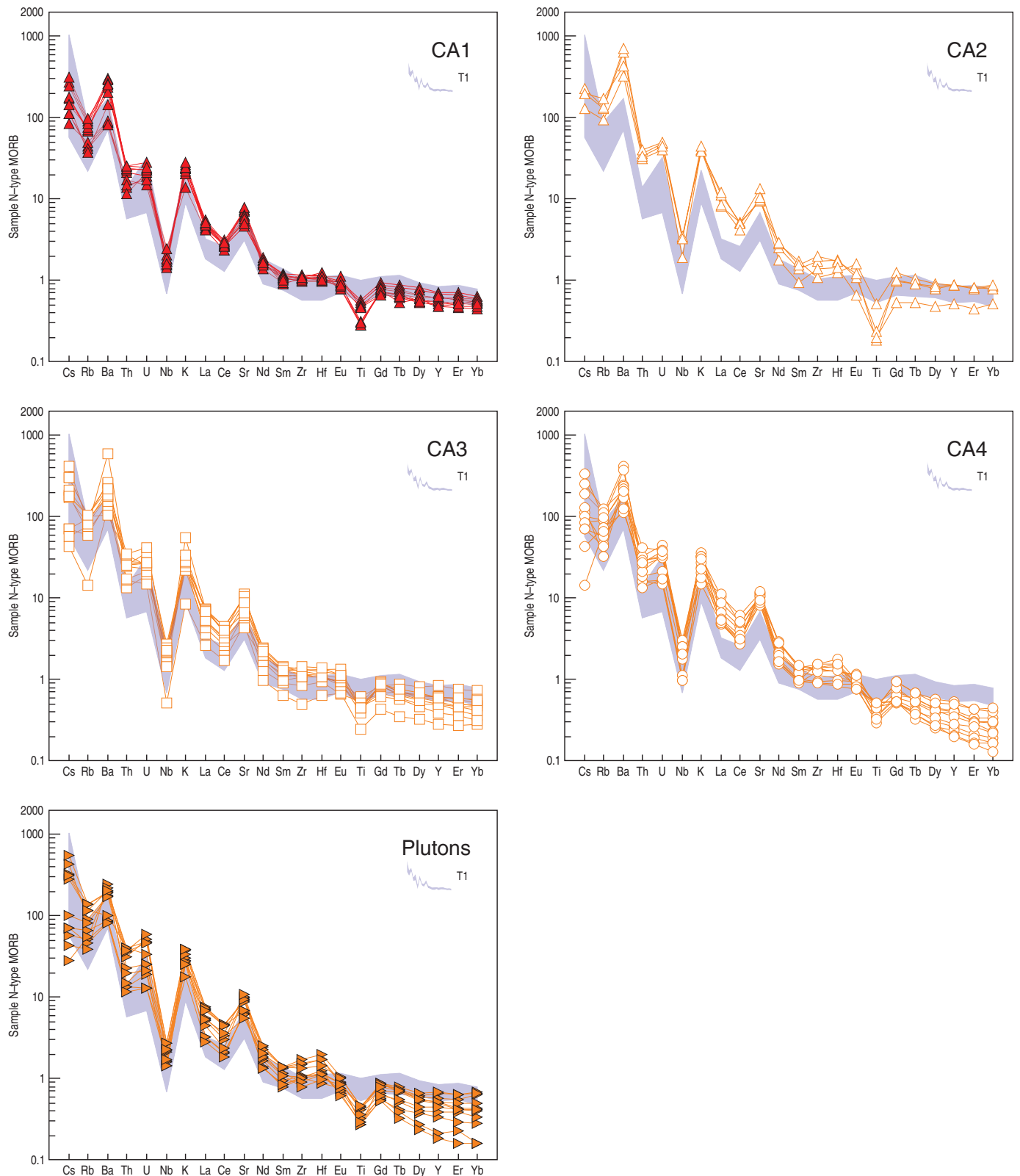


Figure 18. N-MORB-normalized trace-element patterns for the calc-alkaline series of the Combia Volcanic Province. Normalization values from Taylor & McLennan (1985). Symbols as in Figure 12. Group T1 tholeiitic lavas are shown for comparison. Plutonic rocks are plotted separately.

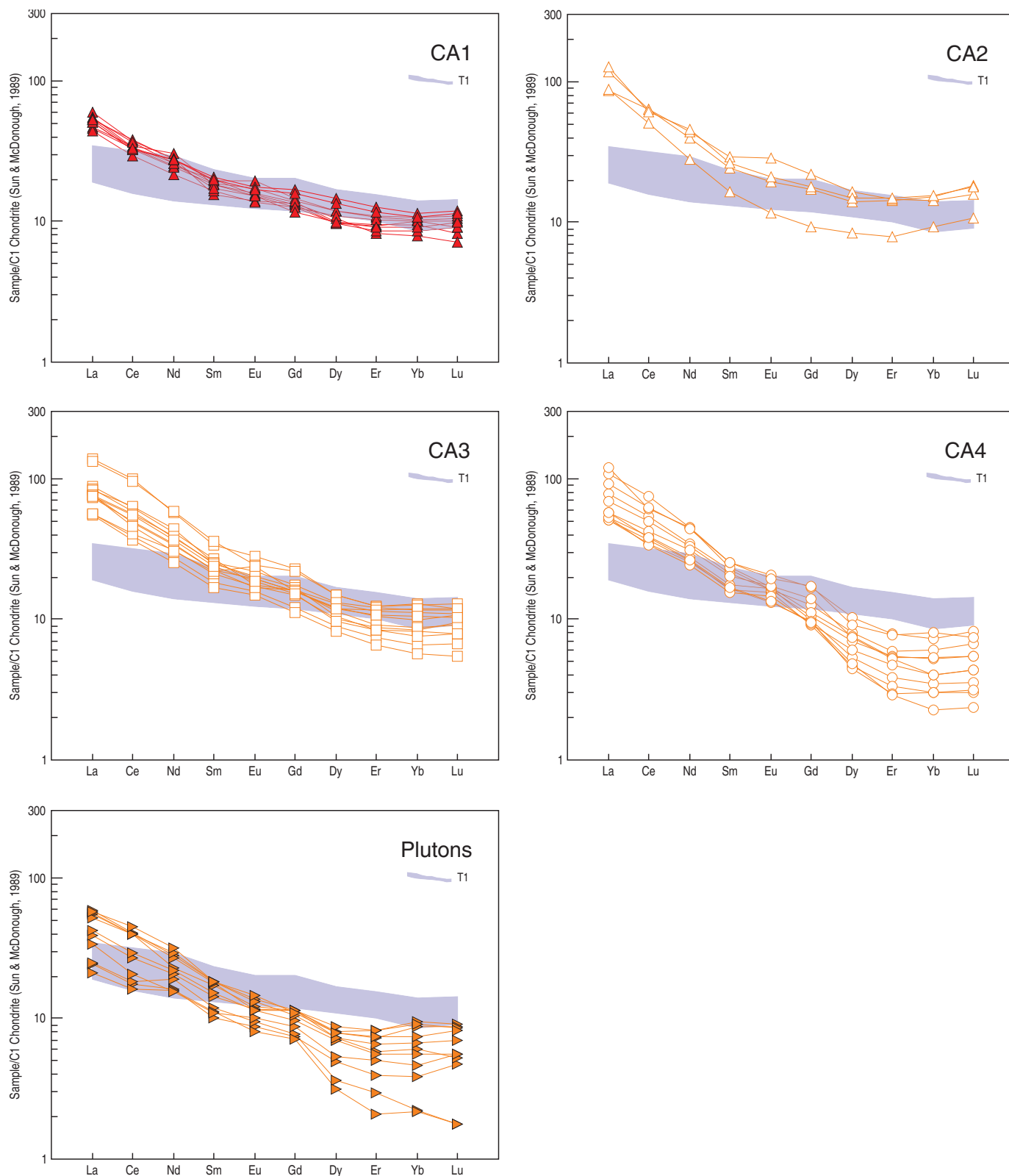


Figure 19. Figure REE patterns normalized to chondrite for the calc-alkaline series of the Combia Volcanic Province. Normalization values from Sun & MacDonough (1974). Symbols as in Figure 12. Group T1 tholeiitic lavas are shown for comparison. Plutonic rocks are plotted separately.

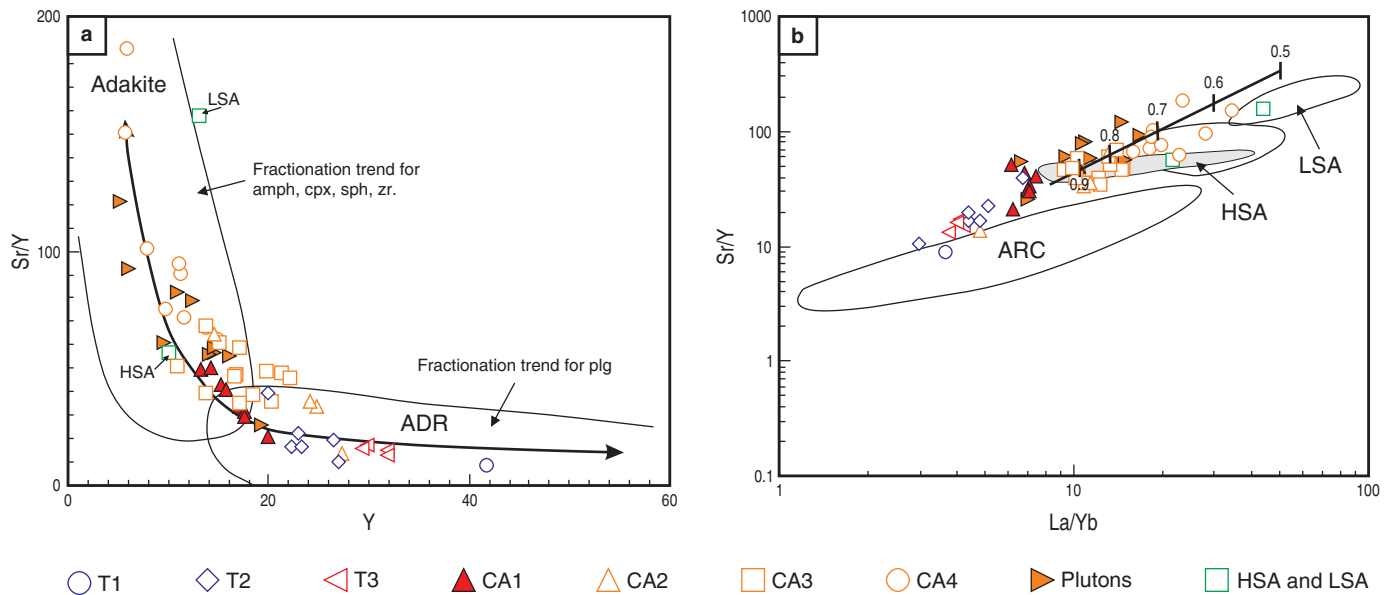


Figure 20. Diagrams showing adakite definitions. Only lavas with $\text{SiO}_2 > 56$ are plotted. **(a)** Diagram showing Sr/Y vs. Y distribution between adakites and “normal” arc andesite, dacite, and rhyolite (ADR) lavas (modified after Drummond & Defand, 1990; Richards & Kerrich, 2007). The fractionation trend for various minerals is also shown (after Richards & Kerrich, 2007). **(b)** Sr/Y vs. La/Yb diagram with fields for High Silica Adakites (HSA), Low Silica Adakites (LSA), and “ordinary” arc magmas (ARC) after Martin et al. (2005). Also shown the calculated fractional crystallization trend of garnet and amphibole as the main fractionating phases (see text for details).

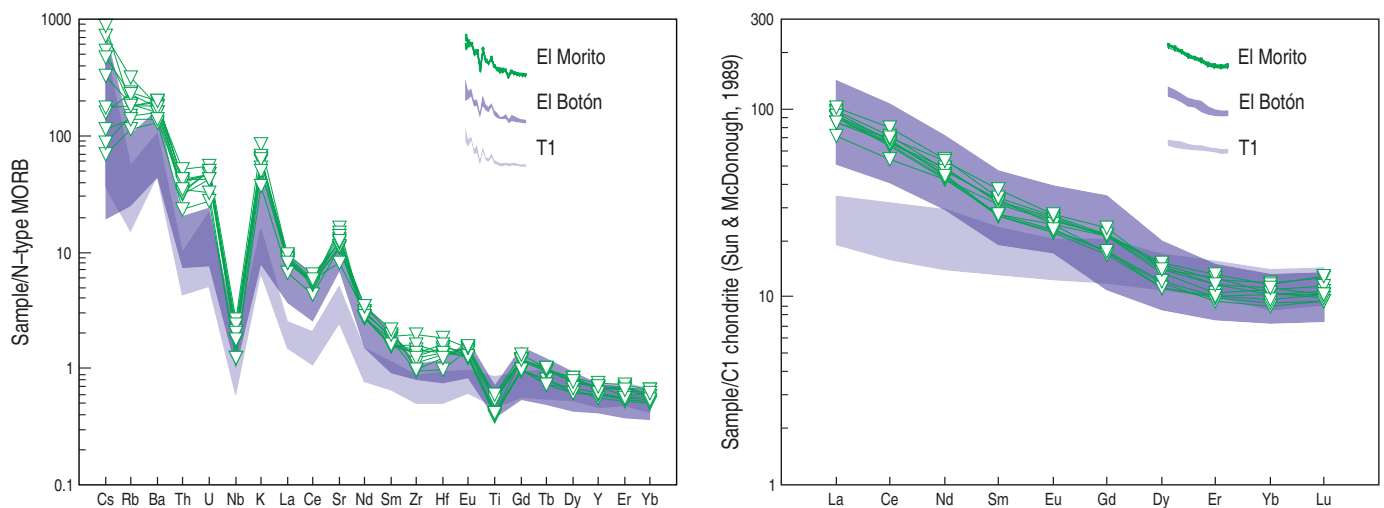


Figure 21. N-MORB-normalized trace-element patterns and REE patterns normalized to chondrite for the shoshonitic series of the Combia Volcanic Province (El Morito lavas). Normalization values from Taylor & McLennan (1985) and Sun & MacDonough (1974). Symbols as in Figure 12. Shown for comparison are El Botón lavas (Zapata & Rodríguez, 2011) and T1 tholeiitic lavas.

12 and 6 Ma (Figure 24) had occurred. Younger ages between 6 and 4 Ma (Figure 24; see Table 1 of the Supplementary Information 2) would represent cooling ages of ca. 6 Ma intrusions and associated hydrothermal activity, not intrusion or formation ages. Middle Miocene intermediate magmatism in western Colombia began between ca. 14 and 12 Ma with a widespread magmatism affecting both the Western Cordillera and the Cauca valley (on both southern and northern segments). Nevertheless, this magmatism was especially intense in the northern part of

the Cauca valley and mainly concentrated along the Cauca Fault, which possibly served as a magma emplacement conduit (Figure 24). $^{40}\text{Ar}/^{39}\text{Ar}$ determined ages for these shallow volcanic intrusives lie within this range (Figure 24). Cerro Tusa, one of the most outstanding vestiges of this magmatism, and considered a volcanic plug (Calle & Gonzalez, 1980; Grosse, 1926), yields a reliable $^{40}\text{Ar}/^{39}\text{Ar}$ in hornblende age of 7.93 ± 0.14 Ma (Figure 25a). Garnet-bearing shallow volcanic intrusive porphyries, north of Jericó, yield two $^{40}\text{Ar}/^{39}\text{Ar}$ ages in hornblende of ca. 8.8

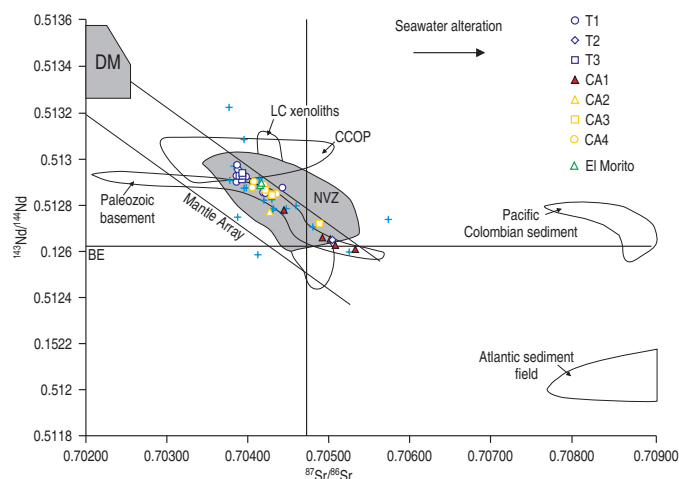


Figure 22. $^{143}\text{Nd}/^{144}\text{Nd}$ vs. $^{87}\text{Sr}/^{86}\text{Sr}$ diagram. Comparison of the CF and CSVI rock data with the Northern Volcanic Zone. Northern Volcanic Zone (NVZ) data from James & Murcia (1984), Francis et al. (1977), Hawkesworth et al. (1979), Barragan et al. (1998), Bourdon et al. (2002), Errázuriz-Henao et al. (2019); Caribbean-Colombian oceanic plateau (CCOP) data from Kerr et al. (1996, 1997); Pacific Colombian Sediment from Errázuriz-Henao et al. (2019), Atlantic Sediment Field taken from data compilation plot from Errázuriz-Henao et al. (2019), Lower Crustal (LC) xenoliths from Weber et al. (2002). Main oceanic mantle reservoirs after Zindler and Hart (1986): Depleted Mantle (DM), and Bulk Silicate Earth (BE).

Ma (Figure 25b, 25c). These ages overlap the explosive volcanic deposits associated with the CF.

Different pyroclastic density current units, exposed near the Amagá River (Figure 25d) and along the Morro Plancho, Concordia (Figure 25e, 25f), were dated and presented here, all yielding the same age, ca. 8.5 Ma. Samples were obtained from outcrops with altitudinal differences of ca. 1000 m. The Morro Plancho sequence is located at ca. 1500 masl, whereas the Amagá River sequence is located at ca. 500 masl. Because these two sequences yield the same age and have identical petrographic characteristics, we interpret them as part of the same deposit or at least formed by subsequent eruptions. Transtensional displacements could explain the outcrop positions along NW–SE to N–S faults. The ages obtained for the explosive deposits are concordant with previously published ages for the CSVI surrounding the Amagá Basin area (Figure 24). Jaramillo et al. (2019) report an age of ca. 8.3 Ma for the overlying pyroclastic sequence, including lithic breccia deposits, the same as that reported on the other side of the Amagá Basin between Jericó, Támesis, and Jardín. Based on the ages reported here for the pyroclastic density current units, we suggest that these ages could be genetically linked with lithic breccia deposits.

The Irra Formation correlates by lithology, time, and space with the CF. This formation, deposited to the south of the CF, within the Cauca River valley, is a succession of interbedded polymictic conglomerates and reworked pyroclastic material

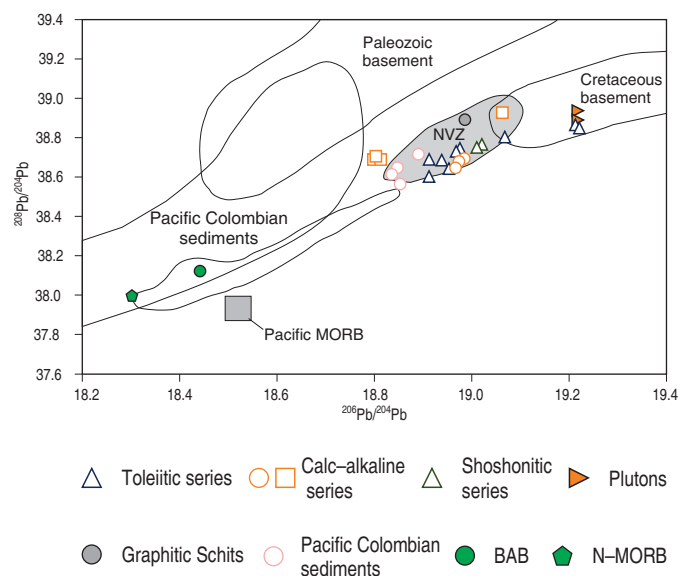


Figure 23. $^{208}\text{Pb}/^{204}\text{Pb}$ vs. $^{206}\text{Pb}/^{204}\text{Pb}$ diagram showing the Pb isotopic composition for samples of the Combia Volcanic Province. Data from Tassinari et al. (2008), Leal-Mejía (2011), and Bernet et al. (2020), in comparison with potential inputs (plot modified from data compilation plot from Marín-Cerón et al., 2010, 2019). NVZ: Northern Volcanic Zone. Colombian Pacific sediments data from Errázuriz-Henao et al. (2019), mean N-MORB and BAB from Gale et al. (2013).

packages (Sierra, 1994). The age of the pyroclastic deposits, late Miocene (6.3 ± 0.2 Ma fission tracks in zircon; Toro et al., 1999), overlaps with those obtained for some subvolcanic intrusives emplaced along the Cauca River depression (e.g., Irra porphyry; Támesis Stock, Marmato porphyry, La Felisa Stock). Considering that (i) the mentioned pyroclastic deposits are coeval with corresponding magmatic intrusives in each area, and (ii) the Cauca River depression and the Amagá Basin intrusives correspond to the same continuous magmatism, which affected the Western Cordillera, we propose that the volcano-sedimentary member of the CF and at least the upper members (A and B) of the Irra Formation represent a coeval singular geological event that is recorded in adjacent extensional basins.

6. Garnet-Bearing Samples

Garnet-bearing porphyritic rocks in the Neogene middle Cauca valley were first reported from the Chinchiná and Palestina areas (García, 1983). Later, garnets were described from two localities in the Jericó area (Dunia, 2005; Tejada & Betancourt, 2006; Tejada et al., 2007) and Tesorito and El Poma in the Colombian Middle Cauca Metallogenic Belt (Bissig et al., 2017). The composition is variable and will be detailed elsewhere (Hoyos et al., submitted). Zircon U–Pb and new $^{40}\text{Ar}/^{39}\text{Ar}$ ages (Figure 25a–c) for garnet-bearing porphyritic

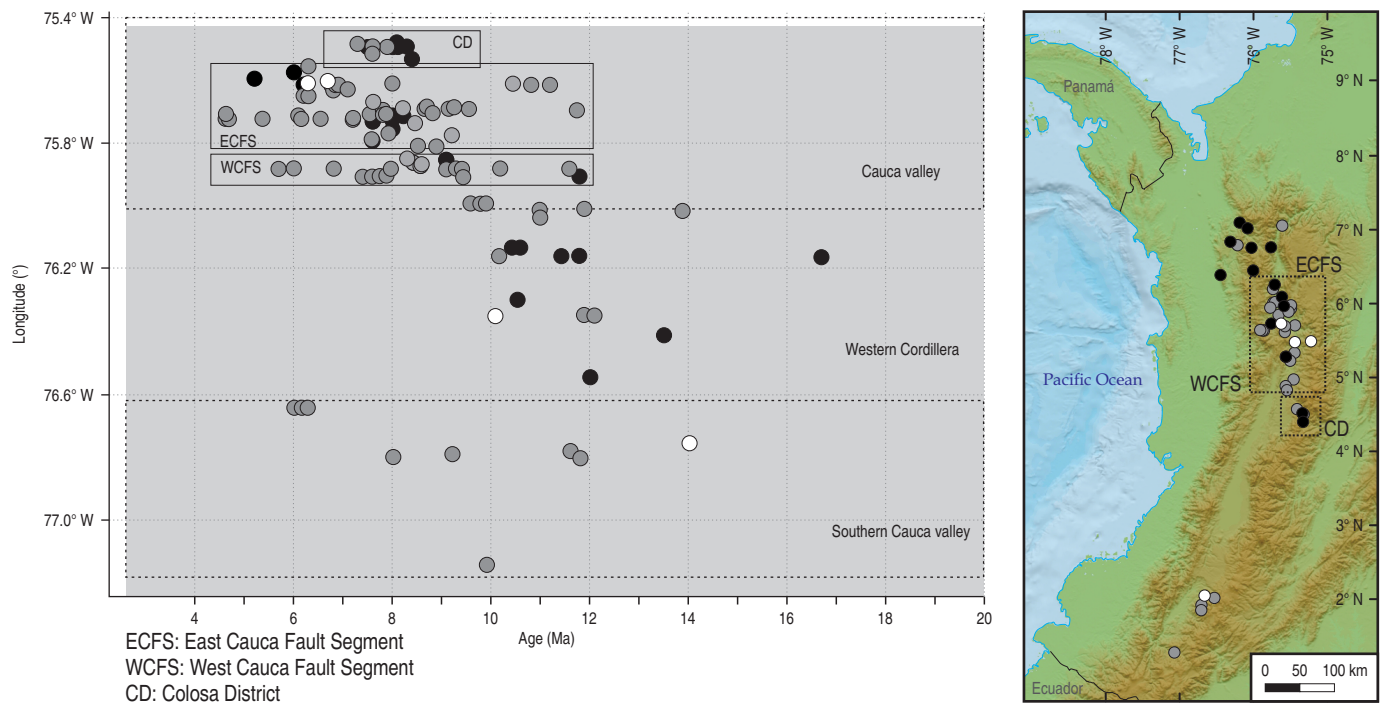


Figure 24. Age distribution of the Miocene intrusive, subvolcanic, and volcanic rocks from western Colombia, including the Combia Formation magmatic rocks. **(a)** Age (Ma) versus Longitude (°). **(b)** Geographic distribution of compiled analyses. Colour in symbols varies with rock composition: Basic rocks (black), intermediate rocks (gray), differentiated rocks (white). Plotted samples correspond to Table 1 of the Supplementary Information 2.

ic rocks indicate that these rocks formed at ca. 12 Ma in El Poma location and at ca. 9 Ma in El Tesorito and Jericó locations during the early stages of magmatic activity in the Cauca valley. The Jericó $^{40}\text{Ar}/^{39}\text{Ar}$ ages possibly represent cooling ages, and therefore magmatic crystallization ages are likely to be slightly older. Nevertheless, these magmas crystallize at shallow crustal levels, and thus cooling was fast, and the differences in both ages are small.

To constrain the significance of these rocks within the CF, we present the mineral chemistry of two garnet-bearing samples (MJG-132 and MJG-134) from the Jericó area and one andesite sample from Cerro Tusa (MW-1) (Figure 26). The analyzed minerals were garnet, plagioclase, amphibole phenocrysts, and microlith matrix phases (see Tables 1, 2, 3 of the Supplementary Information 3).

6.1. Garnet

Garnet is mainly almandine, characterized by XFe compositions ranging from 0.54 to 0.61, XMg compositions ranging from 0.14 to 0.20, and XCa from 0.16 to 0.23 (Figure 26a–c). Generally, garnet crystals show a darker pink core and a colorless rim. Furthermore, there is a compositional break in larger garnets, with garnet compositions being more Ca-rich in the centers (e.g., garnet in sample MJG-134 varies in terms of XCa content, from approximately 0.66 to 0.58, and

XMg from approximately 0.44 to 0.45), and more Mn and Mg enriched at the rims. Consequently, at least two garnet generations are preserved (core Grt 1 and rim Grt 2) (Figure 26). The presence of Mn–Mg-enriched and Ca-depleted overgrowth garnets indicates an abrupt change in crystallization conditions during their formation within the magma. Depleted Ca garnets would represent the second generation (Grt 2), which in turn shows a slight Ca increase towards the outermost rim (Figure 26c).

Three scenarios could explain these zonation profiles: (1) Post-formation diffusion at garnet rims under the growth of a new crystallization phase within the magma (e.g., plagioclase coronas around garnet are common, and zonation could therefore suggest Ca depletion due to Ca–plagioclase formation). Nevertheless, the slight increase in Ca from the inner Grt 2 to the outermost rim precludes this possibility. Furthermore, plagioclase coronas are common in similar porphyritic garnet-bearing rocks, where zonation profiles are flat (e.g., Bissig *et al.*, 2017). (2) Changes in physicochemical conditions of the magma after the crystallization of Grt 1. This could happen because of the introduction of a different liquid component (magma mixing or fluid introduction), assimilation of wall rock material, or transition to shallower crustal levels, where a different composition of garnet would crystallize. Any of these processes would explain the coupled Ca, Mn, and Mg profiles shown. (3) The second garnet formation reflects the

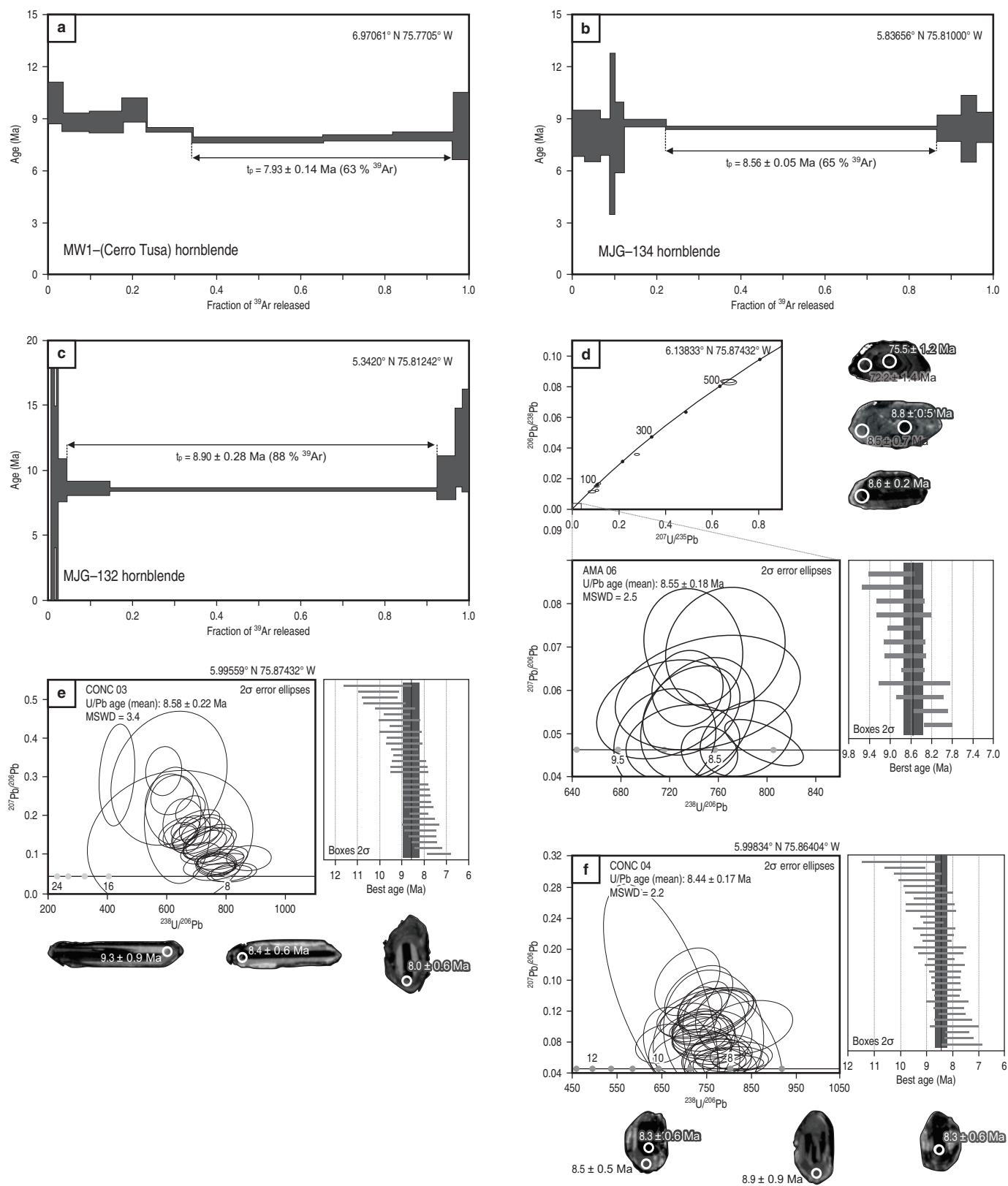


Figure 25. New $^{40}\text{Ar}/^{39}\text{Ar}$ ages from **(a)** Cerro Tusa and **(b–c)** Jericó garnet-bearing intrusive. **(d–f)** U–Pb ages from pyroclastic density current deposits from Concordia–Cauca river section.

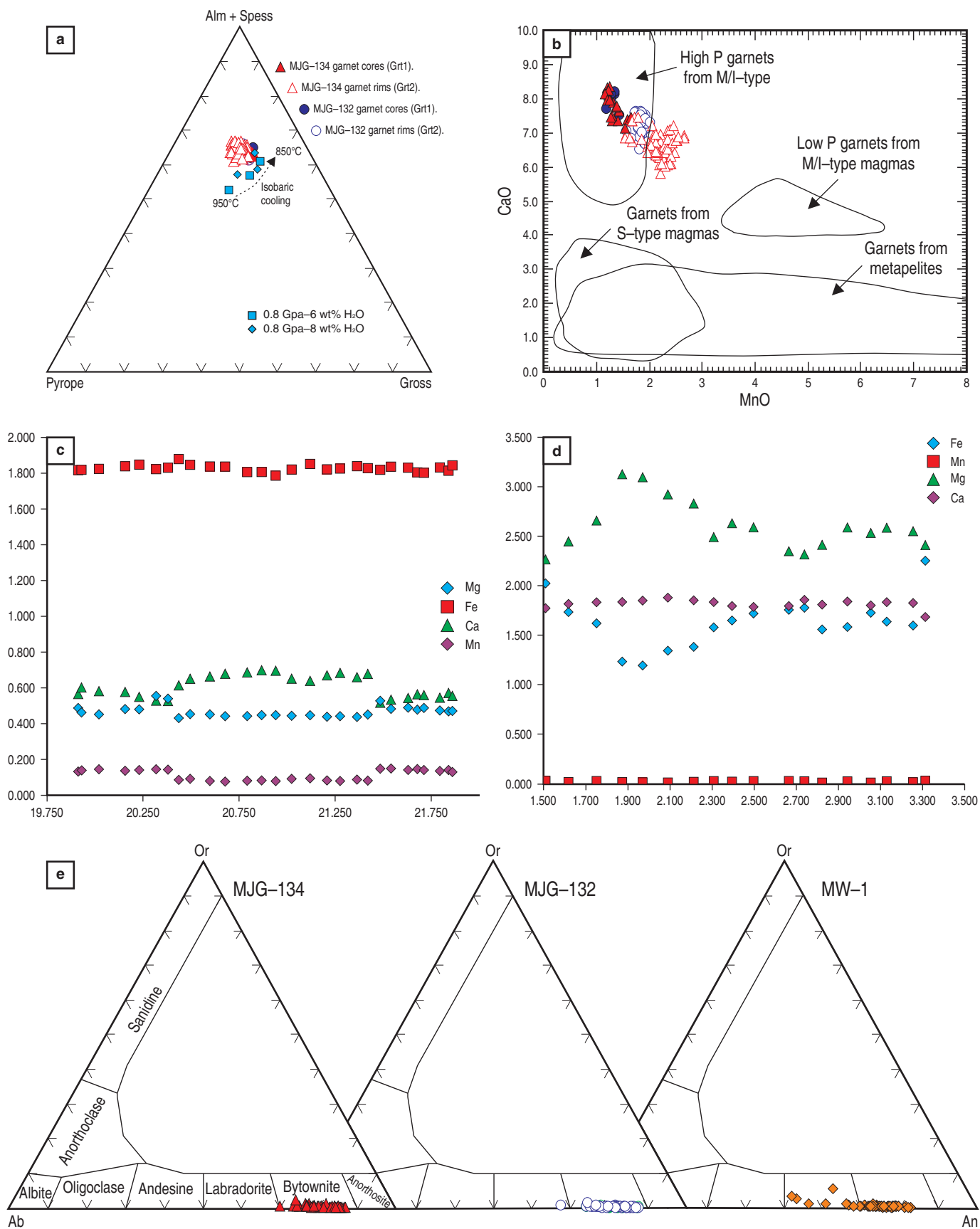


Figure 26. Mineral chemistry of garnet, amphibole, and plagioclase in the Combia Formation porphyritic rocks. **(a)** Garnet phenocryst composition on the Grss–Alm–Py diagram. Experimental garnet compositions and isobaric cooling trend from Alonso–Perez et al. (2009) are also shown. **(b)** CaO and MnO binary diagram. Fields are from Harangi et al. (2001) and references therein. **(c)** Representative garnet zonation profile. **(d)** Representative amphibole zonation profile. **(e)** Plagioclase composition in the Ab–An–Or ternary diagram.

introduction of a new crystallization phase in the magma (e.g., plagioclase), which would change the fractionated liquid's overall Ca composition.

The CF garnet compositions are similar to those reported from El Tesorito and El Poma (Bissig et al., 2017). They also resemble the experimental garnets obtained by Alonso–Perez et al. (2009) from andesitic compositions with 6 to 8 wt% H₂O at 0.8 GPa and 850 to 900 °C. Furthermore, according to these authors, under these experimental conditions, the modal amount of garnet at 0.8 GPa decreases with a decrease in H₂O at the expense of plagioclase and amphibole formation (grt + liq1 = amph + plg + liq2), which would agree with the petrographic evidence (i.e., plagioclase rims and amphibole rims) shown by CSVI garnet phenocrysts (Figure 10c).

6.2. Plagioclase

Plagioclase phenocrysts in all samples are oscillatory zoned (Figure 10a). Most of them are classified as bytownite. Overall cores are more calcium-enriched than rim compositions, although some variability is present, and zonation is less well developed in the Cerro Tusa sample (Figure 26e). Plagioclase inclusions in garnets are more calcic, similar in composition to cores in zoned phenocrysts. Cerro Tusa matrix microliths are labradorite.

6.3. Amphibole

Amphibole in garnet-bearing samples is mainly pargasitic hornblende, and Mg# ranges from 0.439 to 0.693. Most phenocrysts show a compositional break, with more Mg-rich and Al- and Fe-poor cores than rim compositions (Figure 26d). Nevertheless, some amphiboles show composite zoning profiles. There is also evidence of some reverse zoning at the crystal rims, possibly due to magma–crystal interactions during matrix cooling. Amphibole inclusions in garnet are more pargasitic than matrix crystals. Some amphiboles enclose smaller garnet crystals, indicating crystal growth after Grt 1 was already formed.

Amphiboles in the andesitic magma of Cerro Tusa have an overall darker rim than their centers, but zonation is nevertheless patchy. Even though cores are slightly more Mg-rich, chemical variation is present to a much lesser extent than garnet-bearing samples. The compositions are mainly ferro-pargasitic, and Mg# ranges from 0.223 to 0.337.

To obtain further constraints on magma crystallization depths, thermobarometric calculations were performed on amphibole crystals (Figure 27). Estimations of pressure and temperature were calculated using an empirical calibration based on the composition of amphibole from calc-alkaline magmas, proposed by Ridolfi & Renzulli (2012) and Ridolfi et al. (2010). The results obtained are plotted in Figure 27 and listed in Table 1 of the Supplementary Information 4.

Pressures obtained using the calibration range between 309 and 502 MPa, which correspond to ca. 18 km depth calculated for cores and ca. 11 km depth for rims, considering an upper crustal density of 2.7 g/cm³. The temperature calculations for these samples range between 950 °C in the cores and 880 °C in the rims (Figure 27a). These temperatures agree with the PT constraints for the garnet determined above.

Although all analyzed crystals are close to the boundary of compositionally consistent amphiboles (dashed lines in Figure 27a), some of them exceed the H₂O melt stability limit. However, the estimated water contents account for uncertainties of 15% (Figure 27b). Pressure and temperature characterization of these crystals indicate that the analyzed amphiboles crystallized close to the instability boundary, making these crystals prone to destabilization with small P–T changes.

Further constraints on pressure and temperature conditions can be obtained via a comparison with compositions of experimentally obtained amphiboles. Crystallization and melting experiments have shown that the contents of Al₂SiO₅, Mg#, and Na+K in amphibole are pressure- and temperature-dependent (Alonso–Perez et al., 2009; Ribeiro et al., 2016; Samaniego et al., 2010). Amphibole from the garnet-bearing samples overlaps the high-pressure (HP) compositional fields (>400 MPa) in Al₂SiO₅, Mg#, and Na+K for amphibole plots (after Ribeiro et al., 2016) and is somewhat higher than the calculated pressures and temperatures from geothermobarometric calculations shown above.

Physical conditions during the last magma evolution stages are difficult to evaluate via mineral chemistry. However, the amphibole reaction rims found in the CSVI intrusives, especially in the Amagá Basin–CSV (Figure 10b), suggest that these rocks respond to water loss throughout the melt adiabatic ascent from the reservoir to upper-level magmatic chambers (Rutherford & Hill, 1993). Therefore, magmas resided in shallow chambers prior to intrusion into the AF sedimentary beds or eruption to the surface.

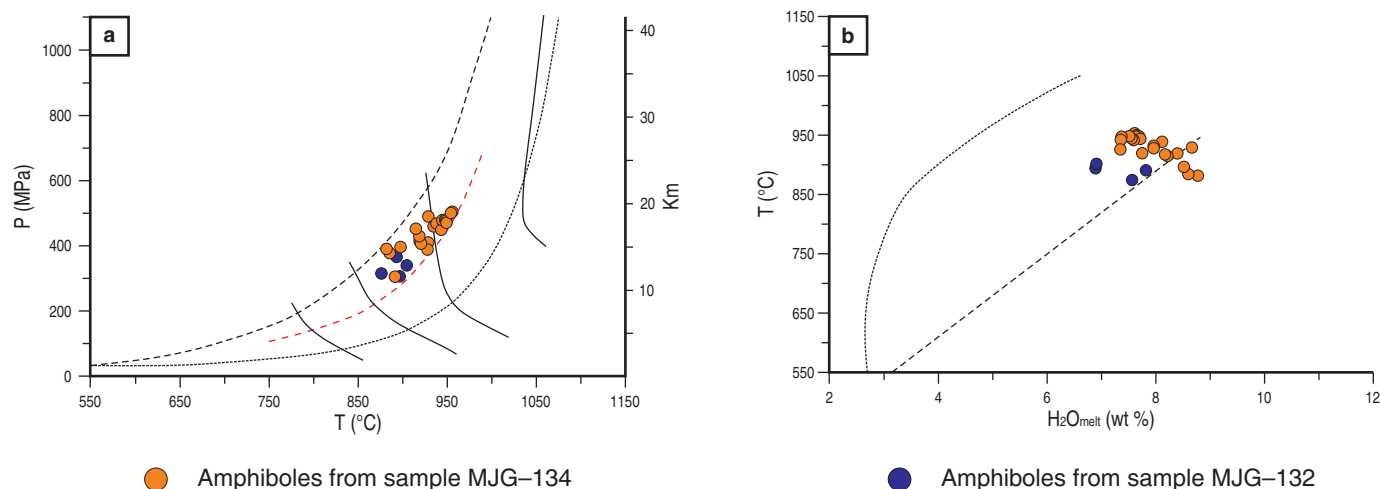


Figure 27. Estimated pressures and temperatures for the Jericó garnet-bearing intrusives (MJG-132 and MJG-134). **(a)** Pressure (MPa) vs. Temperature (°C) and **(b)** Temperature (°C) vs. H₂O melt (wt%). Pressures and temperatures were calculated after Ridolfi & Renzulli's (2012) formulation based on amphibole composition. Mineral data and calculations are presented in Table 1 of the Supplementary Information 4.

7. Discussion

7.1. Garnet-Bearing Rocks

Few worldwide localities report primary garnet in volcanic rocks. As a primary phenocryst, garnet is more common in per-aluminous magmas (Harangi *et al.*, 2001), such as the Pyrenean dacite–rhyolite suites (e.g., Gilbert & Rogers, 1989; Muñoz, 1992), the Trinity Peninsula in Antarctica (e.g., Hamer & Moyes, 1982), and NW England (e.g., Fitton, 1972; Thirlwall & Fitton, 1983). Primary garnets in metaluminous rocks (e.g., andesites) occur in volcanism-related settings in NE Japan (Miyashiro, 1955; Kano & Yashima, 1976; Kawabata & Takafuji, 2005; Shuto *et al.*, 2013), Central Anatolia (e.g., Aydar & Gourgaud, 2002), the Northland Arc in New Zealand (Bach *et al.*, 2012; Day *et al.*, 1992; Green, 1992; Smith *et al.*, 1989), and evolved magmas in the Pannonian Basin (e.g., Embey–Iszstín *et al.*, 1985; Harangi *et al.*, 2001). Furthermore, Green (1992) used the terms S-type, M-type, or I-type originally proposed by Chappell & White (1974) for granitoids, for garnet-bearing volcanic rocks.

Green (1977, 1992) determined that the CaO content in garnet is dependent on the magma type and the pressure and temperature of crystallization. Garnets formed under high-pressure conditions are characterized by high CaO (>5 wt%) and, as pressure decreases, MnO contents tend to increase (> 3wt%) without a coupled decrease in CaO.

Garnets occurring in CSVI rocks are similar to garnets crystallized in M-type and I-type intermediate and mafic magmas at high pressures (Figure 26a). In addition, they have a CaO-rich core, which is surrounded by CaO-poor secondary garnet. Consequently, this evidence suggests at least two growth stages,

which is also reflected by amphibole phenocryst zonation. Interestingly, these rocks have shown to have abundant xenoliths, and interestingly, some garnet-bearing samples have more radiogenic Sr–Nd isotope values within the whole suite, which could indicate the addition of a crustal component (Figure 22)

Ca-rich almandine garnet is not stable in high-pressure magmas, and it is likely to be completely reabsorbed in long-residence magma chambers under shallow crustal conditions. Thus, garnet survival in volcanic rocks is expected to be a function of rapid magma ascent through the crust (e.g., Fitton, 1972; Gilbert & Rogers, 1989; Harangi *et al.*, 2001). Nevertheless, the addition of a Mn component increases garnet stability (Green, 1972), which could account for preserving some of the garnet in the CSVI. Secondary overgrowth (Grt 2) would increase the possibility of garnet preservation. An additional factor in garnet stability determined in recent studies is the presence of H₂O-content in the magmatic liquid (Alonso-Perez *et al.*, 2009). For some of the CSVI Group CA1 magmas it is possible that garnet was reabsorbed, and therefore is not present as a phenocrystal phase.

Amphibole in these samples also indicates at least two formation stages evidenced by the differences in calculated pressures and temperatures in cores and rims (17–19 km–950 °C and 11 km–900 °C, respectively). Furthermore, the outermost amphibole rims and sieve textures in plagioclase indicate degasification and chemical/physical disequilibrium (respectively) during the last stages of magma ascent to the surface (Figure 28).

Therefore, we conclude that the garnet-bearing magmas in the CSVI suite show at least three formation stages through phenocrystal evolution: (i) Magma formation and crystallization of Grt1 and Amph1, (ii) changes in physicochemical conditions either due to pressure decrease or magma contamination,

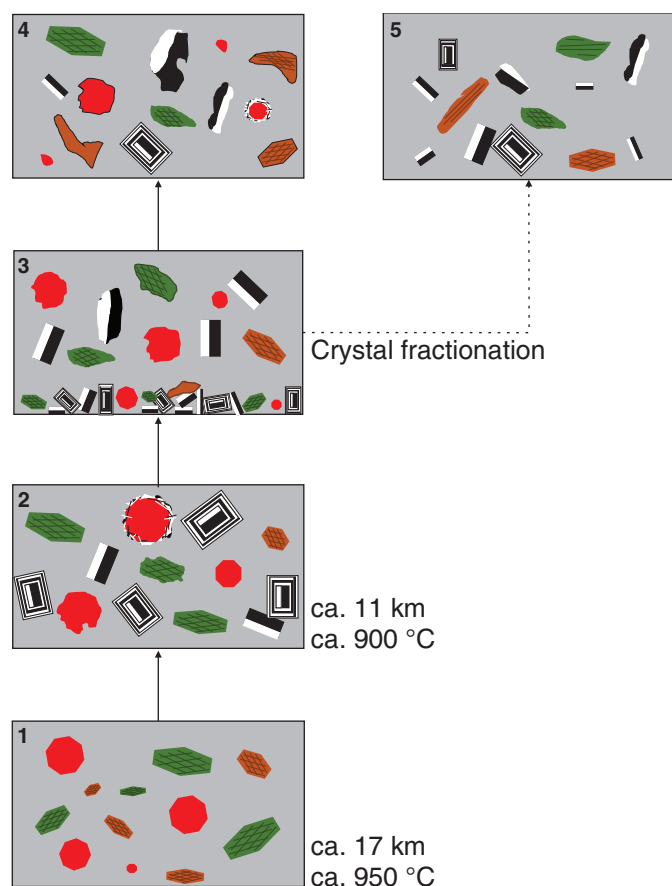


Figure 28. Magma crystallization model proposed for CSVI calc-alkaline rocks. Stages: (1) Early phenocrysts formation phases at ca. 17 to 19 km deep and ca. 950 °C; (2) reabsorption of early formed phenocrysts and crystallization of the second generation of phenocrysts at ca. 11 km and ca. 900 °C; (3) removal of some phenocrysts to evolve into stages 4 and 5; (4) early formed phenocrysts disequilibrium and degasification/dehydration textures in amphibole and plagioclase due to chemical (magma mixing) and physical (P–T changes) variation in shallow magma chambers; and (5) adakitic magmas formed via crystal fractionation.

whereby Grt2 and Amph2 are formed, and possibly the onset of extensive Plg crystallization, and (iii) degasification and rapid ascent to the surface (Figure 28).

7.2. The Adakite Connection

The CSVI has been linked to adakite formation (Bissig et al., 2017; Borrero & Toro-Toro, 2016; Jaramillo et al., 2019). As shown previously, most of the calc-alkaline series have all the characteristics of adakitic magmas. Adakites are rocks that have received considerable attention due to their significance in understanding crustal recycling at convergent margins, and their similarities with the Archean Tonalite–Trondhjemite–Granodiorite series are essential to understand Earth’s initial differentiation and the onset of plate tectonic movement (see Castillo,

2012 for a review). The general REE patterns of adakite are considered to indicate that garnet is involved in the formation process of these magmas, as garnet controls REE fractionation, most likely by being formed during melting, and therefore retaining HREEs in favor of LREEs.

Various adakite formation models have been hypothesized, generally involving the melting of young ocean crust in subduction zone settings (cf. Castillo, 2012; e.g., Defant & Drummond, 1990). Nevertheless, some adakites are thought to form via high-pressure (HP) fractionation of water-rich mantle melts (Hidalgo & Rooney, 2010, 2014; Macpherson et al., 2006; Ribeiro et al., 2016; Richard & Kerrich, 2007) or by AFC processes (i.e., mantle melts are reinjected into a shallow crustal magma chamber; e.g., Castillo et al., 1999; Ribeiro et al., 2016). Under the HP conditions, model fractionating phases that determine the adakite character would be garnet and HP amphibole, as the magma would be within the stability field of these minerals (Castillo, 2006; Macpherson et al., 2006; Ribeiro et al., 2016; Richards & Kerrich, 2007). The presence of water in the system would promote amphibole and garnet crystallization, and delay plagioclase fractionation (Müntener et al., 2001). The adakites formed via fractionation are very similar to High Silica Adakites compositions (Martin et al., 2005).

Under the HP fractionation scenario garnet-bearing samples from the CSVI could represent possible “primitive” magmas, where garnet and amphibole have not been separated from the melt. This would account for the less differentiated REE profiles of Group CA1 samples (Figure 19). If, garnet and amphibole, and plagioclase to a lesser extent, are separated from the melt through time, the result should correspond to at least some of the calc-alkaline rocks. To test this hypothesis, we applied the Rayleigh equilibrium fractionation formula and considered the garnet-bearing samples as a starting composition for magma differentiation. We used the partition coefficients proposed by Hidalgo et al. (2007) for amphibole, clinopyroxene, magnetite, and plagioclase, and the partition coefficients of Irving & Frey (1978) for garnet. Our results show that the magma composition of group CA3 can be obtained by fractionation of 18:8:2:2 amphibole–garnet–magnetite–pyroxene (Figure 29), with 80% remaining melt. The listric patterns of Group CA4 magmas can also be obtained by approximately fractionating 20:6 amph:grt in Group CA2 magmas and 80 to 85% remaining melt. Consequently, our assumptions adjust to the model of adakite formation via crystal fractionation of an arc magma (Alonso-Perez et al., 2009; Macpherson et al., 2006; Richards & Kerrich, 2007).

We also used the Dy/Dy* versus Dy/Yb diagram of Davidson et al. (2013) to determine amphibole and clinopyroxene vs. garnet fractionation (Figure 30). The Dy/Dy* versus Dy/Yb quantifies the curvature seen in many chondrite-normalized REE patterns due to mineral fractionation. Amphibole and clinopyroxene can significantly decrease Dy/Dy*, but amphibole

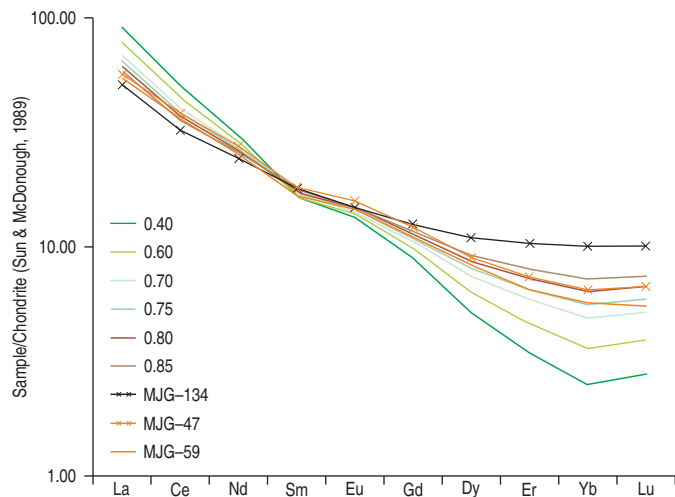


Figure 29. C1 Chondrite normalized REE patterns for Rayleigh fractionation modelling of Group CA1 garnet-bearing sample MJG-134. Patterns for 40%, 60%, 70%, 75%, 80%, and 85% remaining melt are shown. Samples MJG-47 and MJG-59 of Group CA2 are shown for comparison.

has greater effect on reducing Dy/Yb. The figure shows the CVP data. The calc-alkaline data show less well-defined trends than the tholeiitic series, except for Group CA1. This group offers a broad linear array parallel to the tholeiitic series and the calculated primitive composition plots towards a more LREE-enriched MORB. The other rocks of the series tend towards the middle and upper crust composition, which, according to Davidson et al. (2013), would suggest that either the primitive arc magmas differentiated towards continental crust-like compositions or mixed with it during differentiation. Nevertheless, a considerably higher Dy/Yb trend is evident in samples from groups CA3 and CA4, further suggesting that garnet was involved during differentiation.

7.3. Crustal Input and Magma Origin

Evidence of interaction between a mantle source and a crustal contaminant is given by the trace element characteristics that magmas attain when these processes occur. Various ratios have been used as proxies to determine the nature of this interaction (e.g., Pearce, 2008; Plank, 2005).

On the Th/Yb vs. Nb/Yb plot of Pearce (2008) (Figure 31), magmatic rocks containing a large recycled crustal component (e.g., continental margins and subduction zones) have Th/Yb ratios that lie above the MORB–OIB array and are the product of selective Th addition (Pearce, 2008). In this diagram, the tholeiitic series plots in a tight compositional cluster above the N–MORB to E–MORB composition transition, which can be interpreted as either (i) a modified depleted mantle source or (ii) representing crust–magma interaction processes. There is only a slight vertical increase in Th/Yb from the more primitive basalts

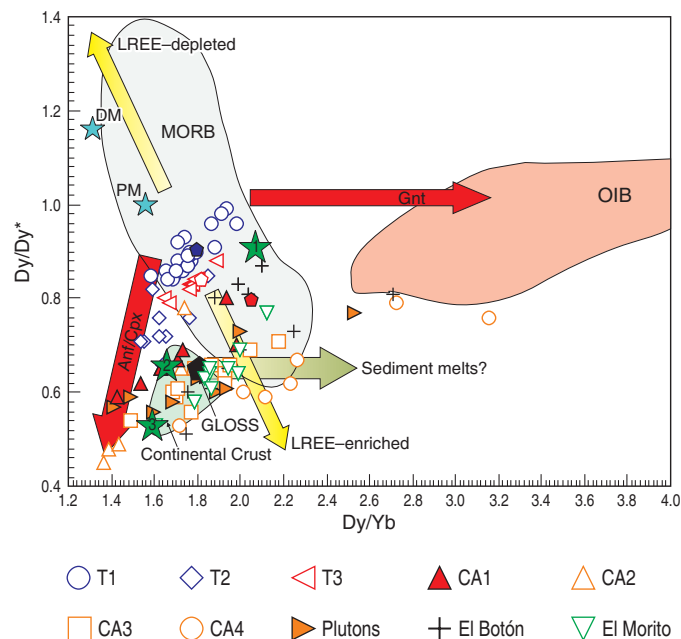


Figure 30. Dy/Dy* vs. Dy/Yb diagram after Davidson et al. (2013). $Dy/Dy^* = Dy_N / (La_N 4/13 \times Yb_N 9/13)$. Arrows indicate mineral control and melting. (PM) primitive mantle; (DM) depleted mantle; (GLOSS) average global subducting sediment; numbers in green stars: 1 = Upper Continental Crust, 2 = Middle Continental Crust, and 3 = Lower Continental Crust. Pentagons denote recalculated primitive magmas at 48% SiO₂.

(Group T1) towards the Group T2 samples. The calc-alkaline series shows an overall parallel trend above the mantle array and commences above the E–MORB, with the garnet-bearing samples. This trend suggests either fractional crystallization of a magma formed from a more enriched mantle source than the tholeiitic series or crustal assimilation. Nevertheless, the more ⁸⁷Sr/⁸⁶Sr-enriched samples do not show the highest Th/Yb values, suggesting that fractional crystallization is an important process of the calc-alkaline series. The shoshonite series defines a well-developed curved trend together with the less differentiated El Botón arc data (Rodríguez & Zapata, 2014), suggesting assimilation and fractional crystallization.

TiO₂/Yb vs. Nb/Yb relations of basaltic rocks indicate original mantle source compositions of magmatic rocks, as they are independent of alteration and subduction enrichment processes (Pearce, 2008) (Figure 31). Most samples plot on the MORB array. Group T1 of the tholeiitic series spreads from the N–MORB towards the E–MORB transition, whereas Group T2 clusters around the transition line. The calc-alkaline series is also shown and is less homogeneous but plots towards E–MORB and spreads towards higher TiO₂/Yb values.

The Th/La ratio has been used as an indicator of sediment input into arc systems, as the excess of Th is considered to derive from subducted sediments (Plank, 2005). The Th/La and Sm/La ratios for the tholeiitic and calc-alkaline series show

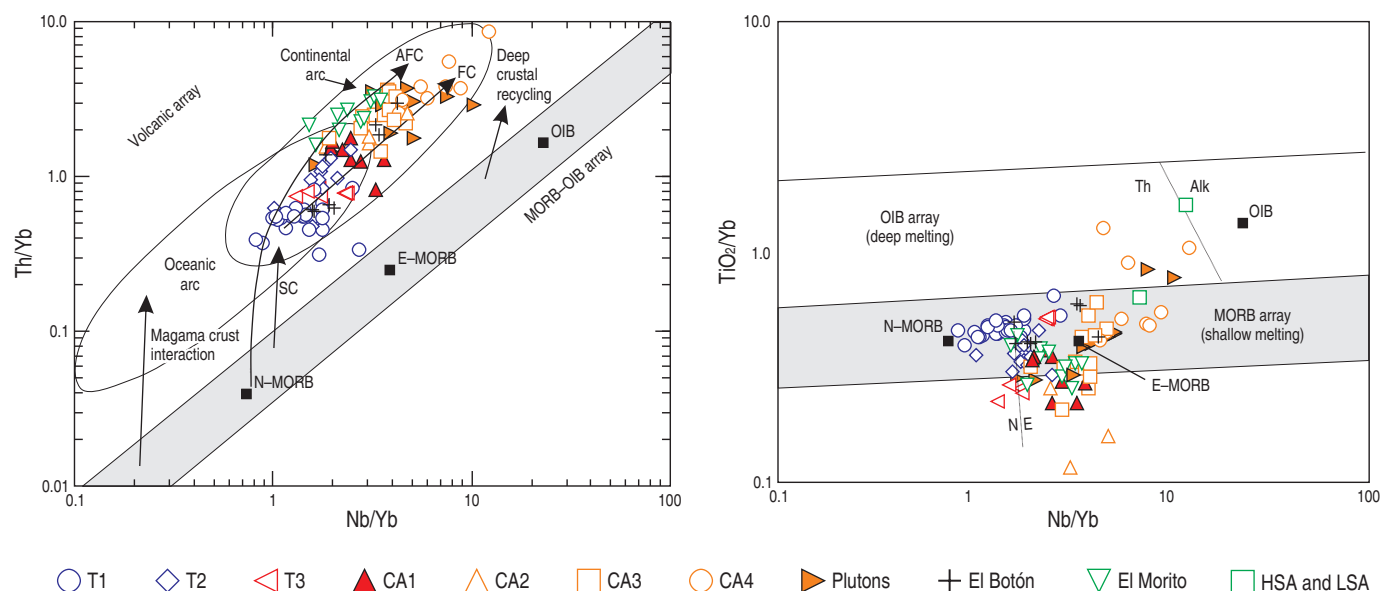


Figure 31. Th/Yb vs. Nb/Yb and TiO_2 vs. Nb/Yb plots of Pearce (2008) for the Combia Volcanic Province rocks. SC: Sediment Component, AFC: Assimilation and Crustal Contamination, FC: Fractional Crystallization.

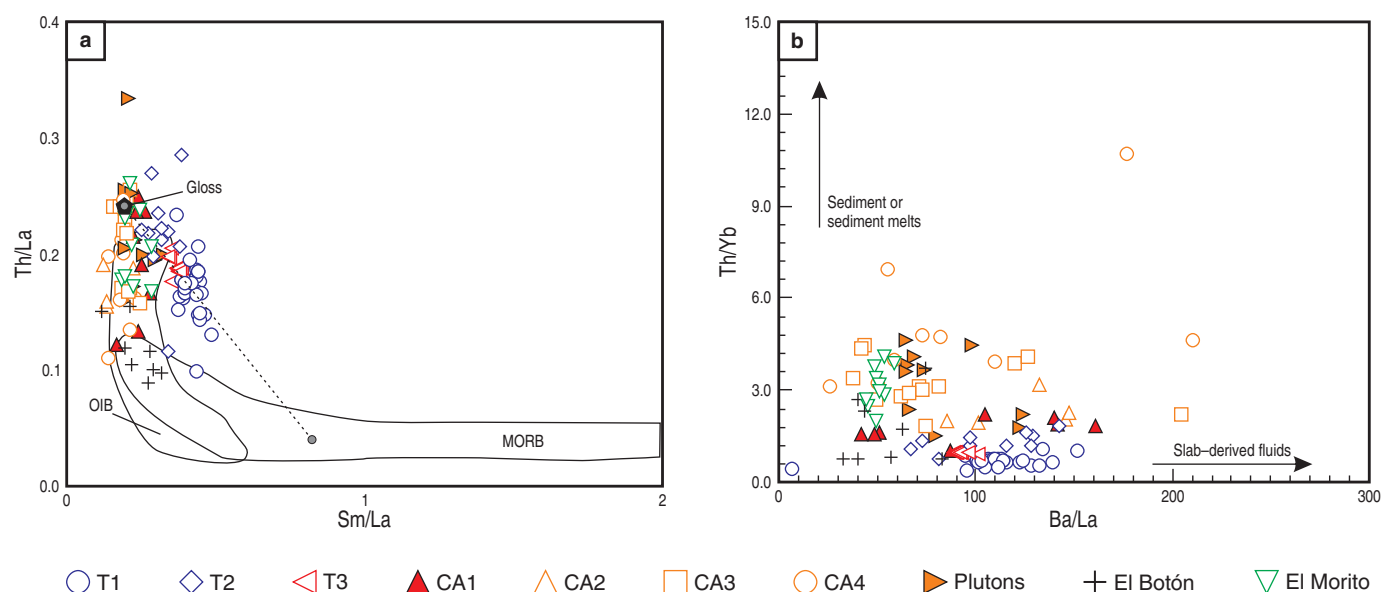


Figure 32. (a) Th/La vs. Sm/La (after Plank 2005) for the Combia Volcanic Province rocks. GLOSS from Plank & Langmuir (1998). **(b)** Th/Yb vs. Ba/La (after Woodhead et al., 2001).

two distinct trends and define the variable influence of subducted sediment (Figure 32). The regression line calculated for the tholeiitic series indicates a somewhat enriched MORB endmember mixed with possible sediment. Interestingly, the calculated endmember is similar to the Global Subducting Sediment composition GLOSS from Plank & Langmuir (1998). The calc-alkaline and shoshonite series denote a vertical trend that suggests a more enriched mantle endmember mixing with a sedimentary component. Additional constraints are given by the

Ba/La ratio, which indicates slab dehydration fluids, as Ba is a mobile element, whereas La is immobile in fluids (Staudigel et al., 1996; Woodhead et al., 2001). The CF tholeiitic series plots towards a high Ba/La ratio (up to 150) and defines a linear trend that suggests the influence of slab-derived fluids. In both diagrams Group T2 plots above the T1 and T3 Groups, towards the garnet-bearing samples, suggesting contamination. The CF and CSVI calc-alkaline and shoshonitic series plot toward higher Th/Yb, indicating a sediment component for these rocks.

In the Dy/Dy* versus Dy/Yb diagram of Davidson et al. (2013) (Figure 30), the samples plot towards an LREE-enriched mantle array, and the more differentiated groups gradually spread towards lower Dy/Dy*. Davidson et al. (2013) suggest that this may be due to the variable incorporation of sediment. The tholeiitic series plots on the MORB field and individual trends for the defined groups tend to show positive slopes, suggesting clinopyroxene differentiation. The tholeiitic Groups T1 and T3 plot parallel to one another, “stepping down” towards higher Dy/Yb and lower Dy/Dy*. Group T2 does not follow the same parallel trend, plotting towards Group CA1, suggesting contamination. The calculated primitive melts (SiO₂ at 48%) plot towards the center of the field defined by MORB data.

The Sr–Nd radiogenic isotope data for the CF and CSMV rocks are low and generally fall into the mantle array. There is a spread towards more enriched Sr, which indicates some variable contribution of a sediment/crustal component. Most of the tholeiitic rocks are less radiogenic than the shoshonitic and calc-alkaline rocks. The calc-alkaline series partially overlaps, which suggests that a similar source formed them. Nevertheless, some CSMV samples plot towards more enriched sediment or crustal Sr values and include some of the garnet-bearing samples. Therefore, garnet-bearing samples probably show evidence of crustal or sediment contamination. As shown previously, these rocks carry xenoliths, and there is evidence that the magmas that formed these rocks ascended in three distinct phases and thus were exposed to changes in magma composition, be it by the addition of another magma, continental crust, or sediment components. Jaramillo et al. (2019) determined that the more evolved magmas of the CSMV formed at deeper crustal levels (ca. 50 km for dacites, ca. 17 km for basalts), which would enable more assimilation and homogenization for these rocks. Lead isotope systematics also confirm the interaction of various components, including the mantle wedge, oceanic sediment, and a crustal endmember, the Cretaceous basement, that comprises accreted rocks.

7.4. The Shoshonitic Series

One crucial aspect is the evidence of shoshonitic magmatism (12.5 and 9 Ma; Zapata & Rodríguez, 2011) in the Amagá Basin (Jaramillo, 1976; Rodríguez & Zapata, 2014; this study), which is associated with a more widespread event that includes El Botón basalts to the west (Figure 2). The known age for this magmatism in the Amagá Basin (9.1 ± 0.7 Ma in Restrepo et al., 1981a), and the absarokite intrusion in the CF, described by Jaramillo (1976), suggest that volcanism was coeval with other volcanic activity.

Reverse Petrogen calculations on the more primitive samples of El Botón basalts indicate that these rocks melted in the lower crust, at ca. 10 kbar and ca. 1250 °C (Krein et al. in review). In the Dy/Dy* versus Dy/Yb diagram of Davidson et al. (2013) (Figure 30), the shoshonitic samples define a different,

steeper trend than the other series, plotting from high Dy/Yb MORB compositions, towards upper continental crust compositions. The trend suggests mainly amphibole or clinopyroxene fractionation in the formation of the more evolved rocks.

Shoshonitic magmas form in various tectonic settings, including within plates, continental rifts, ocean islands, oceanic arcs, back-arc extensional zones, and continental arcs (Müller et al., 1992). The Colombian shoshonitic rocks are related to the continental arc after the collision of the Chocó–Panamá Block (Lara et al., 2018). Basic to intermediate shoshonitic magmas are generally considered to have formed by low degrees of melting of previously modified mantle rocks, where LILEs and LREEs have been transferred from a subducting slab (e.g., Aldanmaz et al., 2000; Morrison, 1980). Th–Ba–Nb systematics indicate addition of subducted sediment melts and crystal fractionation processes in the formation of these rocks in the CVP.

7.5. Tectonic Scenario

In this review, we consider the following important aspects for the interpretation of the Combia Volcanic Province:

1. Field relationships in the Amagá Basin indicate a volcanic province that formed due to the presence of a short-lived magmatic event resulting from transtensional tectonics in a sedimentary basin. The underlying extensional event of the Amagá Basin would have begun during the early Miocene (23–21 Ma), indicated by the sedimentation of the AF (Lara et al., 2018; Ramírez et al., 2015), and it seems to be associated with Panamá–Chocó Block docking against the South American Plate approximately 25–23 Ma (Farris et al., 2011) via a fast-oblique convergence phase along a sinistral strike-slip fault (Müller et al., 2008).
2. The magmatism along the Cauca River valley and the Amagá Basin can be divided into tholeiitic, calc-alkaline, and shoshonitic series. The calc-alkaline includes garnet-bearing andesites and adakites. Nb–Ta and Zr negative anomalies in all series are evidence of a subduction zone setting. The tholeiitic magma series originated from fractionation of a heterogeneous mantle source modified by variable degrees of slab-derived fluids. Adakites are the result of garnet and amphibole fractionation and crustal contamination. Shoshonites possibly formed by fractionation of magmas created by low degrees of melting of mantle source modified through addition of a sediment/crustal component.
3. Tholeiitic magmatism is a unique feature of the Amagá Basin, and therefore we propose the term Combia Volcanic Province (CVP). However, records of shoshonitic, calc-alkaline (garnet-bearing and adakitic) magmatism are present in other areas. Specifically, shoshonitic magmatism is present in the northwest (Figure 2; Rodríguez & Zapata, 2014). There are records, from 12.5 to 9 Ma, of

garnet-bearing and adakite magmatism in the south (Figure 2; Bissig et al., 2017). Adakites are also present to the south of the Amagá Basin and are part of the more recent volcanic activity (e.g., Toro-Toro et al., 2008). Furthermore, after magmatism was established at 9 Ma along the Cauca River valley and the Amagá Basin, the tholeiitic, calc-alkaline, and shoshonitic series coexisted at the same time in the CVP.

4. The mineral chemistry of garnets and amphiboles in garnet-bearing rocks indicates at least three formation–emplacement stages for the calc-alkaline series: (i) Magma formation and crystallization of initial garnet and amphibole, (ii) changes in physicochemical conditions triggering Plg crystallization, and (iii) degasification and rapid ascent to the surface (Figure 28).
5. The occurrence of shoshonitic, calc-alkaline (incl. garnet-bearing and adakitic), and tholeiitic rocks in the Amagá Basin suggests that magma production occurred at different depths, as was proposed by Jaramillo et al. (2019) for tholeiitic and calc-alkaline magmatism, and through variations in the different involved processes. The shoshonitic rocks formed through fractionation at levels where plagioclase is still stable, whereas adakites developed within the garnet stability field, and therefore at deeper levels. Tholeiitic magmas would have formed from a mantle beneath shallow crustal levels.

As a result, the considerations above allow us to propose two different but coeval sources for the CF and CSVI magmatism in the Cauca extensional basin: A primitive source, modified by dehydration fluids of the previously subducted slab (i.e., tholeiitic magmas) and a more contaminated magma source (i.e., calc-alkaline magmas, most of which are adakitic and shoshonitic).

Vargas & Mann (2013) proposed an east–west–striking slab tear, named Caldas Tear within the subducted Nazca Plate (Figures 1, 33). It separates two distinct subducted slab segments. The Caldas Tear is an extension of the Sandra Ridge, and both constitute a major weakness along the southern flank of the Panamá Arc indenter (Vargas & Mann, 2013). The Sandra Ridge is a volcanic high with a band of seismicity, interpreted as residual or reactivated tectonism along an imperfect late Miocene plate suture (Lonsdale, 1991, 2005).

The ridge subduction setting is a possible scenario for the formation of CVP rocks. Vargas & Mann (2013) argued that the east–west aligned volcanic activity, the formation of adakites (Borrero et al., 2009), and the presence of outlier volcanic centers (e.g., Paipa–Iza and San Diego (Pardo et al., 2005)) are all indicators that the Caldas Tear may penetrate the upper crust as a fault zone and consequently provides a conduit for the upward rise of magmas formed at different levels and hydrothermal fluids produced by slab melting on either side of the Caldas Tear. It would also enable the mixing of melts from these various

sources. An additional aspect is that a slab window would allow the heat supply to melt multiple components of the mantle and overlying crust extensively. The orthogonal configuration of the Sandra Ridge subduction would explain differences in magmatic products on either side of the subducting plates (Thorkelson & Breitsprecher, 2005).

A recently proposed model determines that a flat slab system developed from a typical arc at ca. 14 Ma when magmatic activity was present along Colombia's Pacific margin. Then, at 9 to 6 Ma gradual flattening of the slab occurred, and magmatic activity ceased and was finally renewed after ca. 4 Ma south of the Caldas Tear (Wagner et al., 2017). Under this scenario, the boundary between the northern segment of the modern flat subducting Nazca Plate and the steeper southern segment is determined by the Caldas Tear (Chiarabba et al., 2016; Yarce et al., 2014) controlled the formation of the Amagá Basin. They represent a surface expression of this complex tectonic system during the Miocene, perhaps indicating that magmatic activity occurred during the gradual flattening of the slab. Therefore, the Caldas Tear was already established at ca. 12 Ma.

Jaramillo et al. (2019) suggests that the presence of tholeiitic rocks in the Amagá Basin is linked to the oblique subduction of the Nazca Plate and to the existence of remobilized structural discontinuities. Thus, the presence of tholeiitic rocks is a result of a more significant structural component due to the change in the convergence angle. Although we do not preclude that oblique subduction plays an important role in the formation of the Amagá Basin and therefore is linked to the formation of the CVP, we also consider that other controls such as the Caldas Tear must have played an important role in the generation of this unique Neogene rock association in the northern Andes.

The melting of a homogeneous, previously modified mantle source formed the tholeiitic magma series. Element variability and Nb–Ta–Zr anomalies, typical of subduction, indicate initial modification by enriched fluids (Group T1), mineral fractionation (Group T3), and possible contamination of crustal and/or sedimentary input (Group T2). Therefore, they are likely to melt from the modified mantle wedge above the subducting plate (Figure 33f). The majority of these melts are primitive arc basalts, and some andesitic differentiates, with an overall homogeneous composition, which suggests that most magmas ascended directly to the surface, with few or no modifications. Nevertheless, some of these primitive magmas could have been emplaced into lower crustal magma chambers being subjected to open system processes (assimilation, magma mixing, melt extraction, and fractional crystallization) as proposed by Bryan et al. (2010). This phenomenon has also promoted magma diversification observed in the Cauca River valley (Figure 33).

The calc-alkaline adakite magma series is the product of HP fractionation of enriched mantle melts, which we believe are likely to have formed above the downgoing subduction of the Nazca Plate (Figure 33). Our findings support the model

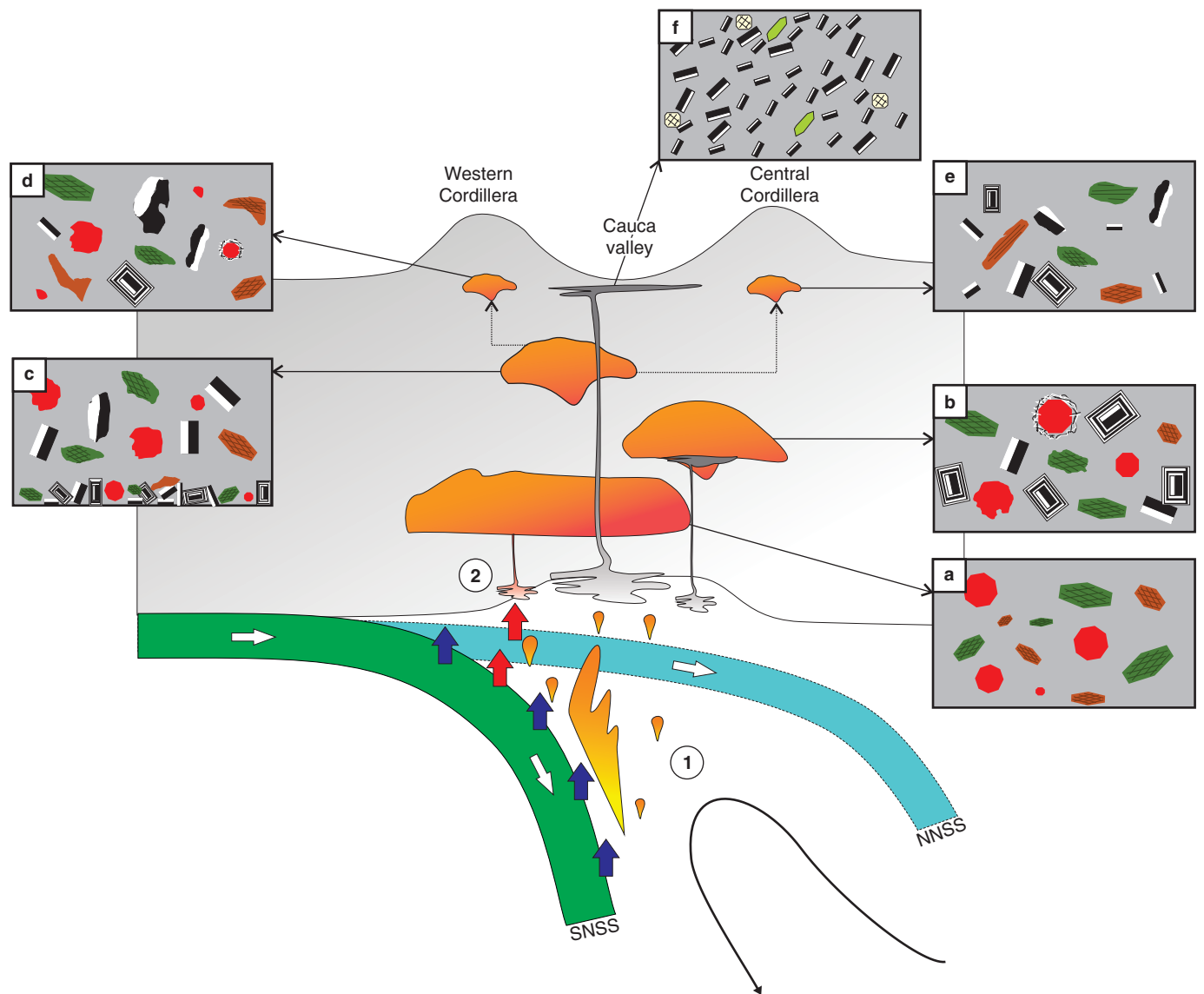


Figure 33. Petro-tectonic model of generation of the Combia Volcanic Province calc-alkaline and tholeiitic magmas (modified from Ribeiro et al., 2016). (1) Dehydration and partial melting occur on the downgoing oceanic crust slab (Nazca Plate), including associated marine sediments that provide incompatible elements to the diverse magmas. The Nazca Plate is split into two segments by the Caldas Tear (Vargas & Mann, 2013): Northern (NNSS) and Southern (SNSS) Subduction Segments. Slab tear provides heat to partial melting (red arrows) of the mantle and overlying crust. (2) High-pressure melts are formed and stall at ca. 18 km, crystallizing garnet and HP amphibole. (a) Plagioclase begins to crystallize and (b) crystal fractionation of garnet, amphibole, and plagioclase operates to generate a wide diversity of magmas (c–e). Tholeiitic magmas from modified mantle sources are emplaced in the upper crust (f). Shoshonitic magmas would fractionate at (a), after magmas separated from the modified mantle.

of Bissig et al. (2017), where the initial hydrous melts in the middle Cauca valley form high-pressure magmatic storage reservoirs, where garnet and high-Mg amphiboles crystallize (Figure 33a). Separation of these minerals from the melt is an essential factor in the adakite-like nature of the resulting fractionated magmas. In the Amagá Basin, new mineral growth (secondary garnet and amphibole) records change magma composition, possibly injecting new mantle melts or crustal contamination. The presence of disequilibrium textures such as sieve textures and reabsorbed phenocrysts and more

radiogenic isotopic signatures supports magma mixing and/or crustal contamination. This scenario is likely to occur at shallower depths, where plagioclase begins to crystallize from the melt (Figure 33b). Fractionation of garnet, amphibole, and to a lesser extent, plagioclase would have occurred at some point in the middle to the upper crust. They formed a wide diversity of magmas (few of them garnet-bearing and most of them garnet-free magmas) beginning from a garnet-bearing magma (Figure 33c–e). We propose that the opening of the Caldas Tear in the downgoing subducting plate is an essential

control for some garnet-bearing magmas. Before the complete fractionation, they reached the surface at the beginning of volcanism in the middle Cauca valley from approximately 12 Ma to 9 Ma (e.g., Hoyos et al., submitted).

Disequilibrium coronas around the amphibole showed that most of these magmas underwent dehydration at low pressures via volcano degassing from a shallow magma chamber (Figure 33d) for a considerable time. Some amphibole crystals present more than one disequilibrium corona, indicating that after a degassing period, the magma chamber was refilled with magma input with a similar composition, allowing the amphibole to regrow around the breakdown corona. This continuous magma replenishment occurred from one magma chamber to another, sometimes with contrasting magmas creating identifiable mingling and mixing textures. Nevertheless, sometimes it would have happened with similar magmas, making it challenging to identify the mixing process.

8. Conclusions

The CF stratigraphy currently divides it between the Lower Member and the Upper Member (Calle & González 1980, 1982; Grosse 1926). However, the CF records highly active volcanism operating in a varying pull-apart basin that frequently changed its topographic relief. Therefore, fluvial environments (and their accommodation spaces) were also adjusted continuously to the new physical features. As a result, the CF documents the utmost heterogeneity of the lithofacies that cannot be constrained to specific isochronous intervals. Accordingly, we propose to stratigraphically group the CF into only one unit.

The magmatic event responsible for the formation of the CF was active between 9 and 6 Ma. During this time, intense magmatic activity dominated the Cauca valley with the intrusion of an essential volume of subvolcanic andesites (including Cerro Tusa and La Pintada Intrusives). Moreover, basaltic intrusions fed composite volcanoes, which formed lava flows, pyroclastic density currents, and lahars, which remobilized the primary volcanic deposits. On the other hand, the so-called 'El Botón Magmatic Arc' (characterized by a shoshonitic affinity and exclusively related Western Cordillera rocks with oceanic affinity) was active prior to the Combian magmatism between 12.5 and 9 Ma. Nevertheless, it was part of the same tectonic event.

The CVP is characterized by the presence of variable magmatic series. They are tholeiitic, calc-alkaline, and shoshonitic. The calc-alkaline series includes adakites and garnet-bearing rocks, whereby the adakites resulted from garnet fractionation within the garnet stability field of andesitic magmas. The geochemical variability shown within the CVP results from the variable contribution of a modified mantle, sediment and crustal components, coupled with differentiation processes. The formation of the CVP is controlled by the Panamá-Chocó docking

against the South American Plate through oblique convergence and the Caldas Tear.

Acknowledgments

The Servicio Geológico Colombiano funded the unpublished data presented here through the project "Caracterización Estratigráfica, Petrogenética y Geocronológica de la Formación Combia, Acuerdo Específico No 009–2004 con la Universidad Nacional de Colombia". Within this project we would like to especially thank Jennifer Andrea BETANCOURT-DEVIA and María Lucía TEJADA-AVELLA for their valuable participation during the fieldwork and sample descriptions. Jhon ORTÍZ-TRUJILLO and Hernando MAHECHA-CARREÑO are also acknowledged. Fabián PANIAGUA-AGUIRRE is thanked for extensive petrography analyses and Jennifer Andrea BETANCOURT-DEVIA for sample processing. The authors wish to acknowledge the Geochronological Research Centre (CP-Geo) and geochemical laboratories of the Universidade de São Paulo. We would also like to thank Eliana MARÍN RINCÓN for her help with graphics and figures. We are very grateful to David BUCHS and Karoly NEMETH, whose thorough and insightful reviews significantly improved this contribution.

References

- Agencia Nacional de Hidrocarburos & Universidad de Caldas. 2011. Estudio integrado de los núcleos y registros obtenidos de los pozos someros (slim holes) perforados por la ANH. Agencia Nacional de Hidrocarburos, unpublished report, 304 p. Manizales.
- Alcárcel-Gutiérrez, F.A. & Gómez, J., compilers, 2017. Mapa Geológico de Colombia 2017. Scale 1:2000000. Servicio Geológico Colombiano. Bogotá.
- Aldanmaz, E., Pearce, J.A., Thirlwall, M.F. & Mitchell, J.G. 2000. Petrogenetic evolution of late Cenozoic, post-collision volcanism in western Anatolia, Turkey. *Journal of Volcanology and Geothermal Research*, 102(1–2): 67–95. [https://doi.org/10.1016/S0377-0273\(00\)00182-7](https://doi.org/10.1016/S0377-0273(00)00182-7)
- Alonso-Perez, R., Müntener, O. & Ulmer, P. 2009. Igneous garnet and amphibole fractionation in the roots of island arcs: Experimental constraints on andesitic liquids. *Contributions to Mineralogy and Petrology*, 157(4): 541–558. <https://doi.org/10.1007/s00410-008-0351-8>
- Álvarez, A.J. 1983. Geología de la cordillera Central y el occidente colombiano y petroquímica de los intrusivos granitoides meso-cenozoicos. *Boletín Geológico*, 26(2): 1–175.
- Aspden, J.A. & Litherland, M. 1992. The geology and Mesozoic collisional history of the Cordillera Real, Ecuador. *Tectonophysics*, 205(1–3): 187–204. [https://doi.org/10.1016/0040-1951\(92\)90426-7](https://doi.org/10.1016/0040-1951(92)90426-7)
- Aydar, E. & Gourgaud, A. 2002. Garnet-bearing basalts: An example from Mt. Hasan, Central Anatolia, Turkey. *Mineralogy*

- and Petrology, 75(3–4): 185–201. <https://doi.org/10.1007/s007100200023>
- Bach, P., Smith, I.E.M. & Malpas, J.G. 2012. The origin of garnets in andesitic rocks from the Northland Arc, New Zealand, and their implication for sub-arc processes. *J Petrology*, 53(6): 1169–1195. <https://doi.org/10.1093/ptrology/egs012>
- Barragan, R., Geist, D., Hall, M., Larson, P. & Kurz, M. 1998. Subduction controls on the compositions of lavas from the Ecuadorian Andes. *Earth and Planetary Science Letters*, 154(1–4): 153–166. [https://doi.org/10.1016/S0012-821X\(97\)00141-6](https://doi.org/10.1016/S0012-821X(97)00141-6)
- Bernet, M., Mesa-García, J., Chauvel, C., Ramírez Londoño, M.J. & Marín-Cerón, M.I. 2020. Thermochronological, petrographic and geochemical characteristics of the Combia Formation, Amagá Basin, Colombia. *Journal of South American Earth Sciences*, 104: 1–21. <https://doi.org/10.1016/j.jsames.2020.102897>
- Bissig, T., Leal-Mejía, H., Stevens, R.B. & Hart, C.J. 2017. High Sr/Y magma petrogenesis and the link to porphyry mineralization as revealed by garnet-bearing I-type granodiorite porphyries of the Middle Cauca Au–Cu Belt, Colombia. *Economic Geology*, 112(3): 551–568. <https://doi.org/10.2113/econgeo.112.3.551>
- Borrero, C. & Toro-Toro, L.M. 2016. Vulcanismo de afinidad adakítica en el Miembro Inferior de la Formación Combia (Mioceno Tardío) al sur de la Subcuenca de Amagá, noroccidente de Colombia. *Boletín de Geología*, 38(1): 87–100. <http://dx.doi.org/10.18273/revbol.v38n1-2016005>
- Borrero, C., Toro, L.M., Alvarán, M. & Castillo, H. 2009. Geochemistry and tectonic controls of the effusive activity related with the ancestral Nevado del Ruiz Volcano, Colombia. *Geofísica Internacional*, 48(1): 149–169.
- Bourdon, E., Eissen, J.-P., Monzier, M., Robin, C., Martin, H., Cotten, J. & Hall, M.L. 2002. Adakite-like lavas from Antisana Volcano (Ecuador): Evidence for slab melt metasomatism beneath the Andean Northern Volcanic Zone. *Journal of Petrology*, 43(2): 199–217. <https://doi.org/10.1093/ptrology/43.2.199>
- Bryan, S.E., Peate, I.U., Peate, D.W., Self, S., Jerram, D.A., Mawby, M.R., Marsh, J.S. & Miller, J.A. 2010. The largest volcanic eruptions on Earth. *Earth-Science Reviews*, 102(3–4): 207–229. <https://doi.org/10.1016/j.earscirev.2010.07.001>
- Calle, B. & González, H. 1980. Memoria explicativa: Geología y geoquímica de la plancha 166 Jericó. Scale 1:100 000. Ingeominas, Internal report 1822, 250 p. Bogotá.
- Calle, B. & González, H. 1982. Memoria explicativa: Geología y geoquímica de la plancha 186 Riosucio. Scale 1:100 000. Ingeominas, Internal report 1878, 120 p. Medellín.
- Calle, B., González, H., de la Peña, R., Escorche, E., Durango, J., Ramírez, O., Alvarez, E., Calderón, M., Álvarez, J., Guarín, G., Rodríguez, C., Muñoz, J. & Durán, J. 1980. Geología de la plancha 166 Jericó. Scale 1:100 000. Ingeominas. Bogotá.
- Castillo, P.R. 2006. An overview of adakite petrogenesis. *Chinese Science Bulletin*, 51(3): 257–268. <https://doi.org/10.1007/s11434-006-0257-7>
- Castillo, P.R. 2012. Adakite petrogenesis. *Lithos*, 134–135: 304–316. <https://doi.org/10.1016/j.lithos.2011.09.013>
- Castillo, P.R., Janney, P.E. & Solidum, R.U. 1999. Petrology and geochemistry of Camiguin Island, southern Philippines: Insights to the source of adakites and other lavas in a complex arc setting. *Contributions to Mineralogy and Petrology*, 134(1): 33–51. <https://doi.org/10.1007/s004100050467>
- Cediel, F., Shaw, R.P. & Cáceres, C. 2003. Tectonic assembly of the northern Andean Block. In: Bartolini, C., Buffler, R.T. & Blickwede, J. (editors), *The circum-Gulf of Mexico and the Caribbean: Hydrocarbon habitats, basin formation, and plate tectonics*. American Association of Petroleum Geologists, Memoir 79, p. 815–848. Tulsa, USA.
- Chappell, B.W. & White, A.J.R. 1974. Two contrasting granite types. *Pacific Geology*, 8: 173–174.
- Chiarabba, C., De Gori, P., Faccenna, C., Speranza, F., Seccia, D., Dionicio, V. & Prieto, G.A. 2016. Subduction system and flat slab beneath the Eastern Cordillera of Colombia. *Geochemistry, Geophysics, Geosystems*, 17(1): 16–27. <https://doi.org/10.1002/2015GC006048>
- Davidson, J., Turner, S. & Plank, T. 2013. Dy/Dy*: Variations arising from mantle sources and petrogenetic processes. *Journal of Petrology*, 54(3): 525–537. <https://doi.org/10.1093/ptrology/egs076>
- Day, R.A., Green, T.H. & Smith, I.E.M. 1992. The origin and significance of garnet phenocrysts and garnet-bearing xenoliths in miocene calc-alkaline volcanics from Northland, New Zealand. *Journal of Petrology*, 33(1):125–161. <https://doi.org/10.1093/ptrology/33.1.125>
- Defant, M.J. & Drummond, M.S. 1990. Derivation of some modern arc magmas by melting of young subducted lithosphere. *Nature*, 347(6294): 662–665. <https://doi.org/10.1038/347662a0>
- Drummond, M.S. & Defant, M.J. 1990. A model for trondhjemite-tonalite-dacite genesis and crustal growth via slab melting: Archean o modern comparisons. *Journal of Geophysical Research: Solid Earth*, 95(B13): 21503–21521. <https://doi.org/10.1029/JB095iB13p21503>
- Dunia. 2005. Complementación geológica, geoquímica y geofísica (magnetométrica) de las planchas 166, 167, 186 y 187. Ingeominas, unpublished report, 576 p. Bogotá.
- Duque-Caro, H. 1990. The Choco Block in the northwestern corner of South America: Structural, tectonostratigraphic, and paleogeographic implications. *Journal of South American Earth Sciences*, 3(1): 71–84. [https://doi.org/10.1016/0895-9811\(90\)90019-W](https://doi.org/10.1016/0895-9811(90)90019-W)
- Embey-Isztin, A., Noske-Fazekas, G., Kurat, G. & Brandstätter, F. 1985. Genesis of garnets in some magmatic rocks from Hungary. *Tschermaks mineralogische und petrographische Mitteilungen*, 34: 49–66. <https://doi.org/10.1007/BF01082457>
- Farris, D.W., Jaramillo, C., Bayona, G., Restrepo-Moreno, S.A., Montes, C., Cardona, A., Mora, A., Speakman, R.J., Glascock, M.D. & Valencia, V. 2011. Fracturing of the Panamanian Isthmus

- during initial collision with South America. *Geology*, 39(11): 1007–1010. <https://doi.org/10.1130/G32237.1>
- Fitton, J.G. 1972. The genetic significance of almandine–pyrope phenocrysts in calc–alkaline Borrowdale Volcanic Group, northern England. *Contributions to mineralogy and petrology*, 36(3): 231–248. <https://doi.org/10.1007/BF00371434>
- Francis, P.W., Moorbath, S. & Thorpe, R.S. 1977. Strontium isotope data for recent andesites in Ecuador and north Chile. *Earth and Planetary Sciences Letters*, 37(2): 197–202. [https://doi.org/10.1016/0012-821X\(77\)90164-9](https://doi.org/10.1016/0012-821X(77)90164-9)
- Gale, A., Dalton, C.A., Langmuir, C.H., Su, Y. & Schilling, J.G. 2013. The mean composition of ocean ridge basalts. *Geochemistry, Geophysics, Geosystems*, 14(3): 489–518. <https://doi.org/10.1029/2012GC004334>
- García, M. 1983. Petrografía detallada de los pórfidos granatíferos de Chinchiná, Caldas. Bachelor thesis, Universidad Nacional de Colombia, 142 p. Bogotá.
- Gelves, J.F., Sierra-Gallego, G. & Márquez, M.A. 2016. Mineralogical characterization of zeolites present on basaltic rocks from Combia geological formation, La Pintada, Colombia. *Microporous and Mesoporous Materials*, 235: 9–19. <https://doi.org/10.1016/j.micromeso.2016.07.035>
- Gilbert, J.S. & Rogers, N.W. 1989. The significance of garnet in the Permo–Carboniferous volcanic rocks of the Pyrenees. *Journal of the Geological Society*, 146(3): 477–490. <https://doi.org/10.1144/gsjgs.146.3.0477>
- Gill, J.B. 1981. *Orogenic andesites and plate tectonics*. Springer-Verlag. 392 p. Berlin. <https://doi.org/10.1007/978-3-642-68012-0>
- Gómez, J., Montes, N.E., Nivia, Á. & Diederix, H., compilers. 2015. Geological Map of Colombia 2015. Scale 1:1 000 000. Servicio Geológico Colombiano, 2 sheets. Bogotá. <https://doi.org/10.32685/10.143.2015.936>
- González, H. 1980. Geología de las planchas 167 Sonsón y 187 Salamina. Scale 1:100 000. *Boletín Geológico*, 23(1): 1–174.
- González, H. 2010. Geoquímica, geocronología de las unidades litológicas asociadas al sistema de fallas Cauca–Romeral, sector centro-sur. Tomo I. Ingeominas, unpublished report, 412 p. Medellín.
- Green, T.H. 1972. Crystallization of calc–alkaline andesite under controlled high–pressure hydrous conditions. *Contributions to Mineralogy and Petrology*, 34(2): 150–166. <https://doi.org/10.1007/BF00373770>
- Green, T.H. 1977. Garnet in silicic liquids and its possible use as a P–T indicator. *Contributions to Mineralogy and Petrology*, 65(1): 59–67. <https://doi.org/10.1007/BF00373571>
- Green, T.H. 1992. Experimental phase equilibrium studies of garnet-bearing I-type volcanics and high-level intrusives from Northland, New Zealand. *Earth and Environmental Science Transactions of The Royal Society of Edinburgh*, 83(1–2): 429–438. <https://doi.org/10.1017/S0263593300008105>
- Grosse, E. 1926. Estudio geológico del terciario carbonífero de Antioquia en la parte occidental de la cordillera Central de Colombia, entre el río Arma y Sacaolal, ejecutado en los años de 1920–1923. Dietrich Reimer, 361 p. Berlin.
- Hamer, R.D. & Moyes, A.B. 1982. Composition and origin of garnet from the Antarctic Peninsula volcanic group of Trinity Peninsula. *Journal of the Geological Society London*, 139(6): 713–720. <https://doi.org/10.1144/gsjgs.139.6.0713>
- Harangi, S., Downes, H., Kósa, L., Szabó, C., Thirlwall, M.F., Mason, P.R.D. & Matthey, D. 2001. Almandine garnet in calc–alkaline volcanic rocks of the northern Pannonian Basin (eastern–central Europe): Geochemistry, petrogenesis and geodynamic implications. *Journal of Petrology*, 42(10): 1813–1844. <https://doi.org/10.1093/petrology/42.10.1813>
- Harmon, R.S., Barreiro, B.A., Moorbath, S., Hoefs, J., Francis, P.W., Thorpe, R.S., Déruelle, B., McHugh, J. & Viglino, J.A. 1984. Regional O–, Sr–, and Pb–isotope relationships in late Cenozoic calc–alkaline lavas of the Andean Cordillera. *Journal of the Geological Society*, 141(5): 803–822. <https://doi.org/10.1144/gsjgs.141.5.0803>
- Hawkesworth, C.J., Norry, M.J., Roddick, J.C., Baker, P.E., Francis, P.W. & Thorpe, R.S. 1979. $^{143}\text{Nd}/^{144}\text{Nd}$, $^{87}\text{Sr}/^{86}\text{Sr}$, and incompatible element variations in calc–alkaline andesites and plateau lavas from South America. *Earth and Planetary Science Letters*, 42(1): 45–57. [https://doi.org/10.1016/0012-821X\(79\)90189-4](https://doi.org/10.1016/0012-821X(79)90189-4)
- Henrichs, I.A. 2013. Caracterização e idade das intrusivas do sistema Pórfiro Yarumalito, magmatismo Combia, Colombia. Doctoral thesis, Universidade Federal do Rio Grande do Sul, 68 p. Porto Alegre, Brasil.
- Hidalgo, P.J. & Rooney, T.O. 2010. Crystal fractionation processes at Baru volcano from the deep to shallow crust. *Geochemistry, Geophysics, Geosystems*, 11(12): 1–29. <https://doi.org/10.1029/2010GC003262>
- Hidalgo, P.J. & Rooney, T.O. 2014. Petrogenesis of a voluminous Quaternary adakitic volcano: The case of Baru volcano. *Contributions to Mineralogy and Petrology*, 168(3): 1–19. <https://doi.org/10.1007/s00410-014-1011-9>
- Hidalgo, S., Monzier, M., Martin, H., Chazot, G., Eissen, J.P. & Cottin, J. 2007. Adakitic magmas in the Ecuadorian volcanic front: Petrogenesis of the Iliniza volcanic complex, Ecuador. *Journal of Volcanology and Geothermal Research*, 159(4): 366–392. <https://doi.org/10.1016/j.jvolgeores.2006.07.007>
- Horton, B.K., Parra, M., Saylor, J.E., Nie, J., Mora, A., Torres, V., Stockli, D.F. & Strecker, M.R. 2010. Resolving uplift of the northern Andes using detrital zircon age signatures. *GSA Today*, 20(7): 4–10. <https://doi.org/10.1130/GSATG76A.1>
- Hoyos, S. & Duque-Trujillo, J.F. 2017. Determinación de focos de emisión en ignimbritas de la Formación Combia a partir de análisis de fábrica magnética. XVI Congreso Colombiano de Geología. *Memoirs*, p. 1301–1302. Santa Marta.
- Hoyos, S., Weber, M., Cárdenas-Rozo, A.L., Cottrell, E., Duque, J.F., Beltrán-Triviño, A., von Quadt, A. & Gómez Tapias, J. 2020. Late Miocene garnet-bearing andesites in the Northern An-

- des and their tectonic implications. Manuscript submitted for publication.
- Irving, A.J. & Frey, F.A. 1978. Distribution of trace elements between garnet megacrysts and host volcanic liquids of kimberlitic rhyolitic composition. *Geochimica et Cosmochimica Acta*, 42(6): 771–787. [https://doi.org/10.1016/0016-7037\(78\)90092-3](https://doi.org/10.1016/0016-7037(78)90092-3)
- James, D.E. & Murcia, L.A. 1984. Crustal contamination in northern Andean volcanics. *Journal of the Geological Society*, 141(5): 823–830. <https://doi.org/10.1144/gsjgs.141.5.0823>
- Jaramillo, J.M. 1976. Volcanic rocks of the rio Cauca Valley, Colombia. Master thesis, Rice University, 46 p. Houston, USA.
- Jaramillo, J.S., Cardona, A., Monsalve, G., Valencia, V. & León, S. 2019. Petrogenesis of the late Miocene Combia volcanic complex, northwestern Colombian Andes: Tectonic implication of short term and compositionally heterogeneous arc magmatism. *Lithos* 330–331: 194–220. <https://doi.org/10.1016/j.lithos.2019.02.017>
- Kano, H. & Yashima, R. 1976. Almandine–garnets of acid magmatic origin from Yamanogawa. *Journal of the Japanese Association of Mineralogists, Petrologists and Economic Geology*, 71(4): 106–119. <https://doi.org/10.2465/ganko1941.71.106>
- Kawabata, H. & Takafuji, N. 2005. Origin of garnet crystals in calc–alkaline volcanic rocks from the Setouchi volcanic belt, Japan. *Mineralogical Magazine*, 69(6): 951–971. <https://doi.org/10.1180/0026461056960301>
- Kennan, L. & Pindell, J.L. 2009. Dextral shear, terrane accretion and basin formation in the northern Andes: Best explained by interaction with a Pacific–derived Caribbean Plate? In: James, K.H., Lorente, M.A. & Pindell, J.L. (editors), *The origin and evolution of the Caribbean Plate*. Geological Society of London, Special Publication 328, p. 487–531. <https://doi.org/10.1144/SP328.20>
- Kerr, A.C., Tarney, J., Marriner, G.F., Nivia, Á., Klaver, G.T. & Saunders, A.D. 1996. The geochemistry and tectonic setting of late Cretaceous Caribbean and Colombian volcanism. *Journal of South American Earth Sciences*, 9(1–2): 111–120. [https://doi.org/10.1016/0895-9811\(96\)00031-4](https://doi.org/10.1016/0895-9811(96)00031-4)
- Kerr, A.C., Marriner, G.F., Tarney, J., Nivia, Á., Saunders, A.D., Thirlwall, M.F. & Sinton, C.W. 1997. Cretaceous basaltic terranes in western Colombia: Elemental, chronological and Sr–Nd isotopic constraints on petrogenesis. *Journal of Petrology*, 38(6): 677–702. <https://doi.org/10.1093/petrology/38.6.677>
- Krein, S.B., Molitor, Z.J. & Grove, T.L. In Review at JGR: Solid Earth. ReversePetrogen: A Multiphase Dry Reverse Fractional Crystallization–Mantle Melting Thermobarometer applied to 13,589 Mid–Ocean Ridge Basalt Glasses.
- Lara, M., Salazar–Franco, A.M. & Silva–Tamayo, J.C. 2018. Provenance of the Cenozoic siliciclastic intramontane Amagá Formation: Implications for the early Miocene collision between Central and South America. *Sedimentary Geology*, 373: 147–162. <https://doi.org/10.1016/j.sedgeo.2018.06.003>
- Leake B.E., Woolley A.R., Arps C.E.S., Birch W.D., Gilbert M.C., Grice J.D., Hawthorne F.C., Kato A., Kisch H.J., Krivovichev V.G., Linthout K., Laird J., Mandarino J., Maresch W.V., Nickel E.H., Schumaker J.C., Smith D.C., Stephenson N.C.N., Ungaretti L., Whittaker E.J.W. & Youzhi G. 1997. Nomenclature of amphiboles: Report of the subcommittee on amphiboles of the International Mineralogical Association Commission on New Minerals and Mineral Names. *Mineralogical magazine*, 61(405): 295–321
- Leal–Mejía, H. 2011. Phanerozoic gold metallogeny in the Colombian Andes: A tectono–magmatic approach. Doctoral thesis, Universitat de Barcelona, 989 p. Barcelona.
- Leal–Mejía, H., Shaw, R.P. & Melgarejo I Draper, J.C. 2019. Spatial–temporal migration of granitoid magmatism and the Phanerozoic tectono–magmatic evolution of the Colombian Andes. In: Cedié, F. & Shaw, R.P. (editors), *Geology and tectonics of northwestern South America: The Pacific–Caribbean–Andean junction*. Frontiers in Earth Sciences. Springer, p. 253–410. Cham, Germany. https://doi.org/10.1007/978-3-319-76132-9_5
- Le Maitre, R.W., Streckeisen, A., Zanettin, B., Le Bas, M.J., Bonin, B., Bateman, P., Bellieni, G., Dudek, A., Efremova, S., Keller, J., Lameyre, J., Sabine, P.A., Schmid, R., Sørensen, H. & Woolley, A.R., editors. 2002. *Igneous rocks: A classification and glossary of terms. Recommendations of the International Union of Geological Sciences Subcommittee on the systematics of igneous rocks*. Cambridge University Press, 236 p. Cambridge, UK. <https://doi.org/10.1017/CBO9780511535581>
- Lesage, G., Richards, J.P., Muehlenbachs, K. & Spell, T.L. 2013. Geochronology, geochemistry, and fluid characterization of the late Miocene Buriticá gold deposit, Antioquia Department, Colombia. *Economic Geology*, 108(5): 1067–1097. <https://doi.org/10.2113/econgeo.108.5.1067>
- Lonsdale, P. 1991. Structural patterns of the Pacific floor offshore of peninsular California. In: Dauphin, J.P. & Simoneit, B.R.T. (editors), *The gulf and peninsular province of the Californias*. American Association of Petroleum Geologists, Memoir 47, p. 87–125. Tulsa, USA.
- Lonsdale, P. 2005. Creation of the Cocos and Nazca Plates by fission of the Farallon Plate. *Tectonophysics*, 404(3–4): 237–264. <https://doi.org/10.1016/j.tecto.2005.05.011>
- MacDonald, W.D. 1980. Anomalous paleomagnetic directions in late tertiary andesitic intrusions of the Cauca depression, Colombian Andes. *Tectonophysics*, 68(3–4): 339–348. [https://doi.org/10.1016/0040-1951\(80\)90183-3](https://doi.org/10.1016/0040-1951(80)90183-3)
- Macpherson, C.G., Dreher, S.T. & Thirlwall, M.F. 2006. Adakites without slab melting: High pressure differentiation of island arc magma, Mindanao, the Philippines. *Earth and Planetary Science Letters*, 243(3–4): 581–593. <https://doi.org/10.1016/j.epsl.2005.12.034>
- Mahecha, H., Ortiz, J., Tejada, M.L., Paniagua, F. & Weber, M. 2006. Cartografía geológica de las vulcanitas de la Formación Combia, en un área de 200 km² en los alrededores del municipio de Jardín, departamento de Antioquia, Colombia. Ingeominas, unpublished report, 27 p. Bogotá.

- Marín-Cerón, M.I., Moriguti, T., Makishima, A. & Nakamura, E. 2010. Slab decarbonation and CO₂ recycling in the southwestern Colombian volcanic arc. *Geochimica et Cosmochimica Acta*, 74(3): 1104–1121. <https://doi.org/10.1016/j.gca.2009.10.031>
- Marín-Cerón, M.I., Leal-Mejía, H., Bernet, M. & Mesa-García, J. 2019. Late Cenozoic to modern-day volcanism in the northern Andes: A geochronological, petrographical, and geochemical review. In: Cedié, F. & Shaw R.P. (editors), *Geology and tectonics of northwestern South America: The Pacific–Caribbean–Andean junction*. *Frontiers in Earth Sciences*. Springer, p. 603–648. Cham, Germany. https://doi.org/10.1007/978-3-319-76132-9_8
- Marriner, G.F. & Millward, D. 1984. The petrology and geochemistry of Cretaceous to recent volcanism in Colombia: The magmatic history of an accretionary plate margin. *Journal of the Geological Society*, 141(3): 473–486. <https://doi.org/10.1144/gsjgs.141.3.0473>
- Martin, H., Smithies, R.H., Rapp, R., Moyen, J.-F. & Champion, D. 2005. An overview of adakite, tonalite–trondhjemite–granodiorite (TTG), and sanukitoid: Relationships and some implications for crustal evolution. *Lithos*, 79(1–2): 1–24. <https://doi.org/10.1016/j.lithos.2004.04.048>
- McPhie, J., Doyle, M. & Allen, R.L. 1993. *Volcanic textures: A guide to the interpretation of textures in volcanic rocks*. Centre for Ore Deposits and Exploration Studies, University of Tasmania, 196 p. Hobart, Australia.
- Miyashiro, A. 1955. Pyroxene garnets in volcanic rocks. *Journal of Geological Society of Japan*, 61(721): 463–470. <https://doi.org/10.5575/geosoc.61.463>
- Miyashiro, A. 1974. Volcanic rock series in island arcs and active continental margins. *American Journal of Science*, 274(4): 321–355. <https://doi.org/10.2475/ajs.274.4.321>
- Montes, C., Bayona, G., Cardona, A., Buchs, D.M., Silva, C.A., Morón, S., Hoyos, N., Ramírez, D.A., Jaramillo, C. & Valencia, V. 2012. Arc–continent collision and orocline formation: Closing of the Central American Seaway. *Journal of Geophysical Research: Solid Earth*, 117(B4), 1–25. <https://doi.org/10.1029/2011JB008959>
- Montes, C., Cardona, A., Jaramillo, C., Pardo, A., Silva, J.C., Valencia, V., Ayala, C., Pérez-Ángel, L.C., Rodríguez-Parra, L.A., Ramírez, V. & Niño, H. 2015. Middle Miocene closure of the Central American Seaway. *Science*, 348(6231): 226–229. <https://doi.org/10.1126/science.aaa2815>
- Morrison, G.W. 1980. Characteristics and tectonic setting of the shoshonite rock association. *Lithos* 13(1): 79–108. [https://doi.org/10.1016/0024-4937\(80\)90067-5](https://doi.org/10.1016/0024-4937(80)90067-5)
- Müller, D., Rock, N.M.S. & Groves, D.I. 1992. Geochemical discrimination between shoshonitic and potassic volcanic rocks in different tectonic settings: A pilot study. *Mineralogy and Petrology*, 46(4): 259–289. <https://doi.org/10.1007/BF01173568>
- Müller, R.D., Sdrolias, M., Gaina, C. & Roest, W.R. 2008. Age, spreading rates, and spreading asymmetry of the world's ocean crust. *Geochemistry, Geophysics, Geosystems*, 9(4): 1–19. <https://doi.org/10.1029/2007GC001743>
- Müntener, O., Kelemen, P.B. & Grove, T.L. 2001. The role of H₂O during crystallization of primitive arc magmas under uppermost mantle conditions and genesis of igneous pyroxenites: An experimental study. *Contributions to Mineralogy and Petrology*, 141(6): 643–658. <https://doi.org/10.1007/s004100100266>
- Muñoz, J.A. 1992. Evolution of a continental collision belt: ECORS–Pyrenees crustal balanced cross-section. In: McClay, K.R., (editor), *Thrust Tectonics*. Springer Science, p. 235–246. London, UK.
- Murcia, H.F., Borrero, C.A., Pardo, N., Alvarado, G.E., Arnosio, M. & Scolamacchia, T. 2013. Depósitos volcánico-clásticos: Términos y conceptos para una clasificación en español. *Revista Geológica de América Central*, 48:15–39.
- Németh, K. & Martin, U. 2007. *Practical volcanology: Lecture notes for understanding volcanic rocks from field based studies*. Geological Institute of Hungary, 221 p. Budapest, Hungary.
- Ordóñez-Carmona, O. 2001. Caracterização isotópica Rb–Sr e Sm–Nd dos principais eventos magmáticos nos Andes colombianos. Doctoral thesis, Universidad de Brasília, 176 p. Brasília.
- Pardo, N., Cepeda, H. & Jaramillo, J. 2005. The Paipa volcano, Eastern Cordillera of Colombia, South America: Volcanic stratigraphy. *Earth Sciences Research Journal*, 9(1): 3–18.
- Pearce, J.A. 2008. Geochemical fingerprinting of oceanic basalts with applications to ophiolite classification and the search for Archean oceanic crust. *Lithos*, 100(1–4): 14–48. <https://doi.org/10.1016/j.lithos.2007.06.016>
- Pindell, J., Kennan, L., Maresch, W.V., Stanek, K.P., Draper, G. & Higgs, R. 2005. Plate–kinematics and crustal dynamics of circum-Caribbean arc–continent interactions: Tectonic controls on basin development in proto-Caribbean margins. In: Avé-Lallemant, H.G. & Sisson, V.B. (editors), *Caribbean–South American Plate interactions, Venezuela*. Geological Society of America, Special Paper 394, p. 7–52. <https://doi.org/10.1130/0-8137-2394-9.7>
- Plank, T. 2005. Constraints from thorium/lanthanum on sediment recycling at subduction zones and the evolution of the continents. *Journal of Petrology*, 46(5): 921–944. <https://doi.org/10.1093/petrology/egi005>
- Plank, T. & Langmuir, C.H. 1998. The chemical composition of subducting sediment and its consequences for the crust and mantle. *Chemical Geology*, 145(3–4): 325–394. [https://doi.org/10.1016/S0009-2541\(97\)00150-2](https://doi.org/10.1016/S0009-2541(97)00150-2)
- Ramírez, D.A., López, A., Sierra, G.M. & Toro, G.E. 2006. Edad y proveniencia de las rocas volcánico-sedimentarias de la Formación Combia en el suroccidente antioqueño, Colombia. *Boletín de Ciencias de la Tierra*, (19): 9–26.
- Ramírez, E., Pardo-Trujillo, A., Plata, A., Vallejo, F. & Trejos, R. 2015. Edad y ambiente de la Formación Amagá, sector de

- Santa Fé de Antioquia–Sopetrán, con base en evidencias palinológicas. XV Congreso Colombiano de Geología. Memoirs, p. 277–281. Bucaramanga, Colombia.
- Restrepo, J.J. 1991. Datación de algunos plutones de Antioquia por el método de trazas de fisión. *Boletín de Ciencias de la Tierra*, (10): 95–107.
- Restrepo, J.J., Toussaint, J.F. & González, H. 1981a. Edades miopliocenas del magmatismo asociado a la Formación Combia, departamentos de Antioquia y Caldas, Colombia. *Geología Norandina*, (3): 21–26.
- Restrepo, J.J., Toussaint, J.F., Zuluaga, J. & Hoyos, P. 1981b. Algunas consideraciones sobre la geología de la parte septentrional de la cordillera Occidental. *Boletín de Ciencias de la Tierra*, (5–6): 85–107.
- Ribeiro, J.M., Maury, R.C. & Grégoire, M. 2016. Are adakites slab melts or high–pressure fractionated mantle melts? *Journal of Petrology*, 57(5): 839–862. <https://doi.org/10.1093/petrology/egw023>
- Richards, J.P. & Kerrich, R. 2007. Special Paper: Adakite–like rocks: Their diverse origins and questionable role in metallogenesis. *Economic Geology*, 102(4): 537–576. <https://doi.org/10.2113/gsecongeo.102.4.537>
- Ridolfi, F. & Renzulli, A. 2012. Calcic amphiboles in calc–alkaline and alkaline magmas: Thermobarometric and chemometric empirical equations valid up to 1130 °C and 2.2 GPa. *Contributions to Mineralogy and Petrology*, 163(5): 877–895. <https://doi.org/10.1007/s00410-011-0704-6>
- Ridolfi, F., Renzulli, A. & Puerini, M. 2010. Stability and chemical equilibrium of amphibole in calc–alkaline magmas: An overview, new thermobarometric formulations and application to subduction–related volcanoes. *Contributions to Mineralogy and Petrology*, 160(1): 45–66. <https://doi.org/10.1007/s00410-009-0465-7>
- Ríos, A.M. & Sierra, M.I. 2004. La Formación Combia: Registro de la relación entre el volcanismo neógeno y la sedimentación fluvial, sección Guineales–Bolombolo, suroeste antioqueño. Bachelor thesis, Universidad EAFIT, 106 p. Medellín.
- Rodríguez, G. & Zapata, G. 2014. Descripción de una nueva unidad de lavas denominada andesitas basálticas de El Morito–correlación regional con eventos magmáticos de arco. *Boletín de Geología*, 36(1): 85–102.
- Rutherford, M.J. & Hill, P.M. 1993. Magma ascent rates from amphibole breakdown: An experimental study applied to the 1980–1986 Mount St. Helens eruptions. *Journal of Geophysical Research: Solid Earth*, 98(B11): 19667–19685. <https://doi.org/10.1029/93JB01613>
- Samaniego, P., Robin, C., Chazot, G., Bourdon, E. & Cotten, J. 2010. Evolving metasomatic agent in the northern Andean subduction zone, deduced from magma composition of the long–lived Pichincha volcanic complex, Ecuador. *Contributions to Mineralogy and Petrology*, 160(2): 239–260. <https://doi.org/10.1007/s00410-009-0475-5>
- Shaw, R.P., Leal–Mejía, H., & Melgarejo I Draper, J.C. 2019. Phanerozoic metallogeny in the Colombian Andes: A tectono–magmatic analysis in space and time. In: Cediél, F. & Shaw R.P. (editors), *Geology and tectonics of northwestern South America: The Pacific–Caribbean–Andean junction*. *Frontiers in Earth Sciences*. Springer, p. 411–549. Cham, Germany. https://doi.org/10.1007/978-3-319-76132-9_6
- Shuto, K., Sato, M., Kawabata, H., Osanai, Y., Nakano, N. & Yashima, R. 2013. Petrogenesis of middle Miocene primitive basalt, andesite and garnet–bearing adakitic rhyodacite from the Ryozen Formation: Implications for the tectono–magmatic evolution of the NE Japan arc. *Journal of Petrology*, 54(12), 2413–2454. <https://doi.org/10.1093/petrology/egt052>
- Sierra, G.M. 1994. Structural and sedimentary evolution of the Irra Basin, northern Colombian Andes. Master thesis, State University of New York, 102 p. Binghamton, USA.
- Smith, I.E.M., Ruddock, R.S. & Day, R.A. 1989. Miocene arc–type volcanic/plutonic complexes of the Northland Peninsula, New Zealand. *Royal Society of New Zealand Bulletin*, 26: 205–213.
- Staudigel, H., Plank, T., White, B. & Schmincke, H.U. 1996. Geochemical fluxes during seafloor alteration of the basaltic upper oceanic crust: DSDP Sites 417 and 418. In: Bebout, G.E., Scholl, D.W., Kirby, S.H. & Platt, J.P. (editors), *Subduction: Top to bottom*. *Geophysical Monograph Series*, 96, p. 19–38. <https://doi.org/10.1029/GM096p0019>
- Stern, C.R. & Kilian, R. 1996. Role of the subducted slab, mantle wedge and continental crust in the generation of adakites from the Andean Austral Volcanic Zone. *Contributions to Mineralogy and Petrology*, 123(3): 263–281. <https://doi.org/10.1007/s004100050155>
- Sun, S.S. & McDonough, W.F. 1989. Chemical and isotopic systematics of oceanic basalts: Implications for mantle composition and processes. In: Saunders, A.D. & Norry, M.J. (editors), *Magmatism in the ocean basins*. *Geological Society of London, Special Publication* 42, p. 313–345. <https://doi.org/10.1144/GSL.SP.1989.042.01.19>
- Tassinari, C.C.G., Díaz–Pinzon, F. & Buenaventura, J. 2008. Age and sources of gold mineralization in the Marmato mining district, NW Colombia: A Miocene – Pliocene epizonal gold deposit. *Ore Geology Reviews*, 33(3–4): 505–518. <https://doi.org/10.1016/j.oregeorev.2007.03.002>
- Taylor, S.R. & McLennan, S.M. 1985. *The Continental Crust: Its composition and evolution; an examination of the geochemical record preserved in sedimentary rocks*. Blackwell Scientific Publications, 312 p. Oxford.
- Tejada, M.L. & Betancourt, J.A. 2006. Cartografía geológica de las vulcanitas de la Formación Combia en un área de 200 km² en los alrededores de los municipios de Jericó y Pueblorrico, departamento de Antioquia, Colombia. Ingeominas, unpublished report, 54 p. Bogotá.
- Tejada, M., Betancourt, J., Nivia, Á., Weber, M. & Gómez, J. 2007. Cartografía geológica y caracterización geoquímica de la For-

- mación Combia en los alrededores de Jericó y Pueblorrico, departamento de Antioquia, Colombia. XI Congreso Colombiano de Geología. Memoirs, CD ROM, 24 p. Bucaramanga.
- Thirlwall, M.F. & Fitton, J.G. 1983. Sm–Nd garnet age for the Ordovician Borrowdale Volcanic Group, English Lake District. *Journal of the Geological Society London*, 140(3): 511–518. <https://doi.org/10.1144/gsjgs.140.3.0511>
- Thorkelson, D.J. & Breitsprecher, K. 2005. Partial melting of slab window margins: Genesis of adakitic and non-adakitic magmas. *Lithos* 79(1–2): 25–41. <https://doi.org/10.1016/j.lithos.2004.04.049>
- Thorpe, R.S., Francis, W.W. & O’Callaghan, L. 1984. Relative roles of source composition, fractional crystallization and crustal contamination in the petrogenesis of Andean volcanic rocks. *Philosophical Transactions of the Royal Society of London, A, Mathematical, Physical and Engineering Sciences*, 310(1514): 675–692. <https://doi.org/10.1098/rsta.1984.0014>
- Toro, G., Restrepo, J.J., Poupeau, G., Sáenz, E. & Azdimousa, A. 1999. Datación por trazas de fisión de circones rosados asociados a la secuencia volcano-sedimentaria de Irra, Caldas. *Boletín de Ciencias de la Tierra*, (13): 28–34.
- Toro–Toro, L.M., Alvarán–Echeverri, M. & Borrero–Peña, C.A. 2008. Rocas con afinidad adakítica al sureste de Manizales: Rasgos petrogenéticos y geoquímicos. *Boletín de Geología*, 30(2): 49–60.
- Touissaint, J.F. 1999. Evolución geológica de Colombia: Precámbrico, Paleozoico, Mesozoico, Cenozoico. Universidad Nacional de Colombia, CD ROM, 243p. Bogotá.
- Vargas, C.A. & Mann, P. 2013. Tearing and breaking off of subducted slabs as the result of collision of the Panama arc–indenter with northwestern South America. *Bulletin of the Geological Society of America*, 103(3): 2025–2046. <https://doi.org/10.1785/0120120328>
- Wagner, L.S., Jaramillo, J.S., Ramírez–Hoyos, L.F., Monsalve, G., Cardona, A. & Becker, T.W. 2017. Transient slab flattening beneath Colombia. *Geophysical Research Letters*, 44(13): 6616–6623. <https://doi.org/10.1002/2017GL073981>
- Weber, M.B.I., Tarney, J., Kempton, P.D. & Kent, R.W. 2002. Crustal make-up of the northern Andes: Evidence based on deep crustal xenolith suites, Mercaderes, SW Colombia. *Tectonophysics*, 345(1–4): 49–82. [https://doi.org/10.1016/S0040-1951\(01\)00206-2](https://doi.org/10.1016/S0040-1951(01)00206-2)
- Woodhead, J.D., Hergt, J.M., Davidson, J.P. & Eggins, S.M. 2001. Hafnium isotope evidence for ‘conservative’ element mobility during subduction zone processes. *Earth and Planetary Science Letters*, 192(3): 331–346. [https://doi.org/10.1016/S0012-821X\(01\)00453-8](https://doi.org/10.1016/S0012-821X(01)00453-8)
- Yarce, J., Monsalve, G., Becker, T.W., Cardona, A., Poveda, E., Alvira, D. & Ordoñez–Carmona, O. 2014. Seismological observations in northwestern South America: Evidence for two subduction segments, contrasting crustal thicknesses and upper mantle flow. *Tectonophysics*, 637: 57–67. <https://doi.org/10.1016/j.tecto.2014.09.006>
- Zapata, G. & Rodríguez, G. 2011. Basalto de El Botón, arco volcánico mioceno de afinidad shoshonítica al norte de la cordillera Occidental de Colombia. *Boletín Ciencias de la Tierra*, (30): 77–91.
- Zapata, G. & Rodríguez, G. 2013. Petrografía, geoquímica y edad de la Granodiorita de Farallones y las rocas volcánicas asociadas. *Boletín de Geología*, 35(1): 81–96.
- Zindler, A. & Hart, S. 1986. Chemical geodynamics. *Annual Review of Earth and Planetary Sciences*, 14(1): 493–571. <https://doi.org/10.1146/annurev.ea.14.050186.002425>

Explanation of Acronyms, Abbreviations, and Symbols:

ADR	Andesite dacite rhyolite	HREE	Heavy rare earth element
AF	Amagá Formation	LILE	Large-ion lithophile element
AFC	Assimilation and fractional crystallization	LOI	Loss on ignition
CF	Combia Formation	LREE	Light rare earth element
CSVl	Cauca Shallow Volcanic Intrusions	MASH	Melting, assimilation, storage, homogenization.
CVP	Combia Volcanic Province	MORB	Mid ocean ridge basalt
E–MORB	Enriched–mid ocean ridge basalt	N–MORB	Normal–mid ocean ridge basalt
GLOSS	Global subducting sediment	OIB	Oceanic island basalt
HP	High–pressure	REE	Rare earth element

Authors' Biographical Notes



Marion WEBER has a PhD in geochemistry from Leicester University and is a full professor at the Departamento de Geociencias y Medio Ambiente from the Universidad Nacional de Colombia Sede Medellín. Research interests comprise metamorphic petrology and geochemistry applied to understand the evolution of the Caribbean region. Dr. WEBER currently holds the position of the museum director of the University Geosciences Museum.



Jose Fernando DUQUE is a PhD geologist from Universidad Nacional Autónoma de México (UNAM) and is an associate professor at Departamento de Ciencias de la Tierra from Universidad EAFIT, Colombia. Dr. DUQUE is interested in regional tectonic processes, using relations between magmatism, deformation, and geodynamic processes to understand evolution of the continental margins overtime.



Susana HOYOS is a PhD student at the Massachusetts Institute of Technology (MIT) in the Department of Earth, Planetary, and Atmospheric Sciences (EAPS).



Andrés L. CÁRDENAS-ROZO has a PhD in geology (paleontology major) from the University of South Florida (USF), and is an associate professor at Departamento de Ciencias de la Tierra from Universidad EAFIT, Colombia. His research interests are related to stratigraphic architecture and obtaining biological and geological signatures from the sedimentary record.



Jorge GÓMEZ TAPIAS is a geologist and has worked as a cartographer at the Servicio Geológico Colombiano for 20 years, during which time, he has authored approximately 70 geological maps. He is the coordinator of the Grupo Mapa Geológico Colombiano of the Dirección de Geociencias Básicas, which was recognized by Colciencias as a research group in 2017. GÓMEZ

is the first author of the Geological Map of Colombia at a scale of 1:1 M —editions 2007 and 2015— and of the 26 map sheets of the Geological Atlas of Colombia at a scale of 1:500 K and is the co-editor of the book *Compilando la geología de Colombia: Una visión a 2015*. Since February 2018, he has served as vice president for South America on the Commission for the Geological Map of the World. He was a co-coordinator and the first author of the Geological Map of South America at a scale of 1:5 M 2019. Since October 2020, he was elected as a member of the International Union of Geological Sciences (IUGS) Nominating Committee for the term 2020–2024. Currently, he is the editor-in-chief of *The Geology of Colombia*. GÓMEZ is in charge of coordinating all the activities related to the project and the editorial process.

Rob WILSON was principal experimental officer and electron probe microanalysis specialist in the Department of Geology at the University of Leicester (UK) before retirement in 2015. He is now an honorary visiting fellow of the School of Geography, Geology & the Environment at the University of Leicester.